1
Non-Diffracting Waves: An Introduction[1]

Erasmo Recami, Michel Zamboni-Rached, Hugo E. Hernández-Figueroa, and Leonardo A. Ambrosio

1.1
A General Introduction

1.1.1
A Prologue

In this chapter, which essentially deals with *exact* solutions to the wave equations, we begin by introducing the topic of non-diffracting waves (NDW), including some brief historical remarks, and by a simple definition of NDWs; afterward we present some recollections – besides of ordinary waves (Gaussian beams, Gaussian pulses) – of the simplest NDWs (Bessel beams, X-shaped pulses, etc.). More details can be found in the first two (introductory) chapters of the volume on *Localized Waves* published [1] in 2008. In section 1.2 we go on to show how to eliminate *any* backward-traveling components (also known as non-causal components), first in the case of ideal NDW pulses, and then, in section 1.3, for realistic, finite-energy NDW pulses. In particular, in section 1.3.1 we forward a general functional expression for any totally-forward non-diffracting pulses. Then, in section 1.4 an efficient method is set forth for the *analytic* description of *truncated* beams, a byproduct of its being the elimination of any need of lengthy numerical calculations. In section 1.5 we explore the not-less-interesting question of the *subluminal* NDWs, or bullets, in terms of two different methods, the second one being introduced as it allows the analytic description of NDWs with $v = 0$ that is of NDWs with a static envelope ("frozen waves" (FW)) in terms of continuous Bessel beam superpositions. The production of such FWs (which, indeed, have been generated experimentally in recent time for optics) is developed theoretically in section 1.6 also for the case of absorbing media. Section 1.7 discusses the role of special relativity and of Lorentz transformations (LTs), which is relevant for the physical comprehension of the whole issue of NDWs. In section 1.8 we present further analytic solutions to the wave equations, with use of higher-order

---

Bessel beams (namely, non-axially symmetric solutions). Next, section 1.9 deals in detail with an application of NDWs to biomedical optics by having recourse to the generalized Lorenz–Mie theory (GLMT). In section 1.10 we exploit the important fact that "soliton-like" solutions can be found also in the rather different case of the ordinary, linear *Schroedinger equation* – which is not a properly said wave equation – within standard quantum mechanics; by also constructing, for instance, a general exact non-diffracting solution for such equation. These "localized" solutions to the Schroedinger equation may a priori be of help for a better understanding, say, of de Broglie's approach and of the particle-wave duality. Some complementary issues are mentioned in the last section.

Let us now start by recalling that diffraction and dispersion are long-known phenomena limiting the applications of beams or pulses.

Diffraction is always present, affecting any waves that propagate in two or three-dimensional (3D) media. Pulses and beams are constituted by waves traveling along different directions, which produces a gradual *spatial* broadening. This effect is a limiting factor whenever a pulse is needed, which maintains its transverse localization, like, for example, in free space communications, image forming, optical lithography, and electromagnetic tweezers, etc.

Dispersion acts on pulses propagating in material media causing mainly a *temporal* broadening, an effect due to the variation of the refraction index with the frequency, so that each spectral component of the pulse possesses a different phase velocity. This entails a gradual temporal widening, which constitutes a limiting factor when a pulse is needed that maintains its *time* width, like, for example, in communication systems.

It has been important, therefore, to develop techniques able to reduce those phenomena. NDW, known also as localized waves, are, indeed, able to resist diffraction for a long distance. Today, NDW are well-established both theoretically and experimentally, and have innovative applications not only in vacuum, but also in material (linear or nonlinear) media, also showing resistance to dispersion. As mentioned, their potential applications are being explored intensively, always with surprising results, in fields like acoustics, microwaves, and optics, and are also promising in mechanics, geophysics [2], and even elementary particle physics [3] and gravitational waves. One interesting acoustic application has been already obtained in high-resolution ultra-sound scanning of moving organs in the human body. We shall see that NDWs are suitable superpositions of Bessel beams. And worth noticing is that peculiar superposition of Bessel beams can be used to obtain "static" NDW fields, with high transverse localization, and whose longitudinal intensity pattern can assume any desired shape within a chosen interval $0 \leq z \leq L$ of the propagation axis; such waves with a *static* envelope [1, 4–7], that we called FW, have been produced experimentally in recent times in the case of optics, as reported elsewhere also in this book. These FWs promise to have very important applications (even in the field of medicine and of tumor curing [8]).

To confine ourselves to electromagnetism, let us recall again the present-day studies on electromagnetic tweezers, optical (or acoustic) scalpels, optical

guiding of atoms or (charged or neutral) corpuscles, optical lithography, optical (or acoustic) images, communications in free space, remote optical alignment, optical acceleration of charged corpuscles, and so on.

1.1.2
Preliminary, and Historical, Remarks

Ordinary beams and pulses are superpositions of plane waves that travel in different directions; this causes diffraction and, consequently, an increasing spatial broadening of the waves during propagation. Incidentally, we are considering here only propagating, that is *non-evanescent,* waves.

Surprisingly, solutions to the wave equations exist, which represent in homogeneous media beams and pulses able to resist the effects of diffraction for long distances. Such solutions are called NDW, or localized waves (LW); even if a better name would be ''limited-diffractions waves'' [9, 10].

The theory of NDWs also allows compensating for effects like dispersion and attenuation. Indeed, in dispersing homogeneous media, it is possible to construct pulses that simultaneously resist the effects *of diffraction and of surface dispersion.* And, in absorbing homogeneous media, it is also possible to construct beams that resist the simultaneous effects *of diffraction and of attenuation.*

For earlier reviews about NDWs, we refer the reader, for instance, to the first two chapters of the *Localized Waves* [1], as well as *Advances in Imaging and Electron Physics* [11], and references therein. There, the reader will find general and formal (simple) introductions to NDWs, with more details on the separate cases of beams and of pulses, as well as on the rather different characteristics of the Bessel and of NDWs, with respect to (w.r.t.) the Gaussian ones. The important properties of the former w.r.t. the latter ones can find application, as well-known and as stressed therein, in all fields in which an essential role is played by a wave–equation (e.g., electromagnetism, optics, acoustics, seismology, geophysics, and also gravitation, and elementary particle physics).

Here, let us only insert the following, quite brief historical information.

The non-diffracting solutions to the wave equations (scalar, vectorial, spinorial etc.) have been in fashion, both in theory and in experiment, for a couple of decades. Rather well known are the ones with luminal or superluminal peak-velocity [1] like the so-called X-shaped waves (see [9, 12, 13] and references therein), which are supersonic in acoustics [10], and superluminal in electromagnetism (see [14]; see also [15] and [16]).

It has already been recognized by Bateman [17] and later on Courant and Hilbert [18], that *luminal* NDWs exist, which are solutions to the wave equations. After subsequent early works, already quoted by us, a great deal of results [19] have been published on NDWs, from both the theoretical and the experimental point of view: initially, taking only free space into account, and, later on, considering more complex media, which exibit effects such as dispersion (see, e.g. [20–22]), nonlinearity [23], anisotropy [24–26], losses [5], and so on. Extensions of this type have been carried out along with the development, for instance, of efficient methods

for obtaining non-diffracting beams and pulses in the subluminal, luminal, and superluminal regimes, thus allowing easier experimental verifications.

Indeed, in recent years, some attention [19, 27–33] started to be paid to the (more ''orthodox'') *subluminal* NDWs, too. It should be stressed that, in any case, the interest in NDWs resides not in their peak-velocity [34–36] but in that they propagate in a homogeneous linear medium without distortion – and in a self-reconstructing way [5, 37, 38] (apart from local variations, in the sense that their square magnitude keeps its shape during propagation, while local variations are shown only by its real, or imaginary, part).

In the past, however, little attention was paid to Brittingham's 1983 paper [39], wherein he obtained *pulse-type* solutions to the Maxwell equations, which propagated in free space as a new kind of *c*-speed ''solitons.'' That lack of attention was partially due to the fact that Brittingham had neither been able to get finite-energy expressions for his ''wavelets'' nor to make suggestions about their practical production. Two years later, however, Sezginer [40] was able to obtain quasi-non-diffracting luminal pulses endowed with a finite energy: Finite-energy pulses are known not to travel undistorted for an infinite distance, but nevertheless propagate without deformation for a long field-depth, much larger than the one achieved by ordinary pulses like the Gaussian ones (see, e.g., [41–52] and references therein).

An interesting problem, indeed, was that of investigating what would happen to the ideal *Bessel beam solution when truncated* by a finite transverse aperture. In 1987 a heuristical answer was found after the quoted series of pioneering papers [41–44] from the experiments by Durnin *et al.* [45, 46], when it was shown that a realistic Bessel beam, passing through a finite aperture, is able to travel keeping its transverse intensity shape approximately unchanged all along a *large* ''depth of field.''

In any case, only after 1985 a general theory of NDWs started to be extensively developed [9, 12, 14, 53–65], both in the case of beams and in the case of pulses. For reviews, see, for instance [1, 11, 13, 48, 50–52, 61] and references within. For the propagation of NDWs in bounded regions (like *wave-guides*), see [66–68] and references therein. For the focusing of NDWs, see, for example [1, 69, 70], and references therein. For recourse to chirped optical X-type waves to obtain pulses capable of recovering their spatial shape both transversally and longitudinally, see, for example, [1, 71] and references therein. Not less important, for the construction of general NDWs propagating in *dispersive* media, see, besides the quoted [20–22], also [72–74]; while, for *lossy* media, see, for example [1, 5, 69, 70] and references therein, and this chapter. Finally, for finite-energy, or truncated, solutions see, for example, [57, 75–79] as well as this chapter.

NDWs have now been produced experimentally [10, 80–83], and are being applied in fields ranging from ultrasound scanning [30, 33, 77, 84] to optics (for the production, e.g., of new type of tweezers [5, 8, 85–87]). All those works have demonstrated that non-diffracting pulses can travel with any arbitrary peak-velocities v, that is with speed v in the range $0 < v < \infty$.

Let us introduce at this point a first mathematical definition of NDWs.

Diffraction, as a spatial transverse spreading, cannot occur in the simple case of one space dimension (1D). Actually, the 1D wave equation

$$(\partial_z^2 - 1/c^2\partial_t^2)\psi(z,t) = 0 \tag{1.1}$$

admits the general solution $\psi = f(z - ct) + g(z + ct)$, quantities f and g being arbitrary (differentiable) functions; and, for instance, a solution of the type $\psi(z - ct)$ travels rigidly along the positive z-direction with speed c. Let us here recall, and stress, that if a wave depends on t and z only through the quantity $z - Vt$, it will be seen as moving without any distortion with the speed V: see, for example [13], and references therein.

Moving on to the 3D case, when the wave equation reads

$$(\nabla_\perp^2 + \partial_z^2 - 1/c^2\partial_t^2)\psi(\mathbf{r}_\perp, z, t) = 0 \tag{1.2}$$

quantity $\nabla_\perp^2$ being the transverse Laplacian, and $\mathbf{r}_\perp$ the transverse position vector (so that $\mathbf{r} = \mathbf{r}_\perp + z\mathbf{k}$), it is natural to look for possible solutions of the type

$$\psi(\mathbf{r}_\perp, z - Vt) \tag{1.3}$$

which would correspond to waves rigidly propagating along z with speed V, whatever the value of V is (see [1, 13]). To check the mentioned possibility, let us go back to Equation 1.2. It is simple to show, then, that an acceptable solution of the type 3 has just to satisfy the equation

$$(\nabla_\perp^2 + (1 - V^2/c^2)\partial_\zeta^2)\psi(\mathbf{r}_\perp, \zeta) = 0 \tag{1.4}$$

where $\zeta \equiv z - Vt$. (Let us explicitly repeat and recall [50] that the shape of any solutions that depend on z and on t only through the quantity $z - Vt$ will always appear the same to an observer traveling along z with the speed V, whatever be (subluminal, luminal, or superluminal) the value of V; that is, such a solution will propagate rigidly with speed V.]

One can therefore realize the following:

1) When $V = c$, Equation 1.4 becomes elliptic; namely, it becomes a Laplace equation in the transverse variables, which prevents the free-space solution from being localizable transversally. In other words, these solutions are plane waves, or plane wave pulses, with scarce practical interest.
2) When $V < c$, Equation 1.4 is still elliptic; more specifically, it is a Laplace equation in the variables $(x, y, \zeta\sqrt{1 - V^2/c^2})$, so that the free-space solutions cannot admit any local maxima or minima. No solutions of physical interest are obtainable.
3) When $V > c$, however, Equation 1.4 is hyperbolic, and it becomes possible to obtain non-diffracting solutions of the type $\psi(\mathbf{r}_\perp, z - Vt)$, both for beams and for pulses.

The latter simple and interesting result shows that, when basing ourselves on Equation 1.4, the solutions that can propagate rigidly (i.e., without any spatial modifications) are those corresponding to $V > c$. In the case of beams, V is

merely the phase velocity; but, in the case of pulses it is the peak velocity (sometimes identified with the group-velocity). Incidentally, it is known that, when one superposes waves whose phase-velocity does not depend on their frequency, such a phase-velocity becomes[2] the actual peak-velocity [50, 67, 88].

Many interesting solutions of this kind exist [1, 9, 10, 14, 57], and some of them will be mentioned in this chapter, and in this very book. From a historical point of view, let us repeat that such solutions to the wave equations (and, in particular, to the Maxwell equations, under weak hypotheses) were predicted theoretically a long time ago [17, 18, 89, 90], mathematically constructed in more recent times [9, 14, 91], and, soon after, produced experimentally [10, 80–83].

However, *it is rather restrictive to define a NDW as a solution of the type* 3, *with V > c*. Actually, *subluminal* NDW solutions to the wave equations also exist [19], and they, too, are rather interesting, as we shall discuss below.

1.1.3
Definition of Non-Diffracting Wave (NDW)

Therefore, it is convenient to formulate a *more comprehensive* definition, wherefrom to derive a much ampler set of solutions (superluminal, luminal, or subluminal) capable of withstanding diffraction, both for infinite distances, in the ideal case (of infinite energy), and for large, but finite distances, in the realistic case (of finite energy).

Let us start by formulating an adequate definition of an *ideal* NDW.

Let us consider a linear and homogeneous wave equation in free space. In cylindrical coordinates (ρ, ϕ, z) and using a Fourier–Bessel expansion, its general solution $\psi(\rho, \phi, z, t)$ can be expressed, when disregarding evanescent waves, as

$$\Psi(\rho, \phi, z, t) = \sum_{n=-\infty}^{\infty} \left[\int_0^\infty dk_\rho \int_{-\infty}^\infty dk_z \int_{-\infty}^\infty d\omega \ k_\rho A_n'(k_\rho, k_z, \omega) J_n(k_\rho \rho) e^{ik_z z} e^{-i\omega t} e^{in\phi} \right]$$

(1.5)

with

$$A_n'(k_\rho, k_z, \omega) = A_n(k_z, \omega) \ \delta \left[k_\rho^2 - \left(\frac{\omega^2}{c^2} - k_z^2 \right) \right]$$

(1.6)

the $A_n(k_z, \omega)$ being arbitrary functions, and $\delta(\cdot)$ the Dirac delta function. It is important to emphasize that the $J_n(k_\rho \rho)$ are *n*-order *Bessel functions*. For simplicity, many authors often confine themselves to the zero-order Bessel functions $J_0(\cdot)$.

An ideal NDW is a wave that must be capable of maintaining indefinitely its spatial form (except for local variations) while propagating. This property may be mathematically expressed, when assuming propagation in the *z*-direction, as follows:

$$\Psi(\rho, \phi, z, t) = \Psi \left(\rho, \phi, z + \Delta z_0, t + \frac{\Delta z_0}{V} \right)$$

(1.7)

---

2) Let us here recall that the group velocity can be written as $v_g = \nabla_k \omega = \partial\omega/\partial k_z \ \mathbf{z}$ only when k_x and k_y remain (almost) constant in the considered superposition, as it happens, for example, in the case of metallic guides.

where Δz_0 is a chosen length, and V is the pulse-peak velocity, with $0 \leq V \leq \infty$. Then, by using Equation 1.5 into Equation 1.7, and taking account of Equation 1.6, one can show [1, 12, 63] that any non-diffracting solution can be written as

$$\Psi(\rho, \phi, z, t) = \sum_{n=-\infty}^{\infty} \sum_{m=-\infty}^{\infty} \left[\int_{-\infty}^{\infty} d\omega \int_{-\omega/c}^{\omega/c} dk_z A_{nm}(k_z, \omega) \right.$$
$$\left. \times J_n \left(\rho \sqrt{\frac{\omega^2}{c^2} - k_z^2} \right) e^{ik_z z} e^{-i\omega t} e^{in\phi} \right] \tag{1.8}$$

with

$$A_{nm}(k_z, \omega) = S_{nm}(\omega)\delta(\omega - (Vk_z + b_m)) \tag{1.9}$$

where $b_m = 2m\pi V/\Delta z_0$ (with m an integer number too, of course), while quantity $S_{nm}(\omega)$ is an arbitrary *frequency spectrum*. Notice that, owing to Equation 1.9, each term in the double sum (1.8), namely in its expression within square brackets, is a truly NDW (beam or pulse); and their sum (1.8) is just the most general form representing *an ideal NDW* according to definition 1.7.

One should also notice that (1.8) *is nothing but a superposition of Bessel beams* with a specific "space–time coupling," characterized by *linear relationships* between their angular frequency ω and their longitudinal wave number k_z.

Concerning such a superposition, the Bessel beams with $\omega/k_z > 0$ ($\omega/k_z < 0$) propagate in the positive (negative) z-direction. As we wish to obtain NDWs propagating in the positive z-direction, the presence of "backward" Bessel beams is not desirable, that is, of "backward components" – often called *non-causal*, as they should be *entering* the antenna or generator. The problems with the backward-moving components, that so frequently plague the localized waves, can be overcome, however, by appropriate choices of the spectrum (1.9), which can totally eliminate those components, or minimize their contribution, in superposition (1.8). Let us notice that often only positive values of ω are considered ($0 \leq \omega \leq \infty$).

Another important point refers to the energy [12, 40, 52, 92] of the NDWs. It is well known that any ideal NDW, that is, any field with the spectrum (1.9), possesses infinite energy. However, finite-energy NDWs can be constructed by concentrating the spectrum $A_{nm}(k_z, \omega)$ in the surrounding of a straight line of the type $\omega = Vk_z + b_m$ instead of collapsing it exactly over that line [12, 63]. In such a case, the NDWs get a finite energy, but, as we know, are endowed with *finite field depths*, that is, they maintain their spatial forms for long (but not infinite) distances.

Despite the fact that expression 1.8, with $A_{nm}(k_z, \omega)$ given by Equation 1.9, does represent ideal NDWs, it is difficult to use it for obtaining analytical solutions, especially when there is the task of eliminating the backward components. This difficulty becomes even worse in the case of finite-energy NDWs. We shall come back to this point in section 1.2.

1.1.4
First Examples

Before going on, let us be more concrete. First of all, let us notice that Equation 1.5, for $n = 0$ and on integrating over k_z, reduces to the less general – but still quite useful – solution

$$\psi(\rho, z, t) = \int_{-\infty}^{\infty} \int_{0}^{\omega/ck_\rho} J_0(k_\rho\,\rho)\ e^{i\sqrt{\omega^2/c^2-k_\rho^2}\,z}\ e^{-i\omega t}\ S(k_\rho, \omega)\ \mathrm{d}k_\rho\ \mathrm{d}\omega \quad (1.10)$$

where $S(k_\rho, \omega)$ is now the chosen spectral function, with only $k_z > 0$ (and we still disregard evenescent waves). We are using the standard relation

$$\frac{\omega^2}{c^2} = k_\rho^2 + k_z^2 \tag{1.11}$$

From the integral solution (1.10) one can get in particular, for instance, the (*non-localized*) Gaussian beams and pulses, to which we shall refer for illustrating the differences of the NDWs w.r.t. them.

The Gaussian beam is a very common (non-localized) beam [93], corresponding to the spectrum

$$S(k_\rho, \omega) = 2a^2\ e^{-a^2 k_\rho^2}\ \delta(\omega - \omega_0) \tag{1.12}$$

In Equation 1.12, a is a positive constant, which will be shown to depend on the transverse aperture of the initial pulse.

The integral solution (1.10), with spectral function (1.12), can be regarded as a *superposition* of plane waves: namely, *of plane waves propagating in all directions (always with $k_z \geq 0$), the most intense ones being those directed along (positive) z* (especially when $\Delta k_\rho \equiv 1/a \ll \omega_0/c$). This is depicted clearly in Figure 1.4 of [1].

On substituting Equation 1.12 into Equation 1.10 and adopting the paraxial approximation (which is known to be just valid if $\Delta k_\rho \equiv 1/a \ll \omega_0/c$), one meets the Gaussian beam

$$\psi_{\mathrm{gauss}}(\rho, z, t) = \frac{a^2\ \exp\left(\frac{-\rho^2}{4(a^2+i\ z/2k_0)}\right)}{(a^2 + i\ z/2k_0)}\ e^{ik_0(z-ct)} \tag{1.13}$$

where $k_0 = \omega_0/c$. We can verify that the magniture $|\psi|$ of such a beam, which suffers transverse diffraction, doubles its initial width $\Delta\rho_0 = 2a$ after having traveled the distance $z_{\mathrm{dif}} = \sqrt{3}\,k_0\Delta\rho_0^2/2$, called the diffraction length. The more concentrated a Gaussian beam happens to be, the more rapidly it gets spoiled.

The most common (non-localized) *pulse* is the Gaussian pulse, which is obtained from Equation 1.10 by using the spectrum [71]

$$S(k_\rho, \omega) = \frac{2ba^2}{\sqrt{\pi}}e^{-a^2 k_\rho^2}e^{-b^2(\omega-\omega_0)^2} \tag{1.14}$$

where a and b are positive constants. Indeed, such a pulse is a superposition of Gaussian beams of different frequency.

Now, on substituting Equation 1.14 into Equation 1.10, and adopting once more the paraxial approximation, one gets the Gaussian pulse:

$$\psi(\rho, z, t) = \frac{a^2 \, \exp \, \left(\frac{-\rho^2}{4(a^2 + iz/2k_0)} \right) \exp \, \left(\frac{-(z-ct)^2}{4c^2 b^2} \right)}{a^2 + iz/2k_0} \tag{1.15}$$

endowed with speed c and temporal width $\Delta t = 2b$, and suffering a progressing enlargement of its transverse width, so that its initial value gets doubled already at position $z_{\text{dif}} = \sqrt{3} \, k_0 \Delta \rho_0^2 / 2$, with $\Delta \rho_0 = 2a$. Let us remember that the paraxial approximation is really valid in the pulse case only if there hold the two conditions $\Delta k_\rho \equiv 1/a \ll \omega_0/c$ and $\Delta \omega = 1/b \ll \omega_0$, imposing a slow variation of the envelope.

1.1.5
Further Examples: The Non-Diffracting Solutions

Let us finally go on to the construction of the two most renowned localized waves [48]: the Bessel beam and the ordinary X-shaped pulse. First of all, let us recall that, when superposing (axially symmetric) solutions of the wave equation in the vacuum, three spectral parameters, (ω, k_ρ, k_z), come into the play, which have, however, to satisfy the constraint (1.11), deriving from the wave equation itself. Consequently, only two of them are independent, and we here choose ω and k_ρ. Such a possibility of choosing ω and k_ρ was already apparent in the spectral functions generating Gaussian beams and pulses, which consisted of the product of two functions, one depending only on ω and the other on k_ρ.

We are going to see that further particular relations between ω and k_ρ (or, analogously, between ω and k_z) can be enforced in order to get interesting and unexpected results, such as the NDWs.

Let us start by imposing a *linear* coupling between ω and k_ρ (it could, actually be shown [46] that it is the unique coupling leading to NDW solutions).

Namely, let us consider the spectral function

$$S(k_\rho, \omega) = \frac{\delta \left(k_\rho - \frac{\omega}{c} \sin \theta \right)}{k_\rho} \, \delta(\omega - \omega_0) \tag{1.16}$$

which implies that $k_\rho = (\omega \sin \theta)/c$, with $0 \leq \theta \leq \pi/2$: a relation that can be regarded as a space–time coupling. Let us add that this linear constraint between ω and k_ρ, together with relation 1.11, yields $k_z = (\omega \cos \theta)/c$. This is an important fact, as an *ideal* NDW *must* contain [12, 48] a coupling of the type $\omega = Vk_z + b$, where V and b are arbitrary constants. The integral function 1.10, this time with spectrum (1.16), can be interpreted as a superposition of plane waves; however, this time the axially-symmetric Bessel beam appears as the result of the *superposition of plane waves whose wave vectors lay on the surface of a cone having the propagation line as its symmetry axis and an opening angle equal to* θ; such θ being called the *axicon angle*. This is shown clearly in Figure 1.5 of [1].

By inserting Equation 1.16 into Equation 1.10, one gets the mathematical expression of the so-called Bessel beam:

$$\psi(\rho, z, t) = J_0\left(\frac{\omega_0}{c}\sin\theta \; \rho\right) \; \exp\left[i \frac{\omega_0}{c}\cos\theta \; \left(z - \frac{c}{\cos\theta}t\right)\right] \tag{1.17}$$

This beam possesses phase-velocity $v_{ph} = c/\cos\theta$, and field transverse shape represented by a Bessel function $J_0(\cdot)$ so that its field is concentrated in the surroundings of the propagation axis z. Moreover, Equation 1.17 tells us that the Bessel beam keeps its transverse shape (which is therefore invariant) while propagating, with central "spot" $\Delta\rho = 2.405c/(\omega\sin\theta)$.

The ideal Bessel beam, however, is not square-integrable in the transverse direction, and is therefore associated with an infinite power flux, that is, it cannot be produced experimentally. One must have recourse to truncated Bessel (TB) beams, generated by finite apertures: In this case the (truncated) Bessel beams are still able to travel a long distance while maintaining their transfer shape, as well as their speed, approximately unchanged [45, 46, 94, 95]. For instance, the field-depth of a Bessel beam generated by a circular finite aperture with radius R is given (if $R \gg \Delta\rho_0 = 2.4/k_\rho$) by

$$Z_{max} = \frac{R}{\tan\theta} \tag{1.18}$$

where θ is the beam axicon angle. In the finite aperture case, the Bessel beam can no longer be represented by Equation 1.17, and one must calculate it by the scalar diffraction theory by using, for example, Kirchhoff's or Rayleigh–Sommerfeld's diffraction integrals. But until the distance Z_{max} one may still use Equation 1.17 for approximately describing the beam, at least in the vicinity of the axis $\rho = 0$, that is, for $\rho \ll R$. To realize how much a TB beam succeeds in resisting diffraction, one can also consider a Gaussian beam, with the same frequency and central "spot," and *compare* their field-depths. In particular, let both the beams have $\lambda = 0.63$ μm and initial central "spot" size $\Delta\rho_0 = 60$ μm. The Bessel beam will possess axicon angle $\theta = \arcsin[2.405c/(\omega\Delta\rho_0)] = 0.004$ rad. In the case, for example, of a circular aperture with radius 3.5 mm, it is then easy to verify that the Gaussian beam doubles its initial transverse width already after 3 cm, while after 6 cm its intensity has become an order of magnitude smaller. By contrast, the TB beam keeps its transverse shape until the distance $Z_{max} = R/\tan\theta = 85$ cm. Afterward, the Bessel beam decays rapidly as a consequence of the sharp cut performed on its aperture (such a cut also being responsible for some intensity oscillations suffered by the beam along its propagation axis), and for the fact that the feeding waves, coming from the aperture, at a certain point eventually get faint. All this is depicted clearly in Figure 1.6 of [1].

It may be useful to repeat that a Bessel beam is characterized by an "extended focus" along its propagation axis, so that its energy cannot be concentrated inside a small region in the transverse plane: It needs, indeed, to be reconstructed continuously by the energy associated with the "lateral rings" (evolving along closing conical surfaces), which constitute its transverse structure. This is quite different from the case of a Gaussian beam, which possesses a point-like focus,

that is, is constructed so as to concentrate its energy within a spot that becomes very small at a certain point of its propagation axis, and afterward diffracts rapidly.

The zeroth-order (axially symmetric) Bessel beam is nothing but one example of localized beam. Further examples are the higher order (not cylindrically symmetric) Bessel beams, described by Equation 1.13 of [1], or the Mathieu beams [49], and so on.

Following the same procedure adopted in the previous subsection, let us construct ordinary X-shaped pulses by using spectral functions of the type

$$S(k_\rho, \omega) = \frac{\delta \left(k_\rho - \frac{\omega}{c} \sin\theta \right)}{k_\rho} \, F(\omega) \tag{1.19}$$

where this time the Dirac delta function furnishes the spectral space–time coupling $k_\rho = (\omega \sin\theta)/c$. Function $F(\omega)$ is, of course, the frequency spectrum; it is left for the moment undetermined. On using Equation 1.19 in Equation 1.10, one obtains

$$\psi(\rho, z, t) = \int_{-\infty}^{\infty} F(\omega) \, J_0 \left(\frac{\omega}{c} \sin\theta \, \rho \right) \, \exp \, \left(\frac{\omega}{c} \cos\theta \, \left(z - \frac{c}{\cos\theta} t \right) \right) \, d\omega \tag{1.20}$$

It is easy to see that ψ will be a pulse of the type

$$\psi = \psi(\rho, z - Vt) \tag{1.21}$$

with a speed $V = c/\cos\theta$ independent of the frequency spectrum $F(\omega)$.

Such solutions are known as X-shaped pulses, and are *non-diffracting* waves in the sense that they obviously maintain their spatial shape during propagation (see e.g., [9, 12, 14] and references therein, as well as the following). Their peak velocity is well-known to be superluminal (see also [34, 35, 96] and references therein). Some relevant, useful comments have been added, for instance, at pages 12–13 of [1].

Now, let us for instance consider in Equation 1.20 the particular frequency spectrum $F(\omega)$ given by

$$F(\omega) = H(\omega) \, \frac{a}{V} \, \exp \, \left(-\frac{a}{V} \, \omega \right) \tag{1.22}$$

where $H(\omega)$ is the Heaviside step-function and a a positive constant. Then, Equation 1.20 yields

$$\psi(\rho, \zeta) \; \equiv \; X = \frac{a}{\sqrt{(a - i\zeta)^2 + \left(\frac{V^2}{c^2} - 1 \right) \rho^2}} \tag{1.23}$$

still with $\zeta \equiv z - Vt$. This solution 1.23 is the well-known ordinary, or "classic," X-wave, which constitutes a simple example of a superluminal (supersonic, in the case of a Acoustics) X-shaped pulse [9, 14]. Notice that function 1.22 contains mainly low frequencies, so that the classic X-wave is suitable for low frequencies only.

Actually, Lu *et al.* first introduced them for acoustics [9, 10]. Soon after having mathematically and experimentally constructed their "classic" (acoustic) X-wave,

they started applying them to ultrasonic scanning, directly obtaining very high quality 3D images. Subsequently, in 1996, there were mathematically constructed (see, e.g., [14] and references therein) the analogous X-shaped solutions to the Maxwell equations, by working out scalar superluminal non-diffracting solutions for each component of the Hertz potential. In reality, Ziolkowski *et al.* [57] had already found in electromagnetism similar solutions for the simple scalar case, called by them *slingshot* pulses; but their pioneering solutions had gone almost unnoticed at that time (1993). In 1997, Saari and Reivelt [80] announced the first production of an X-shaped wave in the optical realm, thus proving experimentally the existence of superluminal non-diffracting electromagnetic pulses. Let us add that X-shaped waves have also been produced easily in nonlinear media [23].

Figure 1.1 depicts (the real part of) an ordinary X-wave with $V = 1.1c$ and $a = 3$ m.

Solutions (1.20) and, in particular, the pulse (1.23) have got an infinite field depth, and an infinite energy as well. Therefore, as was mentioned in the Bessel beam case, one should pass to truncated pulses, originating from a finite aperture. Afterward, our truncated pulses will keep their spatial shape (and their speed) along the depth of field

$$Z = \frac{R}{\tan \theta} \tag{1.24}$$
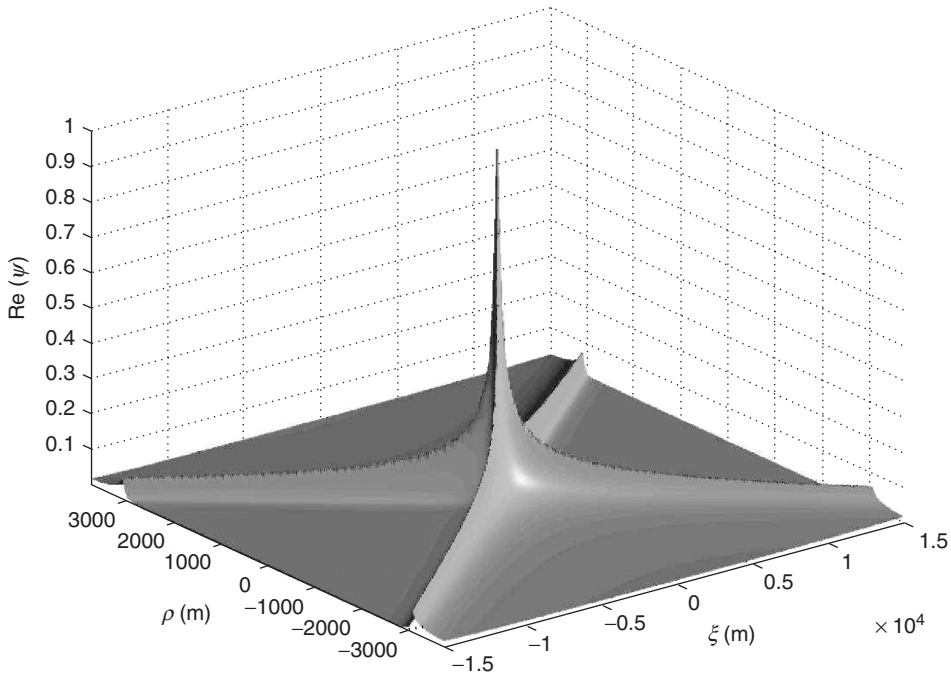
Figure 1.1 Plot of the real part of the ordinary X-wave, evaluated for $V = 1.1c$ with $a = 3$ m.
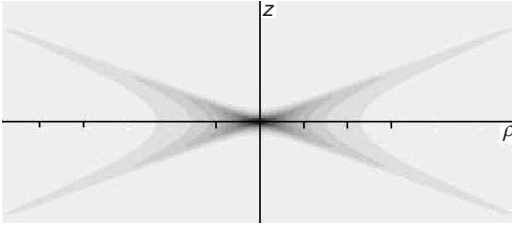
Figure 1.2 All the X-waves (truncated or not) must have a leading cone in addition to the rear cone, such a leading cone having a role even for the peak stability [9]. Long ago, this was also predicted, in a sense, by (non-restricted [1, 13, 14]) special relativity: one should not forget, in fact, that *all* wave equations, and not only Maxwell's, have an intrinsic relativistic structure. By contrast, the fact that X-waves have a conical shape induced some authors to look for (untenable) links – let us now confine ourselves to electromagnetism – between them and the Cherenkov radiation, so as to to deny the existence of the leading cone: But X-shaped waves have nothing to do with Cherenkov, as it has been demonstrated thoroughly in Refs [34, 35, 96]. In practice, when wishing to produce concretely a finite conic NDW, truncated both in space and in time, one is supposed to have recourse *in the simplest case* to a dynamic antenna emitting a radiation cylindrically symmetric in space and symmetric in time [1].

where, as before, R is the aperture radius and θ the axicon angle (and R is assumed to be much larger than the X-pulse spot).

At this point, it is worthwhile presenting Figure 1.2 and its caption.

For further X-type solutions, with less and less energy distributed along their "arms," let us refer the reader to [12, 63] and references therein, as well as to [1]. For example, it was therein addressed the explicit construction of infinite families of generalizations of the classic X-shaped wave, with energy more and more concentrated around their vertex (see, e.g., Figure 1.9 in [1]). Elsewhere, techniques have been found for building up new series of non-diffracting superluminal solutions to the Maxwell equations suitable for arbitrary frequencies and bandwidths, and so on.

1.2
Eliminating Any Backward Components: Totally Forward NDW Pulses

As we mentioned, Equation 1.8, with its $A_{nm}(k_z, \omega)$ given by Equation 1.9, even if representing ideal solutions, is difficult to be used for obtaining analytical solutions with elimination of the "non-causal" components; a difficulty which becomes worse in the case of finite-energy NDWs. As promised, let us come back to these problems putting forth a method [63] for getting exact NDW solutions *totally free of backward components*.

Let us start with Equation 1.5 and Equation 1.6, which describe a general free-space solution (without evanescent waves) of the homogeneous wave equation, and consider in Equation 1.6 a spectrum $A_n(k_z, \omega)$ of the type

$$A_n(k_z, \omega) = \delta_{n\,0} H(\omega) H(k_z) A(k_z, \omega) \tag{1.25}$$

where $\delta_{n\,0}$ is the Kronecker delta function, $H(\cdot)$ the Heaviside function, and $\delta(\cdot)$ the Dirac delta function – quantity $A(k_z, \omega)$ being an arbitrary function. Spectra of the type (1.25) restrict the solutions for the axially symmetric case, with only positive values to the angular frequencies and longitudinal wave numbers. With this, the solutions proposed by us get the integral form

$$\psi(\rho, z, t) = \int_0^\infty d\omega \int_0^{\omega/c} dk_z\, A(k_z, \omega)\, J_0(\rho\sqrt{\omega^2/c^2 - k_z^2})e^{ik_z}e^{-i\omega t} \qquad (1.26)$$

that is, they result to be general superpositions of zero-order Bessel beams propagating in the positive z-direction only. Therefore, any solution obtained from Equation 1.26, be it non-diffracting or not, are *completely free* from backward components.

At this point, we can introduce the *unidirectional* decomposition

$$\begin{cases} \zeta = z - Vt \\[2mm] \eta = z - ct \end{cases} \qquad (1.27)$$

with $V > c$.

A decomposition of this type has been used until now in the context of paraxial approximation only [97, 98]; however, we are going to show that it can be much more effective, giving important results, in the context of exact solutions, and in situations that cannot be analyzed in the paraxial approach.

With Equation 1.27, we can write the integral solution 1.26 as

$$\psi(\rho, \zeta, \eta) = (V - c)\int_0^\infty d\sigma \int_{-\infty}^\sigma d\alpha\, A(\alpha, \sigma)J_0\left(\rho\sqrt{\gamma^{-2}\sigma^2 - 2(\beta - 1)\sigma\alpha}\right)e^{-i\alpha\eta}e^{i\sigma\zeta}$$

$$(1.28)$$

where $\gamma = (\beta^2 - 1)^{-1/2}$, $\beta = V/c$, and where

$$\begin{cases} \alpha = \frac{1}{V-c}\,(\omega - Vk_z) \\[2mm] \sigma = \frac{1}{V-c}\,(\omega - ck_z) \end{cases} \qquad (1.29)$$

are the new spectral parameters.

It should be stressed that superposition (1.28) is not restricted to NDWs: It is the choice of the spectrum $A(\alpha, \sigma)$ that will determine the resulting NDWs.

1.2.1
Totally Forward Ideal Superluminal NDW Pulses

The most trivial NDW solutions are the X-type waves. We have seen that they are constructed by frequency superpositions of Bessel beams with the same phase velocity $V > c$ and *until now* constituted the only known ideal NDW pulses free of backward components. It is not necessary, therefore, to use the present method to obtain such X-type waves, as they can be obtained by using directly the integral

representation in the parameters (k_z, ω), that is, by using Equation 1.26. Even so, let us use our new approach to construct the ordinary X-wave.

Consider the spectral function $A(\alpha, \sigma)$ given by

$$A(\alpha, \sigma) = \frac{1}{V - c} \delta(\alpha) e^{-s\sigma} \tag{1.30}$$

One can notice that the delta function in Equation 1.30 implies that $\alpha = 0 \rightarrow \omega = Vk_z$, which is just the spectral characteristic of the X-type waves. In this way, the exponential function $\exp(-s\sigma)$ represents a frequency spectrum starting at $\omega = 0$, with an exponential decay and frequency bandwidth $\Delta\omega = V/s$.

Using Equation 1.30 in Equation 1.28, we get

$$\psi(\rho, \zeta) = \frac{1}{\sqrt{(s - i\zeta)^2 + \gamma^{-2}\rho^2}} \equiv X \tag{1.31}$$

which is the well-known ordinary X wave.

Focus wave modes (FWMs) [12, 52, 54] are ideal non-diffracting pulses possessing spectra with a constraint of the type $\omega = Vk_z + b$ (with $b \neq 0$), which links the angular frequency with the longitudinal wave number, and are known for their strong field concentrations.

Until now, however, all the known FWM solutions possessed backward spectral components, a fact that, as we know, forces one to consider large-frequency bandwidths to minimize their contribution. However, we are going to obtain solutions of this type free of backward components and able to possess also very narrow frequency bandwidths.

Let us choose a spectral function $A(\alpha, \sigma)$ like

$$A(\alpha, \sigma) = \frac{1}{V - c} \delta(\alpha + \alpha_0) e^{-s\sigma} \tag{1.32}$$

with $\alpha_0 > 0$ a constant. This choice confines the spectral parameters ω, k_z of the Bessel beams to the straight line $\omega = Vk_z - (V - c)\alpha_0$, as it is shown in Figure 1.3.

Substituting Equation 1.32 in Equation 1.28, we have

$$\psi(\rho, \zeta, \eta) = \int_0^\infty d\sigma \int_{-\infty}^\sigma d\alpha \, \delta(\alpha + \alpha_0) e^{-s\sigma} J_0\left(\rho\sqrt{\gamma^{-2}\sigma^2 - 2(\beta - 1)\sigma\alpha}\right) e^{-i\alpha\eta} e^{i\sigma\zeta} \tag{1.33}$$
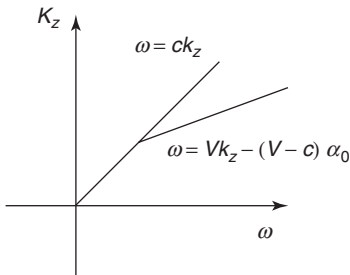
Figure 1.3 The Dirac delta function in Equation 1.32 confines the spectral parameters ω, k_z of the Bessel beams to the straight line $\omega = Vk_z - (V - c)\alpha_0$, with $\alpha_0 > 0$.

which, on using identity 6.616 in [99], results in

$$\psi(\rho, \zeta, \eta) = X \, e^{i\alpha_0 \eta} \, \exp \left[\frac{\alpha_0}{\beta + 1} \left(s - i\zeta - X^{-1} \right) \right] \tag{1.34}$$

where X is the ordinary X-wave given by Equation 1.31.

Equation 1.34 represents an ideal superluminal NDW of the type FWM, but free from backward components.

As we already said, the Bessel beams constituting this solution have their spectral parameters linked by the relation $\omega = V k_z - (V - c)\alpha_0$; thus, by using Equation 1.32 and Equation 1.29, it is easy to see that the frequency spectrum of those Bessel beams starts at $\omega_{min} = c\alpha_0$ with an exponential decay $\exp(-s\omega/V)$, and so possesses the bandwidth $\Delta\omega = V/s$. It is clear that ω_{min} and $\Delta\omega$ can assume any values, so that the resulting FWM, Equation 1.34, can range from a quasi-monochromatic to an ultrashort pulse. This is a great advantage w.r.t. the old FWM solutions.

As an example, we plot in Figure 1.4 one case related with the NDW pulse given by Equation 1.34.

In Figure 1.4 we have a quasi-monochromatic optical FWM pulse, with $V = 1.5c$, $\alpha_0 = 1.256 \times 10^7$ m^{-1}, and $s = 1.194 \times 10^{-4}$ m, which correspond to $\omega_{min} = 3.77 \times 10^{15}$ Hz and $\Delta\omega = 3.77 \times 10^{12}$ Hz, that is to a picosecond pulse with $\lambda_0 = 0.5$ μm. Figure 1.4a shows the intensity of the complex NDW field, while Figure 1.4b shows the intensity of its real part. Moreover, in Figure 1.4b, in the right upper corner, is shown a zoom of this NDW, on the z-axis and around the pulse's peak, where the carrier wave of this quasi-monochromatic pulse shows up.

Now, we apply our method to obtain totally forward *finite-energy* NDW pulses.
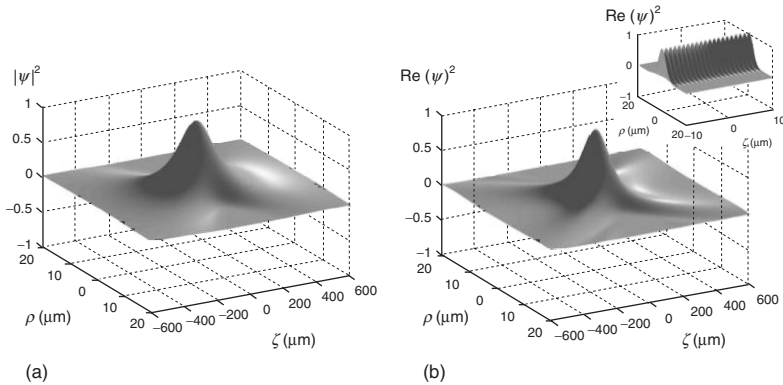
Figure 1.4 The intensity of the (a) complex and (b) real part of a quasi-monochromatic, totally "forward," superluminal optical focus wave mode pulse, with $V = 1.5c$, $\alpha_0 = 1.256 \times 10^7$ m^{-1} and $s = 1.194 \times 10^{-4}$ m, which correspond to $\omega_{min} = 3.77 \times 10^{15}$ Hz, and $\Delta\omega = 3.77 \times 10^{12}$ Hz, that is to a picosecond pulse with $\lambda_0 = 0.5$ μm.

1.3
Totally Forward, *Finite-Energy* NDW Pulses

Finite-energy NDW pulses are *almost* non-diffracting in the sense that they can retain their spatial forms, resisting to the diffraction effects, for long (but not infinite) distances.

There exist many analytical solutions representing finite-energy NDWs [12, 52, 54], but, once more, all the known solutions suffer from the presence of backward components. We can overcome this limitation.

We are missing out here the subluminal NDWs, which will be addressed in section 1.5, where also the particularly interesting case of the NDWs ''at rest'' (Frozen Waves) will be briefly considered.

Superluminal finite-energy NDW pulses, with peak velocity $V > c$, can be obtained by choosing spectral functions in Equation 1.26, which are concentrated in the vicinity of the straight line $\omega = Vk_z + b$ instead of lying on it. Similarly, in the case of luminal finite-energy NDW pulses the spectral functions in Equation 1.26 have to be concentrated in the vicinity of the straight line $\omega = ck_z + b$ (note that, in the luminal case, one must have $b \geq 0$).

Indeed, from Equation 1.29 it is easy to see that, by our approach, finite-energy superluminal NDWs can actually be obtained by concentrating the spectral function $A(\alpha, \sigma)$ entering in Equation 1.28, in the vicinity of $\alpha = -\alpha_0$, with α_0 a *positive* constant. And, analogously, the finite-energy luminal case can be obtained with a spectrum $A(\alpha, \sigma)$ concentrated in the vicinity of $\sigma = \sigma_0$, with $\sigma_0 \geq 0$.

To see this, let us consider the spectrum

$$A(\alpha, \sigma) = \frac{1}{V - c} H(-\alpha - \alpha_0) e^{a\alpha} e^{-s\sigma} \tag{1.35}$$

where $\alpha_0 > 0$, $a > 0$ and $s > 0$ are constants, and $H(\cdot)$ is the Heaviside function.

Owing to the presence of the Heaviside function, the spectrum (1.35), when written in terms of the spectral parameters ω and k_z, has its domain in the region shown in Figure 1.5.

We can see that the spectrum $A(\alpha, \sigma)$ given by Equation 1.35 is more concentrated on the line $\alpha = \alpha_0$, that is, around $\omega = Vk_z - (V - c)\alpha_0$, or on $\sigma = 0$ (i.e. around $\omega = ck_z$), depending on the values of a and s; more specifically, the resulting solution will be a superluminal finite-energy NDW pulse, with peak velocity $V > c$, if $a \gg s$, or a luminal finite-energy NDW pulse if $s \gg a$.
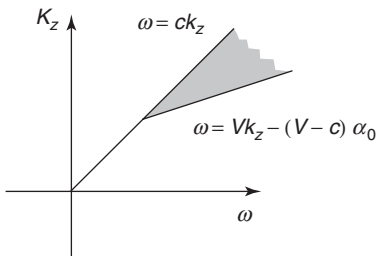
Figure 1.5 The spectrum (1.35), when written in terms of the spectral parameters ω and k_z, has its domain indicated by the shaded region.

Inserting the spectrum 1.35 into 1.28, we have

$$\psi(\rho, \zeta, \eta) = \int_0^\infty d\sigma \int_{-\infty}^{-\alpha_0} d\alpha \ e^{a\alpha} e^{-s\sigma} J_0(\rho\sqrt{\gamma^{-2}\sigma^2 - 2(\beta-1)\sigma\alpha}) e^{-i\alpha\eta} e^{i\sigma\zeta}$$

(1.36)

and, by using identity 6.616 in [99], we get an expression [63] that can be directly integrated to furnish

$$\psi(\rho, \zeta, \eta) = \frac{X \ \exp\left\{-\alpha_0\left[(a-i\eta) - \frac{1}{\beta+1}\left(s - i\zeta - X^{-1}\right)\right]\right\}}{(a-i\eta) - \frac{1}{\beta+1}(s - i\zeta - X^{-1})}$$

(1.37)

As far as we know, the new solution (1.37) is the first one to represent finite-energy NDWs completely free of backward components [63].

Totally Forward, Finite-energy Superluminal *NDW Pulses.* The finite-energy NDW (1.37) can be superluminal (peak-velocity $V > c$) or luminal (peak-velocity c) depending on the relative values of the constants a and s. To see this in a rigorous way, in connection with solution (1.37), in [63] it was calculated how its global maximum of intensity (i.e. its peak), which is located on $\rho = 0$, develops in time. The peak's motion was then obtained by considering the field intensity of (1.37) on the z-axis, that is, $|\psi(0, \zeta, \eta)|^2$, at a given time t, and finding out the value of z at which the pulse presents a global maximum. It was called $z_p(t)$ (the peak's position) this value of z; and the peak velocity was evaluated as $dz_p(t)/dt$.

As shown in [63], superluminal finite-energy NDW pulses may be obtained from (1.37) by putting $a \gg s$. In this case, the spectrum $A(\alpha, \sigma)$ is well concentrated around the line $\alpha = \alpha_0$, and therefore in the plane (k_z, ω) this spectrum starts at $\omega_{min} \approx c\alpha_0$ with an exponential decay and bandwidth $\Delta\omega \approx V/s$.

Defining the field depth Z as the distance over which the pulse's peak intensity retains at least 25% of its initial value[3], one obtains [63] the depth of field

$$Z = \frac{\sqrt{3} \ a}{1 - \beta^{-1}}$$

which depends on a and $\beta = V/c$. Thus, the pulse can get large field depths by suitably adjusting the value of parameter a.

Figure 1.6 shows the space–time evolution, from the pulse's peak at $z_p = 0$ to $z_p = Z$, of a finite-energy superluminal NDW pulse represented by Equation 1.37 with the following parameter values: $a = 20$ m, $s = 3.99 \times 10^{-6}$ m (note that $a \gg s$), $V = 1.005 \, c$, and $\alpha_0 = 1.26 \times 10^7$ m^{-1}. For such a pulse, we have a frequency spectrum starting at $\omega_{min} \approx 3.77 \times 10^{15}$ Hz (with an exponential decay) and the bandwidth $\Delta\omega \approx 7.54 \times 10^{13}$ Hz. From these values and since $\Delta\omega/\omega_{min} = 0.02$, it is an optical pulse with $\lambda_0 = 0.5$ µm and time width of 13 fs. At the distance given by the field depth $Z = \sqrt{3} \ a/(1 - \beta^{-1}) = 6.96$ km the peak intensity is a fourth of its

---

3) We can expect that, while the pulse peak intensity is maintained, the same happens for its spatial form.

Finite-energy superluminal LW pulse
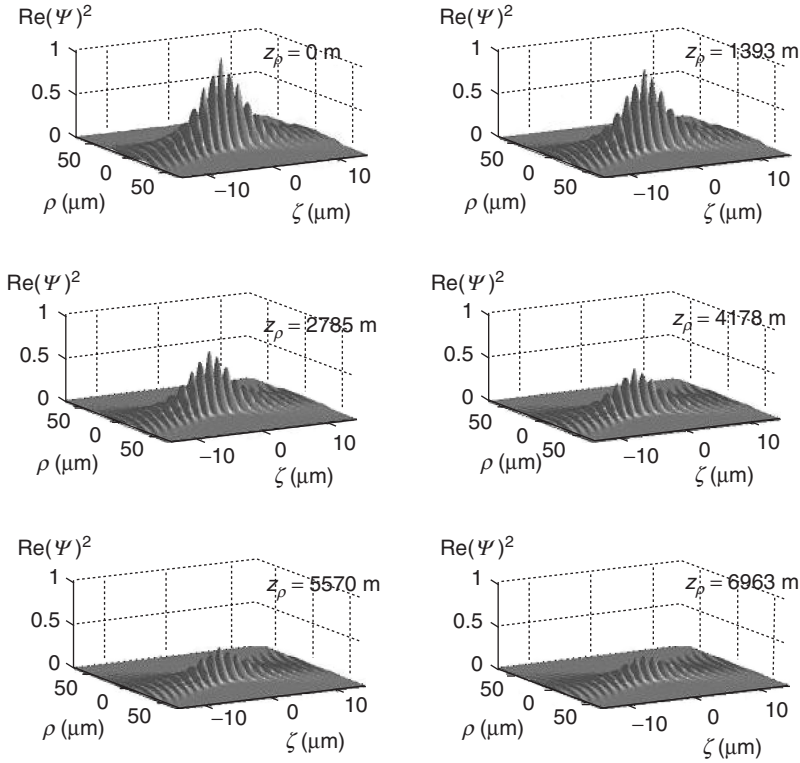
Figure 1.6 The space–time evolution, from the pulse's peak at $z_p = 0$ to $z_p = Z$, of a totally "forward," finite-energy, superluminal non-diffracting wave optical pulse represented by Equation 1.37, with the following parameter values: $a = 20$ m, $s = 3.99 \times 10^{-6}$ m (note that $a \gg s$), $V = 1.005c$ and $\alpha_0 = 1.26 \times 10^7$ m^{-1}.

initial value. Moreover, it is interesting to note that, in spite of the intensity decrease, the pulse's spot size $\Delta\rho_0 = 7.5$ μm remains constant during the propagation.

Totally "Forward", Finite-energy Luminal *NDW Pulses.* Luminal finite-energy NDW pulses can be obtained from Equation 1.37 by making $s \gg a$ (more rigorously, for $s^2 c \gg a^2 V$). In this case, the spectrum $A(\alpha, \sigma)$ is well concentrated around the line $\sigma = 0$ and therefore in the plane (k_z, ω) it starts at $\omega_{\min} \approx c\alpha_0$ with an exponential decay and the bandwidth $\Delta\omega \approx c/a$.

On defining the field depth Z as the distance over which the pulse's peak intensity remains at least 25% of its initial value, one obtains [63] the depth of field

$$Z = \frac{\sqrt{3}\, s}{\beta - 1} \tag{1.38}$$

which depends on s and $\beta = V/c$.
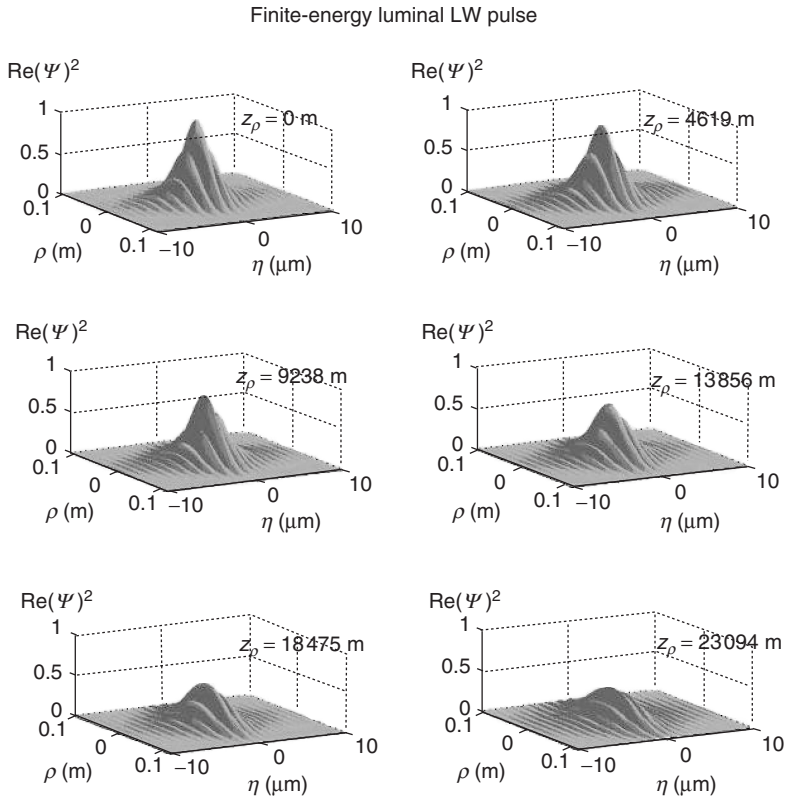
Finite-energy luminal LW pulse

Figure 1.7 The space–time evolution, from the pulse's peak at $z_p = 0$ to $z_p = Z$, of a totally "forward," finite-energy, luminal non-diffracting wave optical pulse represented by Equation 1.37, with $a = 1.59 \times 10^{-6}$ m, $s = 1 \times 10^4$ m (note that $s \gg a$), $V = 1.5c$, $\alpha_0 = 1.26 \times 10^7$ m^{-1}.

Here, we confine ourselves to depict in Figure 1.7 the space–time evolution of such a pulse, from $z_p = 0$ to $z_p = Z$. At the distance given by the field depth $Z = \sqrt{3}\, s/(\beta - 1) = 23.1$ km the peak intensity is just a fourth of its initial value.

We can see from the two examples above, and it can also be shown in a rigorous way, that the superluminal NDW pulses obtained from solution (1.37) are superior to the luminal ones obtained from the same solution, in the sense that the former can possess large field depths and, at the same time, be endowed with strong transverse field concentrations. To obtain more interesting and efficient luminal NDW pulses we should use [12, 63] spectra concentrated around the line $\sigma = \sigma_0 > 0$.

1.3.1
A General Functional Expression for Whatever Totally-Forward NDW Pulses

In the literature concerning NDWs [62] some interesting approaches appear, yielding functional expressions which describe NDWs in closed form. Although

interesting, even the NDWs obtained from those approaches possess backward components in their spectral structure.

A general functional expression, capable of furnishing whatever totally-forward NDW pulses, is, however [63]:

$$\psi(\rho, \phi, \zeta, \eta) = e^{iv\phi} \left(\frac{\gamma^{-1}\rho}{s - i\zeta + X^{-1}} \right)^v X \, F(S) \tag{1.39}$$

with $F(\cdot)$ an arbitrary function, and X the ordinary X-wave (1.31), while S is

$$S = -i\eta - \frac{1}{\beta + 1}(s - i\zeta - X^{-1})$$

Equation 1.39 is, indeed, an exact solution to the wave equation that can yield both ideal and finite-energy NDW pulses, with superluminal or luminal peak velocities. And the NDW solutions obtained from Equation 1.39 are totally free of backward components under the only condition that the chosen function $F(S)$ be regular and free of singularities at all space–time points (ρ, ϕ, z, t).

1.4
Method for the *Analytic* Description of *Truncated* Beams

If we are allowed to set forth some more formal material, we now present an *analytic* method for describing important beams, *truncated* by finite apertures, in the Fresnel regime. The method works in electromagnetism (optics, microwaves, etc.), as well as in acoustics, etc. But we shall here confine ourselves to optics, for conciseness' sake.

Our method [75], rigorous and effective, but rather simple, is based on appropriate superpositions of Bessel–Gauss beams, and in the Fresnel regime is able to describe in analytic form the 3D evolution of important waves, like Bessel beams, plane waves, Gaussian beams and Bessel–Gauss beams, when truncated by finite apertures. One of the advantages of our mathematical method is that one can obtain in a few seconds, or minutes, high-precision results that normally require quite long periods of numerical simulation. Indeed, the coefficients of the Bessel–Gauss beam superpositions are also obtainable in a direct way, without any need for numerical evaluations or optimizations.

1.4.1
The Method

We shall leave understood in all solutions the harmonic time-dependence term exp $(-i\omega t)$. In the *paraxial approximation*, an axially symmetric monochromatic wave field can be evaluated, knowing its shape on the $z = 0$ plane, through the Fresnel diffraction integral in cylindrical coordinates:

$$\Psi(\rho, z) = \frac{-ik}{z} \, e^{i\left(kz + \frac{k\rho^2}{2z}\right)} \int_0^\infty \Psi(\rho', 0) \, e^{ik\frac{\rho'^2}{2z}} \, J_0\left(k\frac{\rho\rho'}{z}\right) \rho' d\rho' \tag{1.40}$$

where, as usual, $k = 2\pi/\lambda$ is the wavenumber and λ the wavelength. In this equation, ρ' reminds us that the integration is being performed on the plane $z = 0$; thus, $\Psi(\rho', 0)$ simply indicates the field value on $z = 0$. An important solution is obtained by considering on the $z = 0$ plane the "excitation" given by

$$\Psi(\rho', 0) = \Psi_{BG}(\rho', 0) = AJ_0(k_\rho \rho') \exp(-q\rho'^2) \tag{1.41}$$

which [100] produces the so-called Bessel–Gauss beam [101]:

$$\Psi_{BG}(\rho, z) = -\frac{ikA}{2zQ} \, e^{ik(z+\frac{\rho^2}{2z})} \, J_0\left(\frac{ikk_\rho \rho}{2zQ}\right) e^{-\frac{1}{4Q}(k_\rho^2 + \frac{k^2\rho^2}{z^2})} \tag{1.42}$$

which is a Bessel beam modulated transversally by the Gaussian function. Quantity $Q = q - ik/2z$, and k_ρ is a constant (namely, the transverse wavenumber associated with the modulated Bessel beam). When $q = 0$, the Bessel–Gauss beam results in the well-known Gaussian beam. The Gaussian beam, and Bessel–Gauss', in Equation 1.42, are among the few solutions to the Fresnel diffraction integral that can be obtained analytically. The situation gets much more complicated, however, when facing beams truncated in space by finite circular apertures; for instance, a Gaussian beam, or a Bessel beam, or a Bessel-Gauss beam truncated via an aperture with radius R. In this case, the upper limit of the integral in Equation 1.40 becomes the aperture radius, and the analytic integration becomes very difficult, requiring recourse to lengthy numerical calculations.

Let us now go on to our method for the description of truncated beams, characterized by simplicity and, in most cases, total analyticity. Let us start with the Bessel–Gauss beam, Equation 1.42, and consider the solution given by the following superposition of such beams:

$$\Psi(\rho, z) = -\frac{ik}{2z} \, e^{ik\left(z+\frac{\rho^2}{2z}\right)} \sum_{n=-N}^{N} \frac{A_n}{Q_n} J_0\left(\frac{i\,k\,k_\rho\,\rho}{2\,z\,Q_n}\right) e^{-\frac{1}{4Q_n}\left(k_\rho^2 + \frac{k^2\rho^2}{z^2}\right)} \tag{1.43}$$

quantities A_n being constants, and Q_n given by

$$Q_n = q_n - \frac{ik}{2z} \tag{1.44}$$

where the q_n are constants that can assume *complex values*. Notice that in this superposition all beams possess the same value of k_ρ. We want the solution (1.43) to be able to represent beams truncated by circular apertures, in the case, as we know, of Bessel beams, Gaussian beams, Bessel–Gauss beams, and plane waves.

Given one such beam, truncated at $z = 0$ by an aperture with radius R, we have to determine the coefficients A_n and q_n in such a way that Equation 1.43 represents with fidelity the resulting beam: If the truncated beam on the $z = 0$ plane is given by $V(\rho)$, we have to obtain $\Psi(\rho, 0) = V(\rho)$, that is to say

$$V(\rho) = J_0(k_\rho \rho) \sum_{n=-N}^{N} A_n e^{-q_n \rho^2} \tag{1.45}$$

The right-hand side of this equation is, indeed, nothing but a superposition of Bessel–Gauss beams, all with the same value of k_ρ, at $z = 0$ (namely, each one of such beams is written at $z = 0$ according to Equation 1.41).

One has to get the values of the A_n and q_n, as well as of N, from Equation 1.45. Once these values have been obtained, the field emanated by the finite circular aperture located at $z = 0$ will be given by Equation 1.43. Remembering that the q_n can be complex, let us make the following choices:

$$q_n = q_R + iq_{In}, \quad \text{with} \quad q_{In} = -\frac{2\pi}{L} n \tag{1.46}$$

where $q_R > 0$ is the real part of q_n, having the *same value* for every n; q_{In} is the imaginary part of q_n; and L is a constant with the dimensions of a square length.

With such choices, and assuming $N \to \infty$, Equation 1.45 gets written as

$$V(\rho) = J_0(k_\rho \rho) \ \exp\left(-q_R \rho^2\right) \sum_{n=-\infty}^{\infty} A_n \ \exp\left(i\frac{2\pi n}{L}\rho^2\right) \tag{1.47}$$

which has then to be exploited for obtaining the values of A_n, k_ρ, q_R, and L.

In the cases of a TB beam or of a truncated Bessel–Gauss (TBG) beam, it it natural to choose quantity k_ρ in Equation 1.47 equal to the corresponding beam transverse wavenumber. In the case of a truncated Gaussian (TG) beam or of a truncated plane (TP) wave, by contrast, in Equation 1.47 it is natural to choose $k_\rho = 0$. In all cases, the product

$$\exp\left(-q_R \rho^2\right) \sum_{n=-\infty}^{\infty} A_n \ \exp\left(i\frac{2\pi n}{L}\rho^2\right) \tag{1.48}$$

in Equation 1.47 has to represent:

(i) a function circ(ρ/R), in the TB or TP cases;
(ii) a function $\exp\left(-q\,\rho^2\right)$ circ(ρ/R), that is, a circ function multiplied by a Gaussian function, in the TBG or TG cases.

Of course (i) is a particular case of (ii) with $q = 0$. It may be useful to recall that the circ-function is the step-function in the cylindrically symmetric case. Quantity R is still the aperture radius, and circ(ρ/R) $= 1$ when $0 \le \rho \le R$, and equals 0 elsewhere.

Let us now show how expression (1.48) can approximately represent the above functions, given in (i) and (ii). To such an aim, let us consider a function $G(r)$ defined on an interval $|r| \le L/2$ and endowed with the Fourier expansion

$$G(r) = \sum_{n=-\infty}^{\infty} A_n \exp\left(\frac{i2\pi nr}{L}\right) \quad \text{for} \quad |r| \le \frac{L}{2} \tag{1.49}$$

where r and L, having the dimensions of a square length, are expressed in square meters (m^2). Suppose now the function $G(r)$ to be given by

$$G(r) = \begin{cases} \exp\left(q_R \, r\right) \exp\left(-q \, r\right) & \text{for} \quad |r| \le R^2 \\ 0 & \text{for} \quad R^2 < |r| < \frac{L}{2} \end{cases} \tag{1.50}$$

where q is a given constant. Then, the coefficients A_n in the Fourier expansion of $G(r)$ will be given by

$$A_n = \frac{1}{L\,(q_R - q) - i2\pi n}\left(e^{(q_R - q - i\frac{2\pi}{L}n)R^2} - e^{-(q_R - q - i\frac{2\pi}{L}n)R^2}\right) \tag{1.51}$$

Writing now

$$r = \rho^2 \tag{1.52}$$

we get that quantity (1.48) in Equation 1.49, and Equation 1.50, can be written as

$$
e^{-q_R \rho^2} \sum_{n=-\infty}^{\infty} A_n e^{i2\pi n \rho^2/L} =
\begin{cases}
e^{-q\,\rho^2} & \text{for } 0 \leq \rho \leq R \\
0 & \text{for } R < \rho \leq \sqrt{L/2} \\
e^{-q_R \rho^2} f(\rho) \approx 0 & \text{for } \rho > \sqrt{L/2}
\end{cases}
\tag{1.53}
$$

where the coefficients A_n are still given by Equation 1.51, and $f(\rho)$ is a function existing on shorter and shorter space intervals, assuming as it maximum value $\exp\,[(q_R - q)R^2]$, when $q_R > q$, or 1, when $q_R \leq q$. As $\sqrt{L/2} > R$, for suitable choices of q_R and L, we shall have that $\exp\,(-q_R \rho^2)\,f(\rho) \approx 0$ for $\rho \geq \sqrt{L/2}$.

Therefore, we obtain

$$
e^{-q_R \rho^2} \sum_{n=-\infty}^{\infty} A_n e^{i2\pi n \rho^2/L} \approx e^{-q\,\rho^2} \, \text{circ}(\rho/R)
\tag{1.54}
$$

which corresponds to case (i), when $q = 0$, and to case (ii). Let us recall once more that the A_n are given by Equation 1.51.

On the basis of what was shown before, we have now in our hands a rather efficient method for describing important beams, truncated by finite apertures, namely the TB, TG, TBG, and TP beams. Indeed, it is enough to choose the desired field, truncated by a circular aperture with radius R, and describe it at $z = 0$ by Equation 1.47.

Precisely:

- In the TBG case the value of k_ρ in Equation 1.47 is the transverse wavenumber of the Bessel beam modulated by the Gaussian function; A_n is given in Equation 1.51; q is related to the Gaussian-function width at $z = 0$. The values L and q_R, and the number N of terms in the series (1.47), are chosen so as to guarantee a faithful description of the beam at $z = 0$ when truncated by a circular aperture with radius R.
- The TB, TG, and TP are special cases of TBG: in TB $q = 0$; in TG $k_\rho = 0$; and in TP $k_\rho = 0$ and $q = 0$

In conclusion, *once we know the chosen beam on the truncation plane (z = 0), the beam emanated by the finite aperture will then be given by solution (1.43). Further details can be found in Ref. [75].*

Let us go on to an important example.

1.4.2
Application of the Method to a TB Beam

For the sake of brevity, we apply our method only to the analytic description of the TB beam.

Let us consider a Bessel beam, with wavelength of 632.8 nm, truncated at $z = 0$ by a circular aperture with radius R, that is to say let us start from
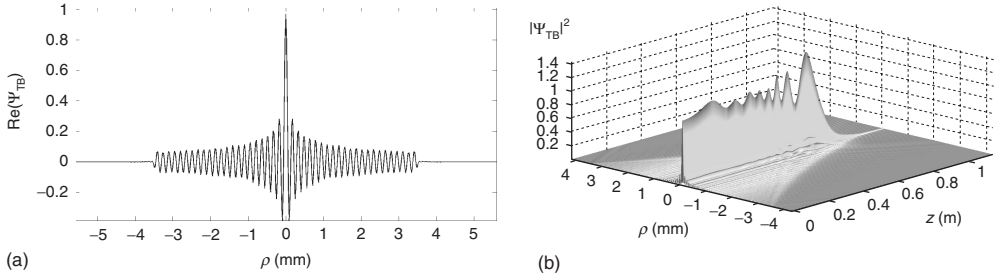
Figure 1.8 (a) Field given by Equation 1.47, representing a Bessel beam at $z = 0$, with $k_\rho = 4.07 \cdot 10^4$ m^{-1} and truncated by a finite circular aperture with radius $R = 3.5$ mm. The coefficients A_n are given by Equation 1.51, with $q = 0$, $L = 3R^2$, $q_R = 6/L$, and $N = 23$. (b) Intensity of a Bessel beam truncated by a finite aperture, as given by solution (1.43).

$\Psi_{\mathrm{TB}}(\rho, 0) = J_0(k_\rho \rho) \, \mathrm{circ}(\rho/R)$. Let us choose $R = 3.5$ mm, and the transverse wavenumber $k_\rho = 4.07 \cdot 10^4$ m^{-1}, which corresponds to a beam spot with radius approximatively equal to $\Delta\rho = 59$ μm.

At $z = 0$ the field is described by Equation 1.47, where the A_n are given by Equation 1.51 and where $q = 0$. In this case, a resonable result can be obtained by the choice $L = 3R^2$, $q_R = 6/L$ and $N = 23$. Let us stress that, as such a choice is not unique, many alternative sets of values L and q_R exist, which also yield excellent results.

Figure 1.8a depicts the field given by Equation 1.47: it represents, with high fidelity, the Bessel beam truncated at $z = 0$. The resulting field, emanated by the aperture, is given by solution (1.43), and its intensity is shown in Figure 1.8b. One can see that the result really corresponds to a Bessel beam truncated by a finite aperture.

1.5
Subluminal NDWs (or Bullets)

Let us now obtain in a simple way non-diffracting *subluminal* pulses, always as exact analytic solutions to the wave equations [19]. We shall adopt in this section a less formal language (perhaps more intuitive or more physical), and we shall confine it to ideal solutions, but such solutions will be constructed for arbitrarily chosen frequencies and bandwidths, once more avoiding any recourse to the non-causal (backward-moving) components. Also, the new solutions can be suitable superpositions of – zeroth-order, in general – Bessel beams, which can be performed by integrating either w.r.t. the angular frequency ω, or w.r.t. the longitudinal wavenumber k_z: Both approaches are treated below. The first one is powerful enough; we sketch the second approach as well, however, as it allows also dealing – from a new starting point – with the limiting case of *zero-speed* solutions. Namely it furnishes a new way, in terms of *continuous* spectra, for obtaining such

("frozen") waves [4–7], so promising also from the point of view of the applications. Some attention is successively paid to the known role of special relativity, and to the fact that the NDWs are expected to be transformed one into the other by suitable Lorentz transformations. We are, moreover, going to mention the case of non-axially symmetric solutions in terms of higher-order Bessel beams. We keep fixing our attention particularly on electromagnetism and optics; however, let us repeat that results of the same kind are valid whenever an essential role is played by a wave equation [like in acoustics, seismology, geophysics, elementary particle physics (as we shall see explicitly in the slightly different case of the Schroedinger equation), and also gravitation (for which we have recently got stimulating new results), and so on].

Subluminal NDWs can also be obtained by suitable superpositions of Bessel beams [19], as in the other cases, but have been rather neglected for the mathematical difficulties in getting analytic expressions for them, as the superposition integral runs over a finite interval. Therefore, almost all the few papers devoted to the subluminal NDWs had recourse to the paraxial [93] approximation [97] or to numerical simulations [29]. Only *one* analytic solution was known [31–33, 56, 63], biased by the inconveniences that its frequency spectrum is very large, that it does not possess a well-defined central frequency, and that backward-travelling [52, 54] components were needed for constructing it. In this section we construct, however, non-diffracting exact solutions with any spectra, in any frequency bands, and for any bandwidths, and without employing [12, 50] backward-traveling components. One can arrive at such (analytic) solutions, both in the case of integration over the Bessel beams' angular frequency ω and of integration over their longitudinal wavenumber k_z.

1.5.1
A First Method for Constructing Physically Acceptable, Subluminal Non-Diffracting Pulses

Axially-symmetric solutions to the scalar wave equation are known to be superpositions of zero-order Bessel beams over the angular frequency ω and the longitudinal wavenumber k_z, that is in cylindrical co-ordinates,

$$\Psi(\rho, z, t) = \int_0^\infty d\omega \int_{-\omega/c}^{\omega/c} dk_z \, \overline{S}(\omega, k_z) J_0 \left(\rho \sqrt{\frac{\omega^2}{c^2} - k_z^2} \right) e^{ik_z z} e^{-i\omega t} \qquad (1.55)$$

where, as usual, $k_\rho^2 \equiv \omega^2/c^2 - k_z^2$ is the transverse wavenumber, and quantity k_ρ^2 has to be positive as evanescent waves are here excluded. We already know that the condition characterizing a NDW is the existence [52, 102] of a linear relation between longitudinal wavenumber k_z and frequency ω for all the Bessel beams entering the superposition. That is to say, in the chosen spectrum for each Bessel beam it has to be [12, 48]

$$\omega = v \, k_z + b \qquad (1.56)$$

with $b \geq 0$. (More generally, as shown in [12], in the plane ω, k_z the chosen spectrum has to call into play, if not exactly such a line, at least a region in the proximity of

a straight-line of that type. In the latter case one obtains solutions endowed with finite energy, and therefore a finite "depth of field").

The requirement (1.56) is a specific space–time coupling, implied by the chosen spectrum $\overline{S}$. Let us recall that Equation 1.56 has to be obeyed by the spectra of any one of the three possible types (subluminal, luminal, or superluminal) of non-diffracting pulses: Indeed, with the choice (1.56), the pulse regains its initial shape after the space-interval $\Delta z_1 = 2\pi v/b$. (But the more general case can be also considered [12, 51] when b assumes any values $b_m = m\,b$ (with m an integer), and the periodicity space-interval becomes $\Delta z_m = \Delta z_1/m$. We are referring ourselves, now, to the real (or imaginary) part of the pulse, as its magnitude is endowed with rigid motion).

Let us first derive in the subluminal case the only exact solution known until recently, the Mackinnon's [31] one, represented by Equation 1.63 below. As the transverse wavenumber k_ρ of each Bessel beam entering Equation 1.55 has to be real, it can be shown easily (as first noticed in Ref. [29]) that in the subluminal case b cannot vanish, but it must be $b > 0$. Then, on using conditions (1.56) and $b > 0$, the subluminal localized pulses can be expressed as integrals over the frequency only:

$$\Psi(\rho, z, t) = \exp\left[-ib\frac{z}{v}\right] \int_{\omega_-}^{\omega_+} d\omega\; S(\omega)\; J_0(\rho k_\rho)\; \exp\left[i\omega\frac{\zeta}{v}\right] \tag{1.57}$$

where now

$$k_\rho = \frac{1}{v}\sqrt{2b\omega - b^2 - (1 - v^2/c^2)\omega^2} \tag{1.58}$$

with

$$\zeta \equiv z - vt \tag{1.59}$$

and with

$$\begin{cases} \omega_- = \frac{b}{1+v/c} \\[2mm] \omega_+ = \frac{b}{1-v/c} \end{cases} \tag{1.60}$$

As anticipated, the Bessel beam superposition in the subluminal case is an integration over a finite interval of ω, which also shows that the backward-travelling components correspond to the interval $\omega_- < \omega < b$. (It could be noticed that Equation 1.57 does not represent the most general exact solution, which, on the contrary, is *a sum* [51] of such solutions for the various possible values of b mentioned above, that is for the values $b_m = m\,b$ with spatial periodicity $\Delta z_m = \Delta z_1/m$. But we can confine ourselves to solution (1.57) without any real loss of generality, as the actual problem is evaluating in analytic form the integral entering Equation 1.57. For any mathematical and physical details, see [51]).

Now, if one adopts the change of variable

$$\omega \equiv \frac{b}{1 - v^2/c^2}\left(1 + \frac{v}{c}s\right) \tag{1.61}$$

Equation 1.57 becomes [29]

$$\Psi(\rho, z, t) = \frac{b}{c} \frac{v}{1 - v^2/c^2} \exp\left[-i\frac{b}{v}z\right] \exp\left[i\frac{b}{v} \frac{1}{1 - v^2/c^2} \zeta\right]$$

$$\times \int_{-1}^{1} ds \, S(s) \, J_0\left(\frac{b}{c} \frac{\rho}{\sqrt{1 - v^2/c^2}} \sqrt{1 - s^2}\right) \exp\left[i\frac{b}{c} \frac{1}{1 - v^2/c^2}\zeta s\right]$$

(1.62)

In the following we shall adhere – as it is an old habit of ours – to some symbols standard in special relativity, as the whole topic of subluminal, luminal, and superluminal NDWs is strictly connected [13, 14, 91] with the principles and structure of special relativity (see [89, 103] and references therein), as we shall mention also in the specific remarks which follow below. Namely, we put $\beta \equiv v/c$ and $\gamma \equiv 1/\sqrt{1 - \beta^2}$.

Equation 1.62 has until now yielded *one* analytic solution, for $S(s) =$ constant: the *Mackinnon solution* [31, 33, 56, 76]

$$\Psi(\rho, \zeta, \eta) = 2\frac{b}{c}v \, \gamma^2 \, \exp\left[i\frac{b}{c} \, \beta\gamma^2 \, \eta\right]$$

$$\times \sin c\sqrt{\frac{b^2}{c^2} \, \gamma^2(\rho^2 + \gamma^2 \, \zeta^2)}$$

(1.63)

which, however, for its above-mentioned drawbacks, is endowed with little physical and practical interest. In Equation 1.63 the sin c function has the ordinary definition $\sin x \equiv (\sin x)/x$, and

$$\eta \equiv z - Vt, \text{ with } V \equiv \frac{c^2}{v}$$

(1.64)

where V and v are related by the *de Broglie relation*. Notice that Ψ in Equation 1.63, and in the following ones, is eventually a function (besides of ρ) of z, t only via quantities ζ and η.

However, we can construct further subluminal pulses, corresponding to any spectrum and devoid of backward-moving components, just by exploiting the fact that in our Equation 1.62 the integration interval is finite, that is, by transforming it into good instead of harm. Let us first observe that Equation 1.62 will also yield exact, analytic solutions for *any* exponential spectra of the type

$$S(\omega) = \exp\left[\frac{i2n\pi\omega}{\Omega}\right]$$

(1.65)

with n any integer number: Which means that for any spectra of this type it holds $S(s) = \exp[in\pi/\beta] \exp[in\pi s]$, as can be checked easily. In Equation 1.65 we have set $\Omega \equiv \omega_+ - \omega_-$. In this more general case, the solution writes

$$\Psi(\rho, \zeta, \eta) = 2b\beta \, \gamma^2 \, \exp\left[i\frac{b}{c} \, \beta \, \gamma^2 \, \eta\right]$$

$$\times \exp\left[in\frac{\pi}{\beta}\right] \sin c\sqrt{\frac{b^2}{c^2} \, \gamma^2 \, \rho^2 + \left(\frac{b}{c} \, \gamma^2 \, \zeta + n\pi\right)^2}$$

(1.66)

Notice also that in Equation 1.66 quantity η is defined as in Equations 1.64 above, where V and v obey the de Broglie relation $vV = c^2$, the subluminal quantity v being the velocity of the pulse envelope, and V playing the role (in the envelope's interior) of a superluminal phase velocity.

We now take *advantage* of the finiteness of the integration limits for expanding any arbitrary spectra $S(\omega)$ in a Fourier series in the interval $\omega_- \le \omega \le \omega_+$, that is:

$$S(\omega) = \sum_{n=-\infty}^{\infty} A_n \ \exp \left[+in\frac{2\pi}{\Omega}\omega \right] \tag{1.67}$$

where (we went back, now, from the s to the ω variable):

$$A_n = \frac{1}{\Omega} \ \int_{\omega_-}^{\omega_+} d\omega \ S(\omega) \ \exp \left[-in\frac{2\pi}{\Omega}\omega \right] \tag{1.68}$$

quantity Ω being defined above.

Then, on remembering the special, "Mackinnon-type" solution (1.66), we can infer from expansion (1.65) that, for any arbitrary spectral function $S(\omega)$, one can work out a rather general axially-symmetric analytic solution for the subluminal case:

$$\Psi(\rho, \zeta, \eta) = 2b\beta \ \gamma^2 \ \exp \left[i\frac{b}{c} \ \beta \ \gamma^2 \ \eta \right]$$

$$\times \sum_{n=-\infty}^{\infty} A_n \ \exp \left[in\frac{\pi}{\beta} \right] \sin c \sqrt{\frac{b^2}{c^2} \ \gamma^2\rho^2 + \left(\frac{b}{c}\gamma^2 \ \zeta + n\pi \right)^2} \tag{1.69}$$

coefficients A_n being still given by Equation 1.68.

The present approach presents several advantages. We can easily choose spectra localized within the prefixed frequency interval (optical waves, microwaves, etc.) and endowed with the desired bandwidth. Moreover, we have seen that spectra can now be chosen such that they have zero value in the region $\omega_- \le \omega \le b$, which is responsible for the backward-traveling components of the subluminal pulse. Even when the adopted spectrum $S(\omega)$ does not possess a known Fourier series (so that the coefficients A_n cannot be exactly evaluated via Equation 1.68), one can calculate approximately such coefficients without meeting any problem, as our general solutions (1.69) will still be exact solutions.

Let us set forth some examples.

1.5.2
Examples

In general, optical pulses generated in the laboratory possess a spectrum centered at some frequency value, ω_0, called the carrier frequency. The pulses can be, for instance, ultra-short, when $\Delta\omega/\omega_0 \ge 1$, or quasi-monochromatic, when $\Delta\omega/\omega_0 \ll 1$, where $\Delta\omega$ is the spectrum bandwidth.

These kinds of spectra can be represented mathematically by a Gaussian function or by functions with similar behavior. One can find various examples in [11, 19].

First example – Let us consider, for example, a Gaussian spectrum

$$S(\omega) = \frac{a}{\sqrt{\pi}} \exp \left[-a^2 (\omega - \omega_0)^2 \right] \tag{1.70}$$

whose values are negligible outside the frequency interval $\omega_- < \omega < \omega_+$ over which the Bessel beams superposition in Equation 1.57 is made, it being $\omega_- = b/(1 + \beta)$ and $\omega_+ = b/(1 - \beta)$. (Let us stress that, once v and b have been fixed, the values of a and ω_0 can afterward be selected in order to kill the backward-travelling components, that correspond, as we know, to $\omega < b$.) The Fourier expansion in Equation 1.67, which yields, with the above spectral function (1.70), the coefficients

$$A_n \approx \frac{1}{W} \exp \left[-in \frac{2\pi}{\Omega} \omega_0 \right] \exp \left[\frac{-n^2 \pi^2}{a^2 W^2} \right], \tag{1.71}$$

constitute an excellent representation of the Gaussian spectrum (1.70) in the interval $\omega_- < \omega < \omega_+$ (provided that, as we requested, our Gaussian spectrum does get *negligible* values outside the frequency interval $\omega_- < \omega < \omega_+$). In other words, a subluminal pulse with frequency spectrum (1.70) can be written as Equation 1.69, with the coefficients A_n given by Equation 1.71: the evaluation of such coefficients A_n being rather simple. Let us repeat that even if the values of the A_n are obtained via a (rather good, by the way) approximation, we based ourselves on the *exact* solution in Equation 1.69.

One can, for instance, obtain exact solutions representing subluminal pulses for optical frequencies (see Figure 1.9). The construction of the considered pulse results are already satisfactory when considering about 51 terms ($-25 \leq n \leq 25$) in the series entering Equation 1.69.

Figure 1.9 shows that pulse, evaluated just by summing the mentioned 51 terms: Figure 1.9a depicts the orthogonal projection of the pulse intensity; Figure 1.9b shows the 3D intensity pattern of the *real part* of the pulse, which reveals the carrier wave oscillations.

Let us stress that the ball-like shape for the field intensity is typically associated with the subluminal NDWs, while the typical superluminal ones are known to be X-shaped [9, 14, 91], as predicted a long time ago by special relativity in its ''non-restricted'' version (see [13, 14, 35, 89, 103] and references therein). Indeed it can be noted that each term of the series in Equation 1.69 corresponds to an ellipsoid or, more specifically, to a spheroid, for each velocity v.

A second example – Let us consider now the very simple case when, within the integration limits ω_-, ω_+, the complex exponential spectrum (1.65) is replaced by the real function (still linear in ω)

$$S(\omega) = \frac{a}{1 - \exp \left[-a(\omega_+ - \omega_-) \right]} \exp \left[a(\omega - \omega_+) \right] \tag{1.72}$$

with a a positive number (for $a = 0$ one goes back to the Mackinnon case). Spectrum (1.72) is exponentially concentrated in the proximity of ω_+, where it
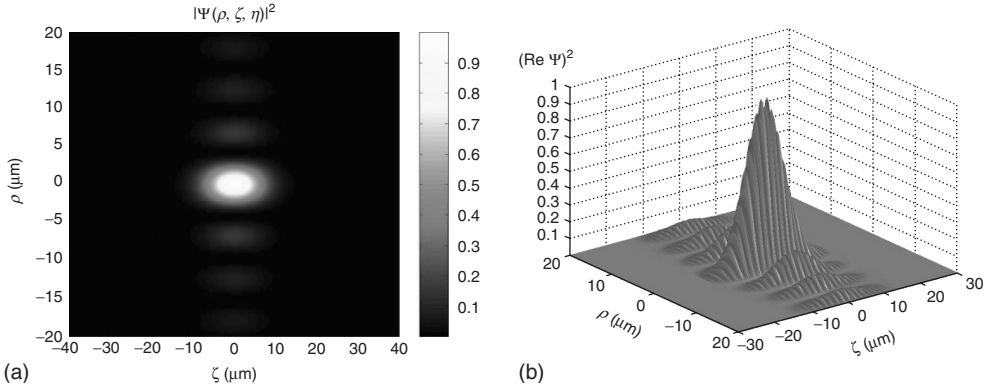
Figure 1.9 (a) The intensity orthogonal projection for a pulse corresponding to Equations 1.70 and 1.71 in the case of an optical frequency, namely for a subluminal pulse with velocity $v = 0.99\, c$, carrier angular frequency $\omega_0 = 2.4 \times 10^{15}$ Hz (i.e., $\lambda_0 = 0.785$ μm) and FWHM bandwidth (that is, full width at half maximum) $\Delta\omega = \omega_0/20 = 1.2 \times 10^{14}$ Hz, which results in an optical pulse of 24 fs. One has also to specify a value for the the frequency: let it be $b = 3 \times 10^{13}$ Hz; as a consequence, one has $\omega_- = 1.507 \times 10^{13}$ Hz and $\omega_+ = 3 \times 10^{15}$ Hz. (This is exactly a case in which the pulse has no backward-traveling components, as the chosen spectrum possesses totally negligible values for $\omega < b$.) (b) The three-dimensional intensity pattern of the *real part* of the same pulse, which reveals the carrier wave oscillations.

reaches its maximum value, and (on the left of ω_+) becomes more and more concentrated as the arbitrarily chosen value of a increases; its frequency bandwidth being $\Delta\omega = 1/a$.

On performing the integration as in the case of spectrum (1.65), instead of solution (1.66) in the present case one eventually gets the solution

$$\Psi(\rho, \zeta, \eta) = \frac{2ab\beta\gamma^2\, \exp\left[ab\gamma^2\right]\, \exp\left[-a\omega_+\right]}{1 - \exp\left[-a(\omega_+ - \omega_-)\right]}$$

$$\times \exp\left[i\frac{b}{c}\, \beta\, \gamma^2\, \eta\right] \operatorname{sinc}\left[\frac{b}{c}\, \gamma^2\, \sqrt{\gamma^{-2}\, \rho^2 - (av + i\zeta)^2}\right] \quad (1.73)$$

This Equation 1.73 appears to be the simplest closed-form solution, after Mackinnon's, as both of them do not need any recourse to series expansions. In a sense, our solution (1.73) may be regarded as the subluminal analogue of the (superluminal) X-wave solution; a difference being that the standard X-shaped solution has a spectrum starting with 0, where it assumes its maximum value, while in the present case the spectrum starts at ω_- and gets increasing afterward until ω_+. It is more important to observe that the Gaussian spectrum has, a priori, two advantages w.r.t. Equation 1.72: It may be more easily centered around any value ω_0 of ω, and, when increasing its concentration in the surroundings of ω_0, the spot transverse width does not increase indefinitely, but tends to the spot-width of a Bessel beam with $\omega = \omega_0$ and $k_z = (\omega_0 - b)/V$, at variance with what happens for spectrum (1.72). Anyway, solution (1.73) is noticeable, as it is really *the simplest*

one. An example is consituted by Figure 1.37 in Refs [11], referring to an optical pulse of 0.2 ps.

1.5.3
A Second Method for Constructing Subluminal Non-Diffracting Pulses

The previous method appears to be very efficient for finding out analytic subluminal NDWs, but it loses its validity in the limiting case $v \rightarrow 0$, as for $v = 0$ it is $\omega_- \equiv \omega_+$ and the integral in Equation 1.57 degenerates, furnishing a null value. By contrast, we are also interested in the $v = 0$ case, as it corresponds, as we said, to some of the most interesting, and potentially useful, NDWs, that is to the "stationary" solutions to the wave equations endowed with a *static* envelope, and that we call Frozen Waves. Before going on, let us recall that the theory of frozen waves was developed initially in [4, 6], by having recourse to discrete superpositions in order to bypass the need of numerical simulations. (In the case of continuous superpositions, some numerical simulations were performed in [104]. However, the method presented in this subsection does allow finding out exact analytic solutions, without any need of numerical simulations, also for FW consisting of *continuous superpositions*).

Actually, we are going to see that the present method works regardless of the chosen field-intensity shape, and in regions with size of the order of the wavelength. It is possible to get such results by starting again from Equation 1.55, with constraint (1.56), but going on – this time – to integrals over k_z, instead of over ω. It is enough to write relation (1.56) in the form $k_z = (\omega - b)/v$, for expressing the exact solutions (1.55) as

$$\Psi(\rho, z, t) = \exp\left[-ibt\right] \int_{k_z\,\text{min}}^{k_z\,\text{max}} dk_z \; S(k_z) \, J_0(\rho k_\rho) \; \exp\left[i\zeta k_z\right] \qquad (1.74)$$

with

$$k_z\,\text{min} = \frac{-b}{c} \, \frac{1}{1+\beta} \, ; \, k_z\,\text{max} = \frac{b}{c} \, \frac{1}{1-\beta} \qquad (1.75)$$

and with

$$k_\rho{}^2 = -\frac{k_z^2}{\gamma^2} + 2\frac{b}{c}\beta k_z + \frac{b^2}{c^2} \qquad (1.76)$$

where quantity ζ is still defined according to Equation 1.59, always with $v < c$.

One can show that the unique exact solution known previously [31] may be rewritten in form (1.75) *with* $S(k_z) =$ constant. Then, on following the same procedure exploited in our first method, one can again observe [11] that any spectra $S(k_z)$ can be expanded, on the interval $k_z\,\text{min} < k_z < k_z\,\text{max}$, into the Fourier series:

$$S(k_z) = \sum_{n=-\infty}^{\infty} A_n \; \exp\left[+in\frac{2\pi}{K}k_z\right] \qquad (1.77)$$

with coefficients given now by

$$A_n = \frac{1}{K} \int_{k_z \min}^{k_z \max} dk_z \; S(k_z) \; \exp\left[-in\frac{2\pi}{K}k_z\right] \tag{1.78}$$

where $K \equiv k_z \max - k_z \min$.

At the end of the whole procedure [11], the general exact solution representing a subluminal NDW, for any spectra $S(k_z)$, can be written eventually:

$$\Psi(\rho, \zeta, \eta) = 2\,\frac{b}{c}\,\gamma^2\,\exp\left[i\frac{b}{c}\,\beta\,\gamma^2\,\eta\right]$$

$$\times \sum_{n=-\infty}^{\infty} A_n \; \exp\left[in\pi\beta\right] \sin c\sqrt{\frac{b^2}{c^2}\,\gamma^2\,\rho^2 + \left(\frac{b}{c}\,\gamma^2\,\zeta + n\pi\right)^2} \tag{1.79}$$

whose coefficients are expressed in Equation 1.78, and where quantity η is defined as above, in Equation 1.64.

Interesting examples could be easily worked out.

1.6
"Stationary" Solutions with Zero-Speed Envelopes: Frozen Waves

Here, we shall refer ourselves to the (second) method, expounded above. Our solution (1.79), for the case of envelopes *at rest*, that is in the case $v = 0$ (which implies $\zeta = z$), becomes

$$\Psi(\rho, z, t) = 2\,\frac{b}{c}\,\exp\left[-ibt\right] \sum_{n=-\infty}^{\infty} A_n \quad \sin c\sqrt{\frac{b^2}{c^2}\,\rho^2 + \left(\frac{b}{c}\,z + n\pi\right)^2} \tag{1.80}$$

with coefficients A_n given by Equation 1.78 with $v = 0$, so that its integration limits simplify into $-b/c$ and b/c, respectively. Thus, one gets

$$A_n = \frac{c}{2b} \int_{-b/c}^{b/c} dk_z \; S(k_z) \; \exp\left[-in\frac{c\pi}{b}k_z\right] \tag{1.81}$$

Equation (1.80) is a new exact solution, corresponding to "stationary" beams with a *static* intensity envelope. Let us observe, however, that even in this case one has an energy propagation, as it can be verified easily from the power flux $\boldsymbol{S}_s = -\nabla\,\Psi_{\mathcal{R}}\,\partial\Psi_{\mathcal{R}}/\partial t$ (scalar case) or from the Poynting vector $\boldsymbol{S}_v = (\boldsymbol{E} \wedge \boldsymbol{H})$ (vectorial case: the condition being that $\Psi_{\mathcal{R}}$ be a single component, A_z, of the vector potential $\boldsymbol{A}$) [14]. We have indicated by $\Psi_{\mathcal{R}}$ the real part of Ψ. For $v = 0$, Equation 1.56 becomes $\omega = b \equiv \omega_0$, so that the particular subluminal waves endowed with null velocity are actually monochromatic beams.

Let us size the present opportunity for presenting here two simple figures (Figures 1.10 and 1.11), which recall, in an intuitive way, some of the geometrical characteristics of our Frozen Waves (FWs).
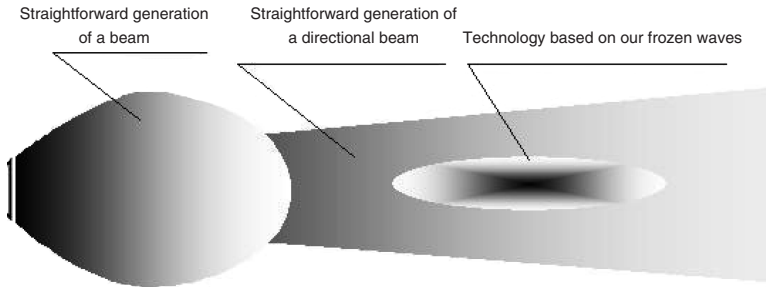
Figure 1.10 See the explications contained in the figures themselves, which apparently refer to ordinary (electromagnetic or acoustical) transmission, to standard directional transmission, and to well-localized transmission allowed by our frozen wave techniques. (Courtesy of Andrei Utkin.)

(a)   (b)   (c)
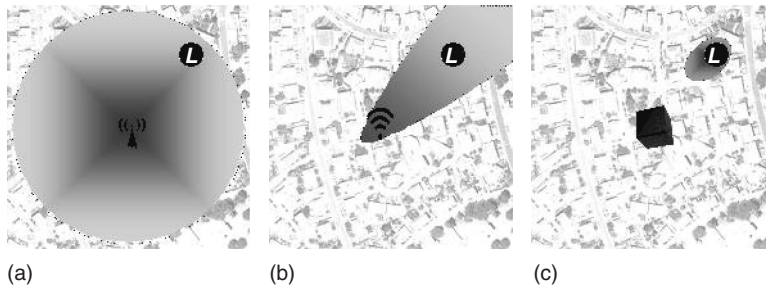
Figure 1.11 Areas covered by the electromagnetic (or acoustic) signals in the case, once more, of (a) omnidirectional trasnsmission, (b) standard directional transmission, and (c) spot-to-spot signal transmission permitted by our frozen wave tecniques. (Courtesy of Andrei Utkin.)

It may be stressed that the present (second) method, without any need of the paraxial approximation, does yield *exact* expressions for (well-localized) beams with sizes *of the order* of their wavelength. It may be noticed, moreover, that the already-known exact solutions – for instance, the Bessel beams – are nothing but particular cases of solution (1.80).

An example – On choosing (with $0 \leq q_- < q_+ \leq 1$) the spectral double-step function

$$S(k_z) = \begin{cases} \frac{c}{\omega_0(q_+ - q_-)} & \text{for } q_-\omega_0/c \leq k_z \leq q_+\omega_0/c \\ \\ 0 & \text{elsewhere,} \end{cases} \tag{1.82}$$

the coefficients of Equation 1.80 become

$$A_n = \frac{ic}{2\pi n\omega_0(q_+ - q_-)} \left[e^{-iq_+\pi n} - e^{-iq_-\pi n} \right] \tag{1.83}$$

The double-step spectrum (1.82) corresponds, with regard to the longitudinal wave number, to the mean value $\overline{k}_z = \omega_0(q_+ + q_-)/2c$ and to the width $\Delta k_z = \omega_0(q_+ - q_-)/c$. From such relations, it follows that $\Delta k_z/\overline{k}_z = 2(q_+ - q_-)/(q_+ + q_-)$.

For values of q_- and q_+ that do not satisfy the inequality $\Delta k_z/\overline{k}_z \ll 1$, the resulting solution will be a *non-paraxial* beam.

An exact solution can be found in Figure 1.38 of [11], which describes a beam with a spot diameter of 0.6 μm (for $\lambda_0 = 1$ μm) and, moreover, with a rather good longitudinal localization. In the case considered therein, about 21 terms in the sum entering Equation 1.81 resulted in being enough for a good evaluation of the series. Such a beam was highly non-paraxial (having $\Delta k_z/\overline{k}_z = 1$) and therefore could not have been obtained by ordinary Gaussian beam solutions, which are valid in the paraxial regime only. Notice that, for simplicity, we are referring ourselves to scalar wave fields only; but, in the case of non-paraxial optical beams, the vector character of the field has to be taken into account.

1.6.1
A New Approach to the Frozen Waves

A noticeable property of our present method is that it allows spatial modeling, even of monochromatic fields (that correspond to envelopes *at rest*, so that, in the electromagnetic cases, one can speak, e.g., of the modeling of ''light-fields at rest''). Let us repeat that such a modeling – rather interesting, especially for applications [8] – was already performed in [4–6] in terms of discrete superpositions of Bessel beams.

But the method presented in the last section allows us to make use of *continuous* superpositions in order to get a predetermined longitudinal (on-axis) intensity pattern, inside a desired space interval $0 < z < L$. Such continuous superposition writes [4, 11]

$$\Psi(\rho, z, t) = e^{-i\omega_0 t} \int_{-\omega_0/c}^{\omega_0/c} dk_z S(k_z) J_0(\rho k_\rho) \quad e^{izk_z} \tag{1.84}$$

which is nothing but the previous Equation 1.72 with $v = 0$ (and therefore $\zeta = z$). In other words, Equation 1.84 does just represent a *null-speed* subluminal wave. The FWs were expressed in the past as discrete superpositions because it was not known at that time how to treat analytically a continuous superposition like Equation 1.84. We are now, however, able to also deal with the relevant integrals: without numerical simulations, as we said, but in terms once more of analytic solutions.

Indeed, the exact solution of Equation 1.84 is given by Equation 1.80, with coefficients (1.81), and one can choose the spectral function $S(k_z)$ in such a way that Ψ assumes the on-axis pre-chosen static intensity pattern $|F(z)|^2$. Namely, the equation to be satisfied by $S(k_z)$, to such an aim, is derived by associating Equation 1.84 with the requirement $|\Psi(\rho = 0, z, t)|^2 = |F(z)|^2$, which entails the integral relation

$$\int_{-\omega_0/c}^{\omega_0/c} dk_z \, S(k_z) \, e^{izk_z} = F(z) \tag{1.85}$$

Equation 1.85 would be trivially solvable in the case of an integration between $-\infty$ and $+\infty$, as it would merely be a Fourier transformation; but, obviously, this is not the case because its integration limits are finite. Actually, there are functions $F(z)$ for which Equation 1.85 is not solvable at all in the sense that no spectra $S(k_z)$ exist obeying the last equation. For instance, if we consider the *Fourier* expansion

$$F(z) = \int_{-\infty}^{\infty} dk_z \, \tilde{S}(k_z) \, e^{izk_z}$$

when $\tilde{S}(k_z)$ does assume non-negligible values outside the interval $-\omega_0/c < k_z < \omega_0/c$, then in Equation 1.85 *no* $S(k_z)$ can forward that particular $F(z)$ as a result.

However, some procedures can be devised, such that one can nevertheless find out a function $S(k_z)$ that approximately (but satisfactorily) complies with Equation 1.85.

The first procedure consists of writing $S(k_z)$ in the form

$$S(k_z) = \frac{1}{K} \sum_{n=-\infty}^{\infty} F\left(\frac{2n\pi}{K}\right) e^{-i2n\pi k_z/K} \tag{1.86}$$

where, as before, $K = 2\omega_0/c$. Then, Equation 86 can be verified easily as guaranteeing that the integral in Equation 1.85 yields the values of the desired $F(z)$ *at the discrete points* $z = 2n\pi/K$. Indeed, the Fourier expansion (1.86) is already of the same type as Equation 1.82, so that in this case the coefficients A_n of our solution (1.80), appearing in Equation 1.81, do simply become

$$A_n = \frac{1}{K} \, F\left(-\frac{2n\pi}{K}\right) \tag{1.87}$$

This is a powerful way for obtaining a desired longitudinal (on-axis) intensity pattern, especially for tiny spatial regions because it is not necessary to solve any integral to find out the coefficients A_n, which, by contrast, are given directly by Equation 1.87.

Figure 1.12 depicts some interesting applications of this method. A few desired longitudinal intensity patterns $|F(z)|^2$ have been chosen, and the corresponding FWs calculated by using Equation 1.80 with the coefficients A_n given in Equation 1.87. The desired patterns are enforced to exist within very small spatial intervals only in order to show the capability of the method to model [19] the field intensity shape also under such strict requirements.

In the following four examples below we considered a wavelength $\lambda = 0.6$ μm, which corresponds to $\omega_0 = b = 3.14 \times 10^{15}$ Hz. Details can be found in [11].

The first longitudinal (on-axis) pattern considered by us is $F(z) = \exp[a(z - Z)]$ for $0 \leq z \leq Z$, and zero elsewhere; that is a pattern with an exponential increase, starting from $z = 0$ until $Z = 10$ μm and with $a = 3/Z$. The intensity of the corresponding FW is shown in Figure 1.12a.

The second longitudinal pattern (on-axis) taken into consideration is the Gaussian one, given by $F(z) = \exp[-q(z/Z)^2]$ for $-Z \leq z \leq Z$, and zero elsewhere, with $q = 2$ and $Z = 1.6$ μm. The intensity of the corresponding FW is shown in Figure 1.12b.

In the third example, the desired longitudinal pattern is supposed to be a super-Gaussian, $F(z) = \exp[-q(z/Z)^{2m}]$ for $-Z \leq z \leq Z$, and zero elsewhere, where m
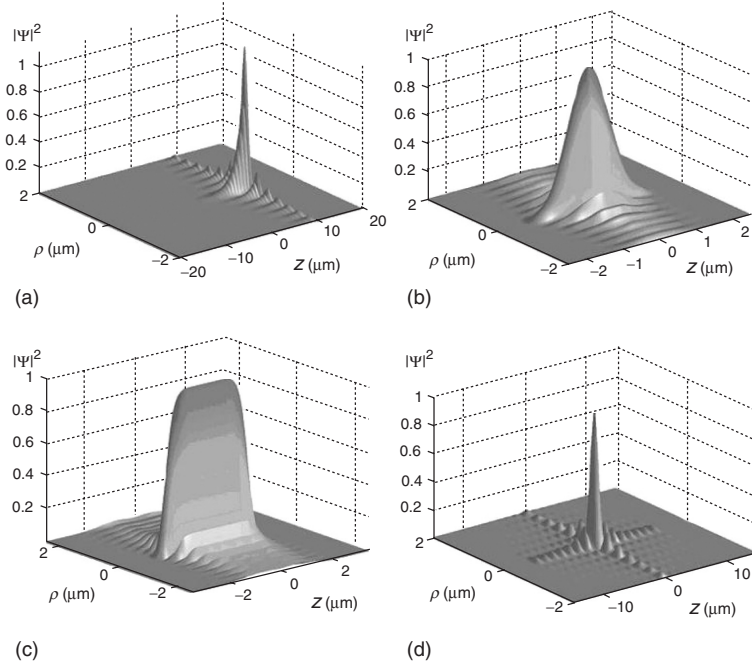
Figure 1.12 Frozen waves with the on-axis longitudinal field pattern chosen as (a) exponential, (b) Gaussian, (c) super-Gaussian, and (d) zero-order Bessel function.

controls the edge sharpness. We choose $q = 2$, $m = 4$ and $Z = 2$ μm. The intensity of the FW obtained in this case is shown in Figure 1.12c.

Finally, in the fourth example, let us choose the longitudinal pattern as being the zero-order Bessel function $F(z) = J_0(q z)$ for $-Z \leq z \leq Z$, and zero elsewhere, with $q = 1.6 \times 10^6$ m^{-1} and $Z = 15$ μm. The intensity of the corresponding FW is shown in Figure 1.12d.

Any static envelopes of this type can be transformed easily into propagating pulses by the mere application of Lorentz Transformations (LT).

Another procedure exists for evaluating $S(k_z)$, based on the assumption that $S(k_z) \approx \tilde{S}(k_z)$, which constitutes a good approximation whenever $\tilde{S}(k_z)$ assumes *negligible* values outside the interval $[-\omega_0/c, \omega_0/c]$. In such a case, one can have recourse to the method associated with Equation 1.77 and expand $\tilde{S}(k_z)$ itself in a Fourier series, eventually getting the relevant coefficients A_n by Equation 1.78. Let us recall that it is still $K \equiv k_z \max - k_z \min = 2\omega_0/c$.

It is worthwhile to call attention to the circumstance that, when constructing FWs in terms of a sum of discrete superpositions of Bessel beams (as it has been done in [4–6, 8, 12]), it is easy to obtain extended envelopes like, for example, "cigars": Where "easy" means using only a few terms of the sum. By contrast, when we construct FWs – following this section – as continuous superpositions, then it is easy to get highly *localized* (concentrated) envelopes. Let us explicitly mention, moreover, that the method presented in this section furnishes FWs that

are no longer periodic along the z-axis (a situation that, with our old method [4–6, 12], was obtainable only when the periodicity interval tended to infinity).

1.6.2
Frozen Waves in Absorbing Media

Let us mention that it is possible to obtain even in *absorbing media* non-diffracting ''stationary'' wave fields capable to assume, approximately, any desired longitudinal intensity pattern within a chosen interval $0 \leq z \leq L$ of the propagation axis z. These new solutions are more easily realizable in practice, to the extent that they are more indicated for the various applications already mentioned.

We know that, when propagating in a non-absorbing medium, the NDWs [4, 6] maintain their spatial shape for long distances. The situation is not the same when dealing with absorbing media. In such cases, both the ordinary and the non-diffracting beams (and pulses) will be attenuated exponentially along the propagation axis.

It can, however be shown that, through suitable superpositions of equal-frequency Bessel beams, it is possible to obtain non-diffracting beams *in absorbing media*, whose longitudinal intensity pattern can assume any desired shape within a chosen interval $0 \leq z \leq L$ of the propagation axis z. For example, one can obtain non-diffracting beams capable of resisting the loss effects, and maintaining the amplitude and spot size of their central core for long distances.

The corresponding method, with some interesting examples, is expounded in [5] and in Chapter 2 of [1].

1.6.3
Experimental Production of the Frozen Waves

Frozen Waves have been produced recently [105] in optics, as reported also in another chapter of this volume; we also expect their production in acoustics, even if at present only simulated experiments have been performed [7].

1.7
On the Role of Special Relativity and of Lorentz Transformations

Strict connections exist between, on one hand, the principles and structure of special relativity and, on the other hand, the whole subject of subluminal, luminal, superluminal localized waves, and it has been expected long time that a priori they are transformable one into the other via suitable Lorentz transformations (see [89, 103, 106–111]).

Let us first confine ourselves to the cases faced in the previous section. Our subluminal localized pulses, which may be called ''wave bullets,'' behave as *particles*; indeed, our subluminal pulses (as well as the luminal and superluminal (X-shaped) ones, that have been so amply investigated in the past literature) do exist

as solutions of any wave equations, ranging from electromagnetism and acoustics or geophysics, to elementary particle physics (and even, as we discovered recently, to gravitation physics). From the kinematical point of view, the velocity composition relativistic law holds also for them. The same is true, in general, for any localized waves (pulses or beams).

Let us start for simplicity by considering, in an initial reference-frame O, just a (v-order) Bessel beam $\Psi(\rho, \phi, z, t) = J_v(\rho k_\rho)\, e^{iv\phi}\, e^{izk_z}\, e^{-i\omega t}$. In a second reference-frame O', moving w.r.t. O with speed u – along the positive z-axis and in the positive direction, for simplicity's sake –, the new Bessel beam it will be observed [111]

$$\Psi(\rho', \phi', z', t') = J_v(\rho' k'_{\rho'})\, e^{iv\phi'}\, e^{iz'k'_{z'}}\, e^{-i\omega' t'} \tag{1.88}$$

obtained by applying the appropriate Lorentz transformation (a Lorentz "boost") with $\gamma = [\sqrt{1 - u^2/c^2}]^{-1}$, and $k'_{\rho'} = k_\rho$; $k'_{z'} = \gamma(k_z - u\omega/c^2)$; $\omega' = \gamma(\omega - uk_z)$; this can be easily seen, for example, by putting $\rho = \rho'$; $z = \gamma(z' + ut')$; $t = \gamma(t' + uz'/c^2)$ directly into Equation 1.88.

Let us now pass to subluminal *pulses*. We can investigate the action of a LT, by expressing them either via the first method, or via the second one, of section 1.5. Let us consider for instance, in the frame O, a v-speed (subluminal) pulse [11] given in section 1.5. When we go on to a second observer O' moving *with the same speed v* w.r.t. frame O, and, still for the sake of simplicity, passing through the origin O of the initial frame at time $t = 0$, the new observer O' will see the pulse [111]

$$\Psi(\rho', z', t') = e^{-it'\omega'_0} \int_{\omega_-}^{\omega_+} d\omega\, S(\omega)\, J_0(\rho' k'_{\rho'})\, e^{iz'k'_{z'}} \tag{1.89}$$

with $k'_{z'} = \gamma^{-1}\omega/v - \gamma b/v$; $\omega' = \gamma b = \omega'_0$; $k'_{\rho'} = \omega'_0/c^2 - k'_{z'}{}^2$, as one gets from the mentioned Lorentz boost [11], with $u = v$ (and γ defined as usual [11]). Notice that $k'_{z'}$ is a function of ω and that here ω' is a constant.

If we explicitly insert into Equation 1.89 the relation $\omega = \gamma(v k'_{z'} + \gamma b)$, which is nothing but a re-writing of the first one of the relations following Equation 1.89 above, then Equation 1.89 becomes [111]

$$\Psi(\rho', z', t') = \gamma v\, e^{-it'\omega_0} \int_{-\omega_0/c}^{\omega_0/c} dk'_{z'}\, \overline{S}(k'_{z'})\, J_0(\rho' k'_{\rho'})\, e^{iz'k'_{z'}} \tag{1.90}$$

where $\overline{S}$ is expressed in terms of the previous function $S(\omega)$, entering Equation 1.89, as follows: $\overline{S}(k'_{z'}) = S(\gamma v k'_{z'} + \gamma^2 b)$. Equation 1.90 describes monochromatic beams with axial symmetry (and also coincides with what was derived from our second method, in section 1.5, when posing $v = 0$).

The conclusion is that a subluminal pulse, given by Equation 1.57, which appears as a v-speed *pulse* in a frame O, will appear [111] in another frame O' (traveling w.r.t. observer O with the same speed v in the same direction z) just as the *monochromatic beam* in Equation 1.90 endowed with angular frequency $\omega'_0 = \gamma b$, whatever be the pulse spectral function in the initial frame O: Even if the kind of monochromatic beam one arrives to does, of course, depend on the chosen $S(\omega)$. The opposite is also true, in general. (Notice, incidentally, that one gets, in particular, a Bessel-type

beam when S is a Dirac's delta-function: $S(\omega) = \delta(\omega - \omega_0)$; moreover, let us notice that, on applying a LT to a Bessel beam, one obtains another Bessel beam, with a different axicon-angle). Let us set forth explicitly an observation that up to now has been noticed only in [19]. Namely, let us mention that, when not starting from Equation 1.57 but from the most general solutions, which – as we have already seen – are *sums* of solutions (1.57) over the various values b_m of b, then a LT will lead us to *a sum* of monochromatic beams – actually, of harmonics (rather than to a single monochromatic beam). In particular, if one wants to obtain a sum of harmonic beams, one has to apply a LT to more general subluminal pulses.

Let us also add that the various superluminal localized pulses get transformed [111] one into the other by the mere application of ordinary Lorentz transformations; while it may be expected that the subluminal and the superluminal NDWs are to be linked (apart from some known technical difficulties, which require a particular caution [35]) by the superluminal Lorentz "transformations" expounded long ago, for example, in [89, 103, 106, 110] and references therein.

Let us recall at this point that, in 1980–1982, special relativity, in its non-restricted version, predicted that, while the *simplest* subluminal *object* is obviously a sphere (or, in the limit, a space point), the simplest superluminal object is, on the contrary, an X-shaped pulse (or, in the limit, a double cone); this is shown in Figure 1.13. The circumstance that the localized solutions to the *wave equations* indeed follow the same pattern is rather interesting, and might be of help – in the case, for example,

(a)   (b)   (c)   (d)
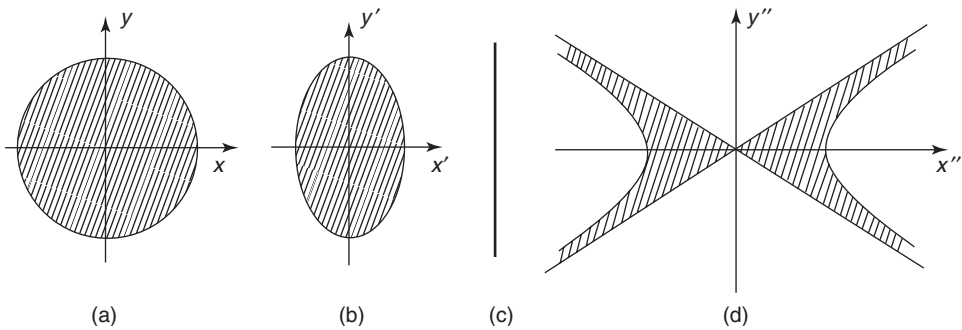
Figure 1.13 From *non-restricted special relativity*, also called "extended special relativity" [35, 103] one can recall the following. An intrinsically spherical (or point-like, at the limit) object appears in the vacuum as an ellipsoid contracted along the motion direction when endowed with a speed $v < c$. By contrast, if endowed with a speed $V > c$ (even if the c-speed barrier cannot be crossed, neither from the left nor from the right), it would appear [35, 89, 103] no longer as a particle, but as occupying the region delimited by a double cone and a two-sheeted hyperboloid – or as a double cone, at the limit –, and moving with superluminal speed V (the cotangent square of the cone semi-angle, with $c = 1$, being $V^2 - 1$). For simplicity, a space axis is skipped. This figure is taken from [89, 103]. It is remarkable that the shape of the localized (subluminal and superluminal) pulses, solutions to the *wave equations*, appears to follow the same behavior; this can have a role for a better comprehension even of the corpuscle/wave duality, that is of de Broglie and Schroedinger wave mechanics. See also Figure 1.14. (Reprinted with kind permission of Società Italiana di Fisica.)

(a)   (b)
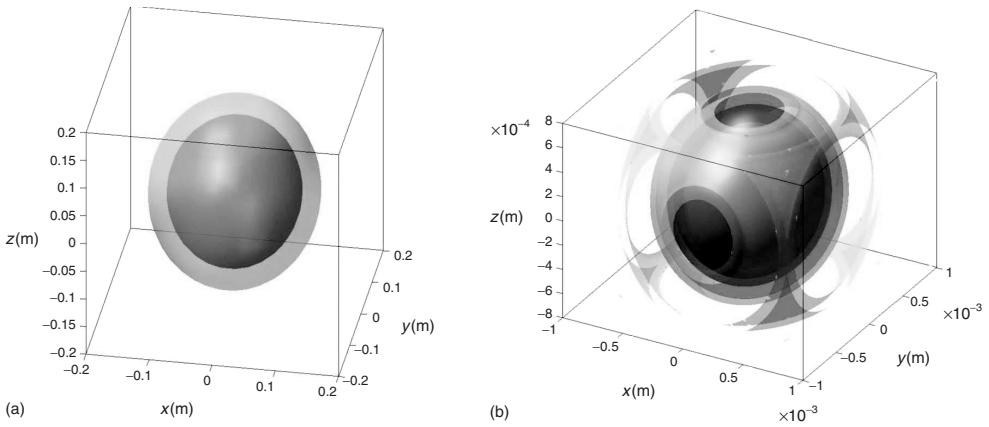
Figure 1.14 In Figure 1.13 we have seen how special relativity (SR), in its non-restricted version, predicted [89, 103] that, while the *simplest* subluminal object is obviously a sphere (or, in the limit, a space point), the simplest superluminal object is, on the contrary, an X-shaped pulse (or, in the limit, a double cone). The circumstance that the localized solutions to the *wave equations* do follow the same pattern is rather interesting, and is expected to be useful – in the case, for example, of elementary particles and quantum physics – for a deeper comprehension of de Broglie's and Schroedinger's wave mechanics. With regard to the fact that the *simplest* subluminal NDWs, solutions to the wave equations, are ''ball-like,'' let us depict, by these figures, in the ordinary three-dimentional space, the general shape of the Mackinnon's solutions as expressed by Equation 1.63, numerically evaluated for $v \ll c$. In (a) and (b) we represent graphically the field iso-intensity surfaces, which, in the considered case, result in being (as expected) just spherical.

of elementary particles and quantum physics – in a deeper comprehension of de Broglie's and Schroedinger's wave mechanics, and of the corpuscle/wave duality. With regard to the fact that the *simplest* subluminal NDWs, solutions to the wave equation, are ''ball-like,'' let us present in Figure 1.14, in ordinary 3D space, the general shape of the simple Mackinnon's solutions, as expressed by Equation 1.63 for $v \ll c$. In such figures we depict graphically the field iso-intensity surfaces, which (as expected) result in being just spherical in the considered case.

We have also seen, among the others, that, even if our first method (Section 1.5.1) cannot *directly* yield zero-speed envelopes, such envelopes ''at rest,'' Equation 1.80, can, however, be obtained by applying a v-speed LT to Equation 1.69. In this way, one starts from many frequencies (Equation 1.69) and ends up with one frequency only (Equation 1.80), as b gets transformed into *the* frequency of the monochromatic beam. Let us add a warning: the topic of superluminal LTs is a delicate one [89, 103, 106, 110], to the extent that the majority of the recent attempts to re-address this question and its applications (see, e.g., [35] and references therein) risk being defective; in some cases, they did not even respect the necessary covariance of the wave equation itself.

Further details on these topics can be found in [1, 11, 13, 14], where, in connection with the fact that the X-shaped pulses are endowed with superluminal peak

velocities, an overview was presented of the various experimental sectors of physics in which superluminal motions do seem to appear. Namely, a bird's-eye view was also given therein of the *experiments* performed until now with evanescent waves (and/or tunneling photons), and with the NDW solutions to the wave equations.

1.8
Non-Axially Symmetric Solutions: The Case of Higher-Order Bessel Beams

Let us stress that until now we paid here attention to exact solutions representing axially-symmetric (subluminal) pulses only, that is to say, to pulses obtained by suitable superpositions of zero-order Bessel beams.

It is, however, interesting to look also for analytic solutions representing *non-*axially symmetric subluminal pulses, which can be constructed in terms of superpositions of ν-order Bessel beams, with ν a positive integer ($\nu > 0$). This can be attempted both in the case of Section 1.5.1 (first method), and in the case of Section 1.5.3 (second method). For brevity's sake, let us take only the first method (Section 1.5.1) into consideration.

One is immediately confronted with the difficulty that *no* exact solutions are known for the integral in Equation 1.62 when $J_0(\cdot)$ is replaced with $J_\nu(\cdot)$. One can overcome this difficulty by following a simple method, which allows obtaining ''higher-order'' subluminal waves in terms of the axially-symmetric ones. Indeed, it is well-known that, if $\Psi(x, y, z, t)$ is an exact solution to the ordinary wave equation, then $\partial\Psi/\partial x$ and $\partial\Psi/\partial y$ are also exact solutions (incidentally, even $\partial^n\Psi/\partial z^n$ and $\partial^n\Psi/\partial t^n$ will be exact solutions). By contrast, when working in cylindrical coordinates, if $\Psi(\rho, \phi, z, t)$ is a solution to the wave equation, quantities $\partial\Psi/\partial\rho$ and $\partial\Psi/\partial\phi$ are *not* solutions, in general. Nevertheless, it is not difficult at all to reach the noticeable conclusion that, once $\Psi(\rho, \phi, z, t)$ is a solution, then

$$\overline{\Psi}(\rho, \phi, z, t) = e^{i\phi}\left(\frac{\partial\Psi}{\partial\rho} + \frac{i}{\rho}\frac{\partial\Psi}{\partial\phi}\right) \tag{1.91}$$

is also an exact solution! For instance, for an axially-symmetric solution of the type $\Psi = J_0(k_\rho\rho) \exp[ik_z] \exp[-i\omega t]$, Equation 1.91 yields $\overline{\Psi} = -k_\rho J_1(k_\rho\rho) \exp[i\phi] \exp[ik_z] \exp[-i\omega t]$, which is actually one more analytic solution. In other words, it is enough to start for simplicity from a zero-order Bessel beam and to apply Equation 1.91, successively, ν times, in order to get as a new solution $\overline{\Psi} = (-k_\rho)^\nu J_\nu(k_\rho\rho) \exp[i\nu\phi] \exp[ik_z] \exp[-i\omega t]$, which is a ν-order Bessel beam.

In such a way, when applying ν times Equation 1.91 to the (axially-symmetric) subluminal solution $\Psi(\rho, z, t)$ in Equations 1.67–1.69 (obtained from Equation 1.57 with spectral function $S(\omega)$), we get the subluminal non-axially symmetric pulses $\Psi_\nu(\rho, \phi, z, t)$ as new analytic solutions; consisting, as expected, of superpositions of ν-order Bessel beams:

$$\Psi_n(\rho, \phi, z, t) = \int_{\omega_-}^{\omega_+} d\omega \ S'(\omega) \ J_\nu(k_\rho\rho) \ e^{i\nu\phi} \ e^{ik_z z} \ e^{-i\omega t} \tag{1.92}$$

where $k_\rho(\omega)$ is given by Equation 1.58, and quantities $S'(\omega) = (-k_\rho(\omega))^\nu S(\omega)$ are the spectra of the new pulses. If $S(\omega)$ is centered at a certain carrier frequency (it is a Gaussian spectrum, for instance), then $S'(\omega)$ too will approximately result to be of the same type.

Now, if we wish the new solution $\Psi_\nu(\rho, \phi, z, t)$ to possess a pre-defined spectrum $S'(\omega) = F(\omega)$, we can first take Equation 1.57 and put $S(\omega) = F(\omega)/(-k_\rho(\omega))^\nu$ in its solution (1.69), and afterward apply to it, ν times, the operator $U \equiv \exp[i\phi][\partial/\partial\rho + (i/\rho)\partial/\partial\phi]$. As a result, we will obtain the desired pulse, $\Psi_\nu(\rho, \phi, z, t)$, endowed with $S'(\omega) = F(\omega)$.

An example – On starting from the subluminal axially-symmetric pulse $\Psi(\rho, z, t)$, given by Equation 1.69 with the *Gaussian* spectrum (1.70), we can get the subluminal, non-axially symmetric, exact solution $\Psi_1(\rho, \phi, z, t)$ by simply calculating

$$\Psi_1(\rho, \phi, z, t) = \frac{\partial \Psi}{\partial \rho}\, e^{i\phi} \tag{1.93}$$

which actually yields the "first-order" pulse $\Psi_1(\rho, \phi, z, t)$, which can be more compactly written in the form:

$$\Psi_1(\rho, \phi, \eta, \zeta) = 2\,\frac{b}{c}\,\nu\,\gamma^2\,\exp\left[i\frac{b}{c}\,\beta\,\gamma^2\,\eta\right]\sum_{n=-\infty}^{\infty} A_n\,\exp\left[in\frac{\pi}{\beta}\right]\psi_{1n} \tag{1.94}$$

with

$$\psi_{1n}(\rho, \phi, \eta, \zeta) \equiv \frac{b^2}{c^2}\,\gamma^2\rho\,Z^{-3}[Z\,\cos Z - \sin Z]\,e^{i\phi} \tag{1.95}$$

where

$$Z \equiv \sqrt{\frac{b^2}{c^2}\,\gamma^2\rho^2 + \left(\frac{b}{c}\,\gamma^2\zeta + n\pi\right)^2} \tag{1.96}$$

This exact solution, let us repeat, corresponds to superposition (1.92), with $S'(\omega) = k_\rho(\omega)S(\omega)$, quantity $S(\omega)$ being given by Equation 1.70. It is represented in Figure 1.15. The *pulse* intensity has a "donut-like" shape.

Let us take the liberty of recalling that in Chapter 2 of [1], in connection with the *frozen waves*, we argued about the possibility of increasing even more our control on their transverse shape also by using higher-order Bessel beams in the FW fundamental superposition Equation 2.74 in [1]. That new approach can be understood and accepted on the basis of simple and intuitive arguments, which can be found in [12].

In Chapter 2 of [1] we showed for example how to obtain a *cylindrical surface of "static" light*, in correspondence with a chosen space interval $0 \leq z \leq L$ (for instance, with $L = 238$ μm).

Figure 1.16 depicts the longitudinal intensity pattern as it was approximately obtained, shifted from $\rho = 0$ to a different value of ρ (in this case, $\rho = 7.75$ μm). Indeed, the resulting field resembles a cylindrical surface of "static" light with a radius of 7.75 μm and length of 238 μm.

$$|\Psi \, (\rho, \, \phi, \, \eta, \, \zeta)|^2$$
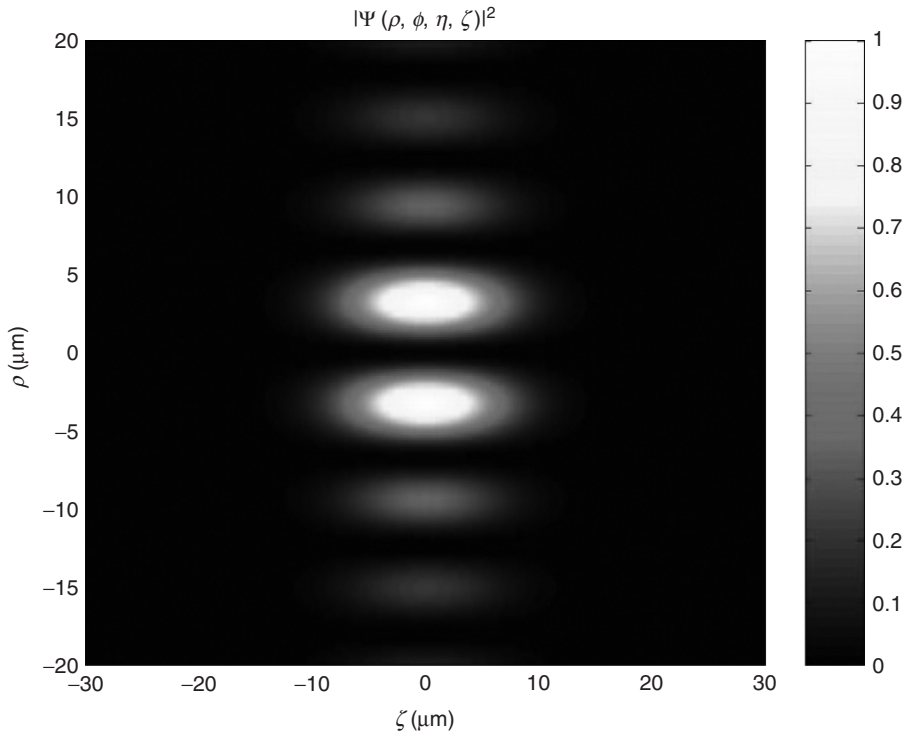
Figure 1.15 Orthogonal projection of the field intensity corresponding to the higher order subluminal *pulse* represented by the exact solution Equation 1.93, quantity Ψ being given by Equation 1.69 with the Gaussian spectrum (1.70). This time, the pulse intensity happens to have a "donut"-like shape.

1.9
An Application to Biomedical Optics: NDWs and the GLMT (Generalized Lorenz-Mie Theory)

Earlier, we mentioned, in several places, the possible applications of NDWs, quoting even a patent of ours [8] regarding FWs. Let us exploit here at least the theoretical aspects of an application in biomedical optics.

As we know, NDWs have become a hot topic in a variety of fields. Let us recall, in particular, that their use, replacing laser beams for achieving multiple traps, has found many potential applications in medicine and biomedicine [112–116]. Even though their multi-ringed structure is not suitable for an effective 3D trap when single beam set-ups are employed, nevertheless, with today techniques for their generation and real-time control, non-diffracting beams have become (better then focused Gaussian beams or others) indispensable "laser-type" beams for biological studies by means of optical tweezing and micromanipulation techniques.

The theory involved in optical trapping and micromanipulation (for a review see, e.g., [117]) is strongly dependent on the relative size and electromagnetic
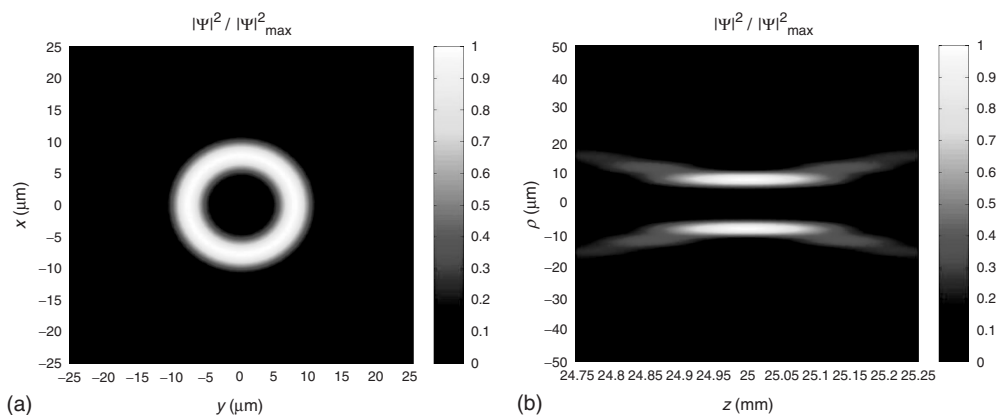
Figure 1.16 (a) Transverse section at $z = L/2$ of the considered higher-order FW. (b) Orthogonal projection of the three-dimensional intensity pattern of the same higher-order FW. Indeed, the resulting field resembles a cylindrical surface of ''static'' light with the chosen radius of 7.75 µm (and the chosen length of 238 µm).

parameters of the scatterer, which is, in general, assumed to have some symmetric shape (sphere, cylinder, ellipsis, etc.). If we take the electromagnetic properties of the particle and of the surrounding medium to be of the same order (as usually happens for biological particles immersed in water or oil), two situations are of particular theoretical interest: the possibility of avoiding, or just eliminating, too large an amount of algebra or numerical calculations.

The first one is met when the size parameter s of the scatterer is much larger than the wavelength λ of the wave ($s \gg \lambda$), so that geometrical optics considerations become the fastest and most convenient way to find out the physical properties of interest [116, 118–120].

The second one, however, concerns very small particles, that is scatterers whose overall dimension may be considered a small fraction of the wavelength ($s \ll \lambda$), so that the Rayleigh theory becomes the most suitable theoretical approach for solving the associated scattering problem [121]. Indeed, both the ray optics method and the Rayleigh theory are extremely accurate within their range of validity, and remain valid for any incident wave (as long as it is adequately modeled).

However, for s close to 1, it results to be difficult to formulate analytic closed-form expressions for the physical properties of interest. In this particular situation none of the two aforementioned approaches is of any help, and one is forced to adopt alternative approaches or techniques, such as the so-called Lorenz−Mie theory (for plane waves and spherical particles) or its generalized version, the GLMT [122−125] for arbitrary wave fields. We adopt the GLMT in this section mainly because it seems to be the most established numerical/theoretical formalism for arbitrary-sized particles in scattering problems (for further methods see, for instance, [126] and references therein).

In the framework of the GLMT and for spherical scatterers, a v-th order paraxial Bessel beam

$$\psi = J_v(k_\rho \rho) \exp \ (i\omega t) \exp \ (iv\phi) \tag{1.97}$$

must be described in terms of the beam-shape coefficients (BSCs) $g^m_{n,\mathrm{TM}}$ and $g^m_{n,\mathrm{TE}}$ (n, m being integers), because of the mathematical structure commonly used for the incident electromagnetic field (which is based on power series expansions in terms of vector spherical harmonics [126]). The BSCs are, thus, the coefficients of such expansion and are responsible for an adequate description of the spatial intensity profile of the wave.

Much effort has been made during the last few years to get reliable and useful descriptions of scalar Bessel beams, envisioning optical trapping and micromanipulation, particle sizing applications and so on. In fact, if the radial component of the electric field, E_R, is given, or known, then the BSCs $g^m_{n,\mathrm{TM}}$ will read [126], in a spherical coordinate system whose origin coincides with the center of the particle, as:

$$\begin{aligned}
g^m_{n,\mathrm{TM}} &= \frac{(2n+1)^2}{2\pi^2 n(n+1)c^{pw}_n} \frac{(n-|m|)!}{(n+|m|)!} \int_0^{2\pi} \int_0^{\pi} \int_0^{\infty} \frac{E_R(r,\theta,\phi)}{E_0} r \Psi_n^{(1)}(kr) \\
&\times P_n^{|m|}(\cos\theta) \exp \ (-im\phi) \sin\theta \ \mathrm{d}(kr) \ \mathrm{d}\theta \ \mathrm{d}\phi
\end{aligned} \tag{1.98}$$

or

$$\begin{aligned}
g^m_{n,\mathrm{TM}} &= \frac{2n+1}{4\pi n(n+1)c^{pw}_n} \frac{(n-|m|)!}{(n+|m|)!} \frac{a}{\Psi_n^{(1)}(ka)} \int_0^{2\pi} \int_0^{\pi} \frac{E_R(r=a,\theta,\phi)}{E_0} \\
&\times P_n^{|m|}(\cos\theta) \exp \ (-im\phi) \sin\theta \ \mathrm{d}\theta \ \mathrm{d}\phi
\end{aligned} \tag{1.99}$$

where Equation (1.99) follows from a suitable choice of the spatial parameter a. In the above expressions, $c^{pw}_n = (-i)^{n+1}(2n+1)/(kn(n+1))$, while k is the wave number in the external medium, and the $\Psi_n^{(1)}$ are spherical Bessel functions; finally, quantities $P_n^{|m|}(\cos\theta)$ are the associated Legendre polynomials and E_0 the electric field strength. The coefficients $g^m_{n,\mathrm{TE}}$ follow from similar considerations.

Unless Equation (1.98) or Equation (1.99) are numerically evaluated, they a priori give us no direct insight into the behavior of the BSCs $g^m_{n,\mathrm{TM}}$ and $g^m_{n,\mathrm{TE}}$, which may or may not be written in terms of any of the following parameters or values: n, m, the size-parameter s, the *spot* $\Delta\rho$ of the impinging Bessel beam, and the perpendicular distance ρ_0 between the optical axis of the beam and the center of the particle. Several researchers have devoted time to the derivation of numerically efficient and fast computing techniques and formulae, instead of simply implementing recursive algorithms for computing triple and double integrations as given by (1.98) and (1.99), respectively [127−131].

We have recently shown that, in spherical coordinates, a scalar ordinary Bessel beam can be accurately described by means of what has been called [132] integral localized approximation (ILA), a method that considerably revolutionized the numerical aspects of the GLMT by making it possible to obtain, in a numerically-efficient way, closed-form expressions [127−133] for the BSCs. For example, a zero-order Bessel beam propagating along axiz z and polarized along x, when

displaced along the x-direction of a distance $\rho_0 = x_0$, has its BSCs, $g_{n,\text{TM}}^m$ and $g_{n,\text{TE}}^m$ given by the simple expressions [132]:

$$g_{n,\text{TM}}^0 = i\frac{2n(n+1)}{2n+1}J_1(\overline{\omega})J_1(\xi)\exp\ (ik_z z_0) \tag{1.100}$$

$$g_{n,\text{TM}}^{m\neq 0} = \frac{1}{2}\left(\frac{-2i}{2n+1}\right)^{|m|-1}$$
$$\times [J_{|m|-1}(\overline{\omega})J_{|m|-1}(\xi) + J_{|m|+1}(\overline{\omega})J_{|m|+1}(\xi)]\exp\ (ik_z z_0) \tag{1.101}$$

$$g_{n,\text{TE}}^0 = 0 \tag{1.102}$$

$$g_{n,\text{TE}}^{\pm|m|\neq 0} = \frac{\mp i}{2}\left(\frac{-2i}{2n+1}\right)^{|m|-1}$$
$$\times [J_{|m|-1}(\overline{\omega})J_{|m|-1}(\xi) - J_{|m|+1}(\overline{\omega})J_{|m|+1}(\xi)]\exp\ (ik_z z_0) \tag{1.103}$$

quantity k_z being the longitudinal wave number, z_0 a constant that accounts for the correct phase of the wave at some observation point, $\overline{\omega} = (n + 1/2)\sin\theta_a$, and $\xi = x_0 k \sin\theta_a$ (θ_a being the axicon angle). Once the BSCs have been found, all the electromagnetic field components can be readily obtained by using double summation expressions [126]. For instance, E_R reads

$$E_r(r,\theta,\phi) = -iE_0\sum_{n=1}^{\infty}(-i)^n(2n+1)\frac{\Psi_n^{(1)}(kr)}{kr}\sum_{m=-n}^{n}g_{n,\text{TM}}^m\pi_n^{|m|}(\theta)\sin\theta\exp\ (im\phi) \tag{1.104}$$

whose original value E_x is given by (1.104) when imposing $E_x = E_r(r = |x_0|, \theta = \pi/2, \phi = 0)$ for $x > 0$ and $E_x = E_R(r = |x_0|, \theta = \pi/2, \phi = \pi)$ for $x < 0$, as we have depicted in Figure 1.17. Unfortunately, the higher the radial displacement ρ_0 of the beam relative to the particle, the higher the number of BSCs that come into play in Equtions 1.100–1.104, or, more generally, in the evaluation of all the physical properties of interest (radiation pressure cross-sections, torques, spatial intensity distribution, and so on). Nevertheless, Equations 1.100–1.103 can speed up numerical calculations by a factor of 100, or even 1000, w.r.t. that expected from a direct use of (1.98) and (1.99) [132]. With such a fast computing technique, together with equivalent expressions for some other specific polarizations, some of the most fundamental trapping properties of (absorbent or lossless) arbitrary size spheres, simple or stratified, with positive or negative refractive indexes have been investigated: The results being more or less in accordance with what should be expected in a real experiment [126, 132, 134, 135]. By "more or less" we mean that the ILA *does not* predict the changes in the intensity profile of the beam, after its passage through the lens system and the objective of the microscope, and so on (a good theoretical approach to this case has recently been demonstrated for a focused Gaussian beam [136, 137]).
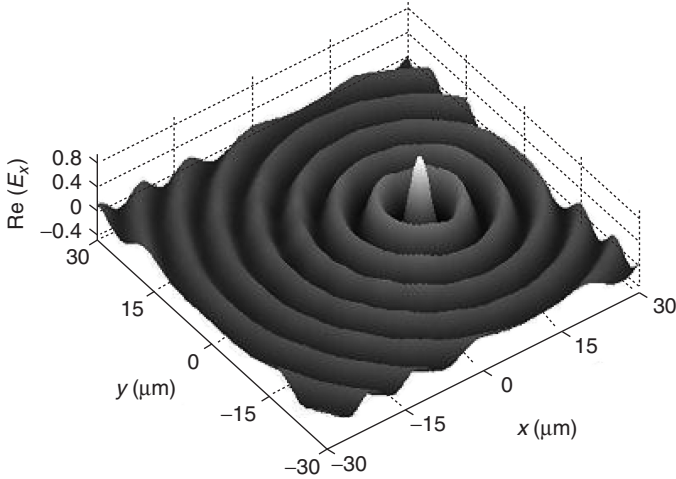
Figure 1.17 The E_x component generated by the generalized Lorenz−Mie theory for an ordinary Bessel beam with $\lambda = 532$ μm. The axicon angle θ_a was chosen to be $5°$, a limiting number for which the paraxial approximation may still be considered valid.

The same approach was more recently applied for the BSCs of higher order Bessel beams, under the paraxial approximation, for studying the optical forces exerted over biological cells [135]. Even though the paraxial restriction may not be adequate in some cases, it allows one to rapidly evaluate the angular and linear momentum transfer characteristics for a wide range of spherical-like, simple or stratified structures and biological particles. Incidentally, if the beam is an authentic ''Maxwellian wave'' (which is not the case for a Gaussian beam), the ILA provides a fast and reliable alternative for investigating scattering problems within the GLMT. It should be emphasized that the formulation in [136, 137] leads to analytical BSC expressions similar to those given by Equations 1.100 and 1.101, thus demonstrating how close the ILA outputs are to the exact quadrature expressions, (1.98) and (1.99) or, equivalently, to what is provided in [136].

One of the particularities of the GLMT is that, when the incident beam is replaced by another one with different parameter *s*, all subsequent formulae and numerical code remain unchanged, avoiding redefinition or inclusion of additional lines in the numerical algorithm, which contains the expressions for the physical parameters to be calculated. Further, once the BSCs for a given Bessel beam are given, any impinging wave constructed by means of a suitable superposition of them can also be easily described and investigated. This is of great interest in the case of static (zero speed) longitudinal intensity patterns, generated by superposing *N* equal-frequency zero-order Bessel beams with different longitudinal wave number – which is the interesting case [4] of the FWs (whose experimental production has been recently realized, let us repeat, for the case of longitudinal intervals of the order [105] of 1 m). Notice that the BSCs of paraxial FWs would simply involve a summation of *N* individual BSCs, each one adequately weighted in order to model
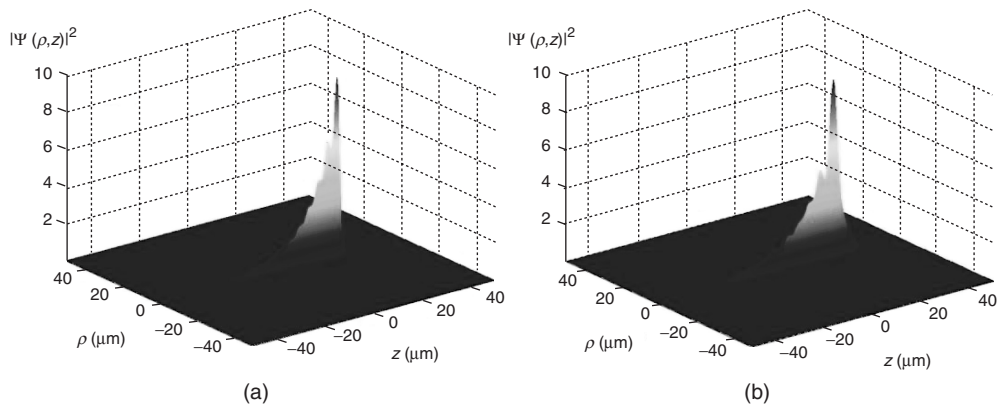
Figure 1.18 (a) A frozen wave with exponential growth, generated by the method in [87] through a superposition of Bessel beams, all with the same frequency $\omega = 6.12 \times 10^{15}$ Hz. (b) Same as (a), but now using integral localized approximation for computing the beam-shape coefficients of each Bessel beam.

some pre-chosen longitudinal intensity pattern. This simple and direct technique enables the description of FWs for a large number of potential applications, as already mentioned elsewhere. Figure 1.18 reveals, for example, the equivalent of the longitudinal exponential intensity pattern first introduced in [4] for mid-range purposes. It is clearly seen that, indeed, the GLMT is capable of handling this new class of ''laser beams'' and provides pretty good results for its associated optical properties, such as the longitudinal radiation pressure cross-section profile of Figure 1.18, as shown in Figure 1.19.

The transverse intensity control provided by the superposition of higher order Bessel beams could also be taken into account by using the analytic expressions for the BSCs, provided, for example, in [135] for single Bessel beams. Finally, future theoretical work may allow one to deal with both scalar and vector FWs, as it is understandable that, once an accurate description of arbitrary order scalar Bessel beams is given, their equivalent vector fields are somehow functions of those same Bessel functions that enter into their expressions, and that can therefore be described by the GLMT in terms of their field components [116, 138].

Bessel beams have also been theoretically introduced as one of the first ''laser beam'' for studying the mechanical properties of simple negative refractive-index (NRI) scatterers [86, 134]. For such particles, the matching condition (i.e., the identity of the impedance of the external medium with that of the particle) is known to produce non-zero radial and scattering optical forces, even if the wave suffers no reflection at the surface of the sphere, in contrast with the ordinary case of positive refractive index particles [139–141]. Using Bessel beams (both in the ray optics and in the GLMT) it has been possible to show, for example, that a given NRI spherical particle can radially be either attracted by or repelled from the bright or dark annular intensity disks. This behavior being strongly affected by how the incident wave distributes itself in space, that is, by its spot and relative transverse distance.
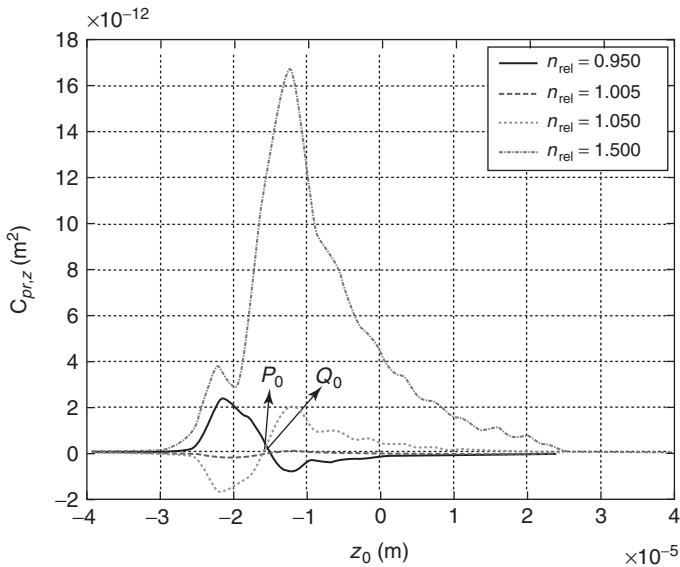
Figure 1.19 Radiation pressure cross-section exerted on a spherical dielectric particle of radius $a = 3.75$ μm as a function of its relative refractive index and of the distance z_0 from $z = 0$. The external medium is assumed to be water. Points of longitudinal stable equilibrium are denoted by P_0 and Q_0.

If the medium inside which the particle is embedded is lossy (or if the scatterer itself is absorbent), it is also possible to conceive the incorporation of diffraction-attenuation resistant beams (DARBs) into some optical tweezers set-up [5, 87], so that any pre-fixed longitudinal intensity provides the experimentalist with the expected optical properties. However, the generation and implementation of DARBs for arbitrary-range applications are still open problems.

1.10
Soliton-Like Solutions to the Ordinary Schroedinger Equation within Standard Quantum Mechanics (QM)

As we know, not only non-linear, but also a large class of linear equations (including the wave equations) admit ''soliton-like'' solutions, which propagate without distortion in one direction. In the case of the (linear) wave equations, for such soliton-like solutions we have used the name of NDWs. It was soon thought that, as these solutions to the wave equations are non-diffracting and particle-like, they are a priori suitable, more than Gaussian's, for describing elementary particle motion, and may well be related with their wave nature [28, 37]. In fact, localized solutions were soon found also for Klein–Gordon and for Dirac equations [28, 37]. In this section we show [3] that, *mutatis mutandis*, non-diffracting solutions exist even for the ordinary (linear) Schroedinger equation within standard quantum

mechanics; where we may obtain both approximate and exact solutions. In the ideal case such solutions (even if localized, and "decaying") are not square-integrable, analogously to plane or spherical waves: one has to show therefore how to obtain finite-energy solutions. The approach can, of course, be extended to a particle moving in the presence of a potential [3].

Little work [38] was done in the past for the case of the ordinary *Schroedinger* equation; see, for example [29, 37]. Indeed, the Schroedinger case is different, as the relation between the energy E and the impulse magnitude $p \equiv |p|$ is quadratic [$E = p^2/(2m)$] in non-relativistic cases, like in Schroedinger's, at variance with the relativistic ones. We might mention that many non-diffracting (especially X-shaped) solutions have been constructed for the linear [41] or nonlinear [42] equations that in optics bear the name of "Schroedinger equation", even if they are mathematically very different from the ordinary Schroedinger's. Moreover, a special kind of non-diffracting packet solutions, in terms of Airy functions, were found in the 1970s for the case of the actual 1D Schroedinger equation and later extended to the 3D case. All that has been recently applied to the case of optics, originating from the discovery of Airy-type waves, now well-known for their remarkable properties [142–146]: Such Airy waves are solutions, once more, to the so-called (linear) Schroedinger equation of optics. But, as we were saying, the non-diffracting solutions to the ordinary Schroedinger equation, within standard quantam machines, are quite apt at describing elementary particles. They will result to be very different from the ones found in optics, both for the mentioned fact that the optical Schroedinger equation is mathematically different from the ordinary Schroedinger equation, and for the fact that our approach and methods are quite different from the ones adopted in optics.

Before going on, let us first recall that in the time-independent realm – or, rather, when the dependence on time is only harmonic, that is, for monochromatic solutions – the (quantum, non-relativistic) Schroedinger equation happens to be mathematically identical to the (classical, relativistic) Helmholtz equation [147–150]. And many trains of localized X-shaped pulses have been found as *superpositions* of solutions to the Helmholtz equation, which propagate, for instance, along cylindrical or co-axial waveguides [66]; however, we shall skip all the cases [67, 68] of this type, as we are concerned here with propagation in free space, even when in the presence of an ordinary potential. Let us also mention that, in the general time-*dependent* case, that is, in the case of pulses, the Schroedinger and the ordinary wave equation are no longer mathematically identical, as the time derivative results are to be of the first order in the former and of the second order in the latter. (It has been shown, nevertheless, that at least in some cases they still share various classes of analogous solutions, differing only in their spreading properties [148]). Moreover, the Schroedinger equation implies the existence of an *intrinsic* dispersion relation, even for free particles; this is another difference to pay attention to: the solutions to the wave equation suffer only diffraction (and no dispersion) in the vacuum, while those of the Schroedinger equation suffer also (an intrinsic) dispersion even in the vacuum.

1.10.1
Bessel *Beams* as Non-Diffracting Solutions (NDS) to the Schroedinger Equation

Let us consider the Schroedinger equation for a free particle (an electron, for example)

$$\overset{2}{\nabla}\psi + \frac{2im}{\hbar}\,\frac{\partial\psi}{\partial t} = 0 \tag{1.105}$$

If we confine ourselves to solutions of the type

$$\psi(\rho, z, \varphi; t) = F(\rho, z, \varphi)\,e^{-iEt/\hbar}$$

their spatial part F is known to obey the reduced equation $\nabla^2 F + k^2 F = 0$, with $k^2 \equiv p^2/\hbar^2$ and $p^2 = 2mE$ (quantity $p \equiv |\boldsymbol{p}|$ being the particle momentum and therefore $k \equiv |\boldsymbol{k}|$ the total wavenumber). Such a reduced equation is nothing but the Helmholtz equation, for which various simple localized-beam solutions are already known: In particular, the so-called Bessel beams, which have been experimentally produced since long time. Actually, let us look – as usual – for factorized solutions (in the simple case of cylindrical symmetry w.r.t. the z-axis), by supposing the constant longitudinal wavenumber $k_z \equiv p_z/\hbar$. (As the present formalism is used both in quantum mechanics and in electromagnetism, with a difference in the customary nomenclature, for clarity's sake let us here stress that $k \equiv p/\hbar; k_\rho \equiv k_\perp \equiv p_\perp/\hbar; \omega \equiv E/\hbar$; while $k_z \equiv k_\parallel = p_\parallel/\hbar \equiv p_z/\hbar$ is often represented by the (for us) ambiguous symbol β). As a consequence, the (transverse) wavefunction obeys a Bessel differential equation, in which it enters the constant transverse wavenumber $k_\rho \equiv p_\rho/\hbar$ with the *condition* $k_\rho^2 = k^2 - k_z^2 \equiv 2mE/\hbar^2 - k_z^2$. To avoid any divergencies, it must be $k_\rho^2 \geq 0$, that is $k^2 \geq k_z^2$; namely, it must hold (see Figure 1.1 in [3]) the constraint

$$E \geq \frac{p_z^2}{2m}$$

A simple solution is therefore [$p \equiv \hbar k$]:

$$\psi(\rho, z; t) = J_0(\rho p_\rho/\hbar)\,\exp\,[i(zp_z - Et)/\hbar] \tag{1.106}$$

together with the above condition. *Equation 1.106 can be regarded as a Bessel beam solution to the Schroedinger equation* (the other Bessel functions are not acceptable here because of their divergence at $\rho = 0$ or for $\rho \to \infty$), with forward propagation (i.e., positive z-direction) for $k_z > 0$. This result is not surprising as – once we suppose the whole time variation to be expressed by the function $\exp\,[i\omega t]$ – both the ordinary wave equation and the Schroedinger equation transform into the Helmholtz equation. Actually, the only difference between the Bessel beam solutions to the wave equation and to the Schroedinger equation consists of the different relationships among frequency, longitudinal, and transverse wavenumber. In other words (with $E \equiv \omega\hbar$):

$$p_\rho^2 = E^2/c^2 - p_z^2, \qquad \text{for the wave equation} \tag{1.107}$$

$$p_\rho^2 = 2mE - p_z^2, \quad \text{for the Schroedinger equation} \tag{1.108}$$

Table 1.1 Comparison of some quantities relevant in the case of a Bessel beam of photons and a Bessel beam of particles (say, electrons), respectively.

Wave equation	Schroedinger equation
$k = \frac{\omega}{c}$	$p = \sqrt{2mE}$
$k_\rho \simeq \frac{r}{f}\,k$	$p_\rho \simeq \frac{r}{f}\,p$
$k_\rho^2 = \frac{\omega^2}{c^2} - k_z^2$	$p_\rho^2 = 2mE - p_z^2$
$k_z^2 = \frac{\omega^2}{c^2}\left(1 - \frac{r^2}{f^2}\right)$	$p_z^2 = 2mE\left(1 - \frac{r^2}{f^2}\right)$

In the case of beams, the experimental production of NDSs to the Schroedinger equation can be *similar* to the one exploited for the NDSs to the wave equations (e.g. in optics or acoustics); see, for example, Figure 1.2 in [50] and references therein, where the simple case of a source consisting in an array of circular slits, or rings, was considered.[4] In Table 1.1 we refer to a Bessel beam of photons and a Bessel beam of for example electrons, respectively. We list therein the relevant quantities having a role, for example in electromagnetism, and the corresponding ones for the Schroedinger equation's spatial part $\hbar^2\nabla^2 F + 2mE\ F = 0$, with $F = R(\rho)\ Z(z)$. The second and the fourth lines have been written down for the so-called simple Durnin *et al.* case, when the Bessel beam is produced by an annular slit (illuminated by a plane wave) located at the focus of a lens [43–46].

In Table 1.1, quantity f is the focal distance of the lens (for instance, an ordinary lens in optics and a magnetic lens in the case of Schroedinger charged wavepackets), and r is the radius of the considered ring. [In connection with the last line of Table 1.1, let us recall that in the wave equation case the phase-velocity ω/k_z is almost independent of the frequency (at least for limited frequency intervals, like in optics), and one gets a constant group-velocity and an easy way to build up X-shaped waves. By contrast, in the Schroedinger case, the phase-velocity of each (monochromatic) Bessel beam depends on the frequency, which makes it difficult to generate an ''X-wave'' (i.e. a wave depending on z and t only via the quantity $z - Vt$) by using simple methods, as per Durnin *et al.*, based on the Bessel beams' superposition. In the case of charged particles, one should compensate such a velocity variation by suitably modifying the focal distance f of the Durnin's lens, for example on having recourse to an additional magnetic, or electric, lens].

Before going on, let us stress that one could easily eliminate the restriction of axial symmetry. In such a case, in fact, solution (1.106) would become

$$\psi(\rho, z, \varphi; t) = J_n(\rho p_\rho/\hbar)e^{izp_z/\hbar}\ e^{-iEt/\hbar}\ e^{in\varphi}$$

4) For pulses, however, the generation technique must deviate from optics, as in the Schroedinger equation case the phase velocity of the Bessel beams produced through an annular slit would depend on the energy.

with n an integer. The investigation of not cylindrically-symmetric solutions is interesting, especially in the case of localized *pulses*; and we shall deal with them in the following.

1.10.2
Exact Non-Diffracting Solutions to the Schroedinger Equation

Coming to the problem of finding out "soliton-like" solutions to the *ordinary* Schroedinger equation, let us switch to a more comprehensive formalism. Namely, in cylindrical coordinates and neglecting evanescent waves, a quite general function ψ of ρ, ϕ, z and t, expressed in terms of Fourier and Hankel transformations, can be written as:

$$\Psi(\rho, \phi, z, t) = \sum_{n=-\infty}^{\infty} \left[\int_0^\infty dk_\rho \int_{-\infty}^\infty dk_z \int_{-\infty}^\infty d\omega \, k_\rho A'_n(k_\rho, k_z, \omega) J_n(k_\rho \rho) e^{ik_z z} e^{-i\omega t} e^{in\phi} \right]$$

(1.109)

Notice that the last equation is nothing but Equation 1.5 in Section 1.1.3 when having in mind a rather general, ideal solution to linear, homogeneous wave equations in free space (still disregarding the evanecsent sector). The essential point, for Equation 1.109 to represent a (general) solution to the Scroedinger equation, is imposing now that the $A_n(k_z, \omega)$ be given by

$$A'_n(k_\rho, k_z, \omega) = A_n(k_z, \omega) \, \delta \left[k_\rho^2 - \left(\frac{2m\omega}{\hbar} - k_z^2 \right) \right]$$

(1.110)

We request moreover that

$$A_n(k_z, \omega) = \sum_{n=-\infty}^{\infty} S_{mn} \, \delta[\omega - (Vk_z + b'_m)]$$

(1.111)

with

$$b'_m = \frac{2m\pi V}{\Delta z_0}$$

(1.112)

The last two equations guarantee that the general solution (1.109) to Equation 1.105 is a NDW, that is a wave capable of indefinitely keeping its spatial shape while propagating. Let us recall that such a property, when assuming propagation in the z-direction, may be mathematically expressed as in Equation 1.7 where Δz_0 is a chosen length, and V is the pulse peak-velocity, with $0 \leq V \leq \infty$. For the moment, the meaning of the spectral parameters k_z, k_ρ, ω appearing above is not important, as they are dumb integration variables.

Notice that in the general solution (1.109), together with Equations 110–112, all Bessel functions $J_n(k_\rho \rho)$, with any n, appear. Just for simplicity, however, we can choose

$$S_{mn} = S'(\omega) \, \delta_{0n} \, \delta_{lm}$$

(1.113)

where the δ s are now Kronecker's symbols and l is a positive integer, so as to reduce ourselves to the mere case of zeroth-order Bessel functions. As we are now dealing with quantum mechanics, let us go on to the new notations

$$k \equiv p/\hbar; \; k_\rho \equiv p_\rho/\hbar; \; k_z \equiv p_z/\hbar; \; \omega \equiv E/\hbar$$

and put $b_l' = 2l\pi V/\Delta z_0 \equiv b/\hbar$.

As the present formalism is used both in quantum mechanics and in electromagnetism, with a difference in the customary nomenclature, for clarity's sake let us repeat once more that $k \equiv p/\hbar; \; k_\rho \equiv k_\perp \equiv p_\rho/\hbar; \; \omega \equiv E/\hbar;$ while $k_z \equiv k_\parallel \equiv p_\parallel/\hbar \equiv p_z/\hbar$.

We can now integrate Equation 1.109 in k_ρ and in k_z, obtaining non-diffracting solutions to the Schroedinger equation as the following superpositions (integrations over the frequency, or the energy) of Bessel-beam solutions [with $b \geq 0$]:

$$\Psi(\rho, z, \zeta) = e^{\frac{-ib}{\hbar V} z} \int_{E_-}^{E_+} dE \, J_0(\rho p_\rho/\hbar) \, S(E) \, e^{i\frac{E}{\hbar V}\zeta} \tag{1.114}$$

where it is still

$$\zeta \equiv z - Vt \tag{1.115}$$

while

$$p_\rho = \frac{1}{V} \sqrt{-E^2 + (2mV^2 + 2b)E - b^2} \tag{1.116}$$

and

$$E_\pm = mV^2 \left(1 \pm \sqrt{1 + \frac{2b}{mV^2}} \right) + b \tag{1.117}$$

Notice that Equation 1.114 (as well as in subsequent equations), the solution Ψ depends on z, besides via ζ only via a phase factor; the modulus $|\Psi|$ of Ψ goes on depending on z (and on t) only through the variable $\zeta \equiv z - Vt$. This means, as we already know, that the magnitude of each solution does not change during propagation, that is the solutions are NDWs and keep their shape while traveling.

The simple integral solution (1.114), which yields non-diffracting solutions with azimutal symmetry, admits of a simple physical interpretation: it implies integrating the Bessel beams $J_0(\rho p_\rho/\hbar) \exp[i\frac{p_z}{\hbar}\zeta] \exp[i\frac{E}{\hbar}t]$, with $p_\rho = \sqrt{2mE - p_z^2}$, in the interval $E_- \leq E \leq E_+$ along the *straight line* $E = Vp_z + b$: This is known to eliminate evanescent waves (Figure 1.20).

Examples. An interesting solution to Equation 1.114 is, for instance, obtained when assuming the *real* exponential spectrum

$$S(E) = s_0 \, \exp[a(E - E_+)] \tag{1.118}$$

a being a positive number, as well as s_0. On integrating [3], we get [$\mathcal{N}$ being a constant]:

$$\Psi(\rho, \eta, \zeta) = \mathcal{N} s_0 2V\sqrt{P} \, \exp[i\frac{mV}{\hbar}\eta] \exp[-aV\sqrt{P}] \frac{\sin Y}{Y} \tag{1.119}$$
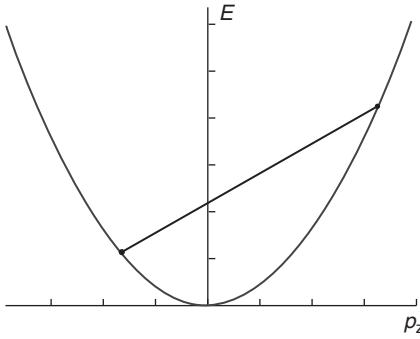
Figure 1.20 The allowed region is the one internal to the parabola, since (to avoid divergencies) it must be $E \geq p_z^2/(2m)$. In this case, the parabola and the chosen straight-line have equations $E = p_z^2/(2m)$ and $E = Vp_z + b$, respectively. The two values of the intersections of this straight-line with the parabola are given in Equation 1.117. Inside the parabola $p_\rho^2 \geq 0$.

where

$$Y \equiv \frac{\sqrt{P}}{\hbar} \sqrt{\rho^2 - (\hbar a V + i\zeta)^2} \tag{1.120}$$

and $P \equiv m^2 V^2 + 2mb$, while $\eta \equiv z - vt$ is a function of b. Notice that for $a = 0$, one ends up with a solution similar to Mackinnon's [31]. Equations 1.119, 1.120 are the simplest closed-form non-diffracting solution to the Schroedinger equation. In Figure 1.3 of [3] we depicted its square magnitude when choosing, for simplicity, $b = 0$ (namely, Figure 3a therein corresponds to $a = E_+/5$, while Figure 3b therein corresponds to $a = 5E_+$).

Some physical (interesting) comments on such results will appear elsewhere. Here, let us only add a few brief comments, illustrated by some more figures. Let us first recall that the non-diffracting solutions to the ordinary wave equations resulted in being roughly *ball-like* when their peak-velocity was subluminal [19, 89], and *X-shaped* [9, 14, 89] when superluminal. Now, let us see what happens in the different case of the Schroedinger equation. Normalizing ρ and ζ, we can write Equation 1.120 as

$$Y = \sqrt{\rho'^2 - (\overline{A} + i\zeta')^2}$$

with $\rho' \equiv \sqrt{P}\rho/\hbar$ and $\zeta' \equiv \sqrt{P}\zeta/\hbar$, while $\overline{A} \equiv aA = \sqrt{P}aV$. For simplicity, let us stick to the case $b = 0$; therefore, the simple relation will hold: $\overline{A} = maV^2$. For the Schroedinger equation, we can observe the following

1) If we choose $\overline{A} = 0$, which can be associated with $V = 0$, we get the solutions in Figure 1.21b, that is a mainly ball-like structure (even if, differently from the ordinary wave equation cases, an X-shaped structure does timidly start to appear).

(a)

(b)
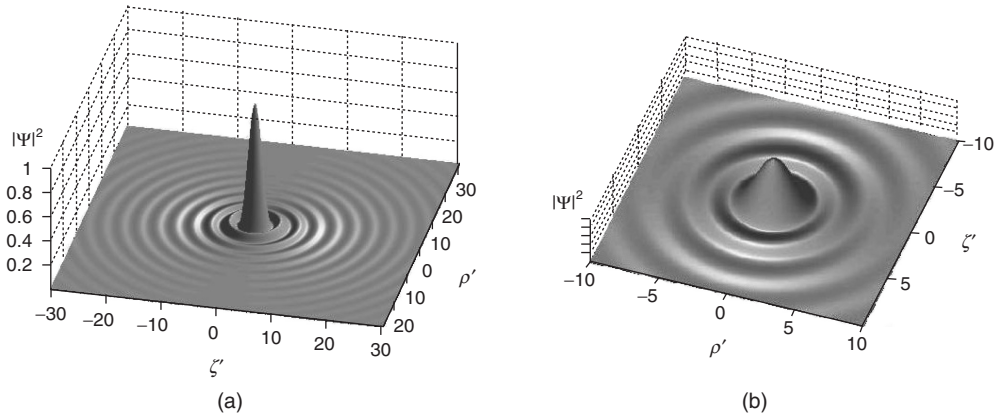
Figure 1.21 Here, and in Figure 1.22, we depict the square magnitude of elementary solutions of the type (1.119), corresponding to the *real* spectrum $S(u) = s_0 \exp [(E - E_+)a]$, as a function of $\rho' \equiv \rho \sqrt{P}/\hbar$ and of $\zeta' \equiv \zeta \sqrt{P}/\hbar$. Quantity a is a positive number (when $a = 0$ one ends up with a solutions similar to Mackinnon's [31]), while b for simplicity has be chosen equal to zero. (a) Corresponds to $a = E_+/5$. For (b), normalized w.r.t. ρ and ζ, we have still assumed for simplicity $b = 0$, so that $\overline{A} = maV^2$. More precisely, it refers to $\overline{A} = 0$ and does clearly show the "ball-like" structure one expects in such a case. It should, however, be noted that, for the Schroedinger equation, also an X-shaped structure always appears – more evident here in (a) – even in the most ball-like solutions.
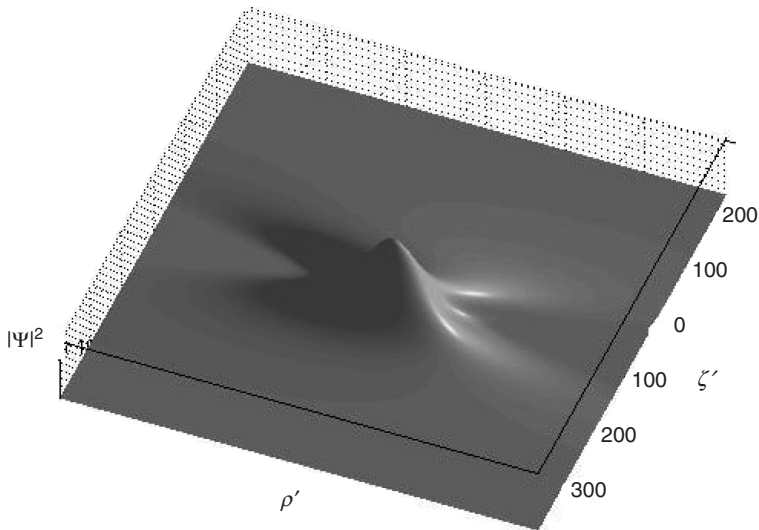
Figure 1.22 The solution, under all the previous conditions, with an increased value of $\overline{A}$, namely with $\overline{A} = 20$. An X-shaped structure more evidently appears, contributing in a more clear way to the general form of the solution (see the text).
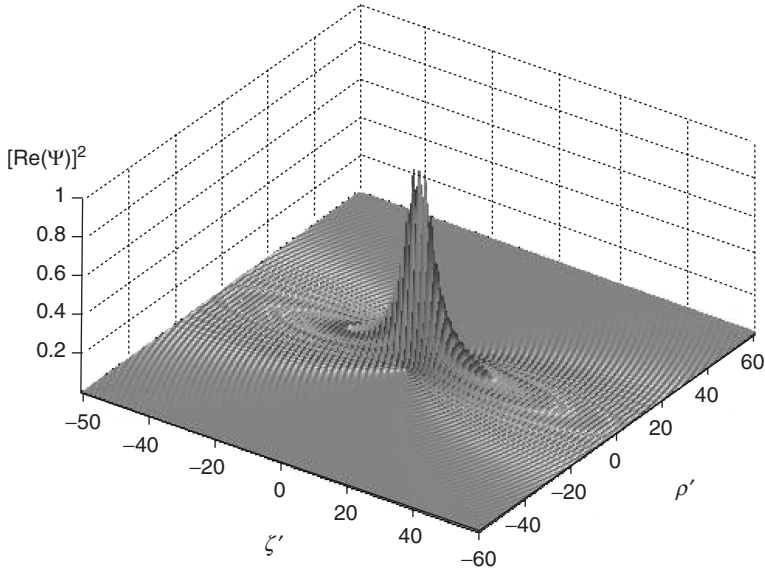
Figure 1.23 The (square of the) real part of Ψ shows, in three-dimension, also some "internal oscillations". This Figure corresponds, for example, to the value $\overline{A} = 5$.

2) If we by contrast increase the value of $\overline{A}$ by choosing, for example, $\overline{A} = 20$ (which can be associated with larger speeds), one notices that an X-shaped structure does evidently contribute. See, for example, Figure 1.22.

3) To have a preliminary idea of the "internal structure" of our soliton-like solutions to the (ordinary) Schroedinger equation, we have to plot, instead of the square magnitude of Ψ, its real or imaginary part. In Figure 1.6 of [3] we chose the square of its real part. Then, even in the $\overline{A} = 0$ case, one can start to see in those figures the appearance of the X shape, which becomes more and more evident as the value of $\overline{A}$ increases. We confine ourselves here to stress that the (square of the) real part of Ψ does also show, in 3D, some "internal oscillations"; see, for example, Figure 1.23 corresponding to the value $\overline{A} = 5$. We shall face elsewhere topics like their possible connections with the de Broglie picture of quantum particles.

1.10.3
A General Exact Localized Solution

Let us go back to the choice of spectrum $S(E)$. As in our Equation 1.114 the integration interval is limited $[E_- < E < E_+]$: In such an interval *any* spectral function $S(E)$ can be expanded into the Fourier series

$$S(E) = \sum_{n=-\infty}^{\infty} a_n \, e^{i \frac{2\pi}{D} n E} \tag{1.121}$$

with

$$a_n = \frac{1}{D} \int_{E_-}^{E_+} dE \, S(E) \, e^{-i\frac{2\pi}{D}nE} \tag{1.122}$$

quantity $S(E)$ being an *arbitrary* function, and D being still defined as $D \equiv E_+ - E_-$. Inserting Equation 1.121 into Equation 1.122, and following [3] the same procedure exploited in the previous subsection, we get the *general exact non-diffracting solution* to the Schroedinger equation in the form

$$\Psi(\rho, \eta, \zeta) = \mathcal{N} \, 2A \, e^{i\frac{mV}{\hbar}\eta} \sum_{n=-\infty}^{\infty} a_n \, \exp\left[i\frac{2\pi}{D}nB \right] \frac{\sin Z}{Z} \tag{1.123}$$

where

$$Z \equiv \sqrt{ \left(\frac{A}{\hbar V}\zeta + n\pi \right)^2 + \frac{P}{\hbar^2}\rho^2 } \tag{1.124}$$

and $A = V\sqrt{P}$; $B = mV^2 + b$, and $\mathcal{N}$ a suitable normalization constant. Notice that solution (1.123) yields non-diffracting solutions with azimuthal symmetry for whatever spectrum $S(E)$ in Equation 1.114. Moreover, it is worthwhile to note that, even when truncating the series in Equation 1.20 at a certain value $n = N$, the solutions obtained is *still* an exact non-diffracting solution to the Schroedinger equation.

We have already mentioned the problem of producing Bessel beams of electrons, instead of optical Bessel beams. As to the possible generating set-ups, an interesting problem from the experimental point of view is that in optics one starts usually from a laser source; in the case of quantum mechanics, one might have recourse to "laser beams of particles," as the ones under investigation for more than a decade.

1.11
A Brief Mention of Further Topics

1.11.1
Airy and Airy-Type Waves

Many non-diffracting (especially X-shaped) solutions have been constructed for the linear [41] or nonlinear [42] equations that in optics bear the name of "Schroedinger equation," even if they are mathematically very different from the ordinary Schroedinger's. Moreover, a special kind of non-diffracting packet solutions, in terms of Airy functions, were found in the 1970s for the case of the actual 1D Schroedinger equation, and extended later to the 3D case. All that has been recently applied to the case of optics, originating the discovery of Airy-type waves, now well-known for their remarkable properties [142–146]. Such Airy waves are solutions, once more, to the so-called (linear) Schroedinger equation of optics.

We wish to repeat here this information, for its intrinsic interest and its relevance, and for the fact that one of the following chapters of this book will be mainly devoted to the Airy waves.

The results presented in Section 1.10 are rather different, however, from the ones found in optics, both for the mentioned fact that the optical Schroedinger equation is mathematically different from the ordinary Schroedinger equation, and for the fact that our approach and methods are quite different from the ones adopted in optics.

1.11.2
"Soliton-Like" Solutions to the Einstein Equations of General Relativity and Gravitational Waves

Some interesting progress has been made by one of us (MZR) in the sector of the Einstein (nonlinearized) equations of general relativity, finding out, therefore, new possible solutions for gravitational waves. But there is no room here for presenting details.

1.11.3
Super-Resolution

Strong super-resolution effects can be attained by suitable superpositions of evanescent Bessel beams. But this topic will be reviewed elsewhere, for the tyranny of space.

Acknowledgments

References

1. Hernandez-Figueroa, H.E., Zamboni-Rached, M., and Recami, E. (eds) (2008) *Localized Waves*, John Wiley & Sons Inc., New York.

2. Recami, E. and Zamboni-Rached, M. (2011) Non-diffracting waves, and Frozen Waves: An Introduction, 121 pages online in Geophysical Imaging with Localized Waves,

Sanya, China, 2011 [UCSC, S. Cruz, Cal.], and refs. therein; available at http://es.ucsc.edu/~acti/sanya/SanyaRecamiTalk.pdf (accessed 27 April 2013).

3. Zamboin-Rached, M. and Recami, E. (2012) Soliton-like solutions to the ordinary Schroedinger Equation within standard QM. *J. Math. Phys.*, **53**, 052102.

4. Zamboni-Rached, M., Recami, E., and Hernández-Figueroa, H.E. (2005) Theory of 'Frozen Waves' [e-print physics/0502105]. *J. Opt. Soc. Am.*, **A11**, 2465–2475.

5. Zamboni-Rached, M. (2006) Diffraction-attenuation resistant beams in absorbing media. *Opt. Express*, **14**, 1804–1809.

6. Zamboni-Rached, M. (2004) Stationary optical wave fields with arbitrary longitudinal shape by superposing equal frequency Bessel beams: Frozen Waves. *Opt. Express*, **12**, 4001–4006.

7. Prego, L.J., Zamboni-Rached, M., Hernández-Figueroa, H.E., and Recami, E. (2012) Producing acoustic frozen waves: simulated experiments. *IEEE Trans. Ultrason. Ferroel. Freq. Control.*, submitted for publication.

8. Recami, E., Zamboni-Rached, M., Hernández-Figueroa, H.E., *et al.* (2011) Method and Apparatus for Producing Stationary (Intense) Wavefields of arbitrary shape. Patent, Application No. US-2011/0100880-.

9. Lu, J.-y. and Greenleaf, J.F. (1992) Non-diffracting X-waves: Exact solutions to free-space scalar wave equation and their finite aperture realizations. *IEEE Trans. Ultrason. Ferroel. Freq. Control.*, **39**, 19–31.

10. Lu, J.-y. and Greenleaf, J.F. (1992) Experimental verification of non-diffracting X-waves. *IEEE Trans. Ultrason. Ferroel. Freq. Control.*, **39**, 441–446.

11. Recami, E. and Zamboni-Rached, M. (2009) Localized waves: A review. *Adv. Imaging Electron. Phys. (AIEP)*, **156**, 235–355.

12. Zamboni-Rached, M., Recami, E., and Hernández-Figueroa, H.E. (2002) New localized Superluminal solutions to the wave equations with finite total energies and arbitrary frequencies. *Eur. Phys. J.*, **D21**, 217–228.

13. Recami, E., Zamboni-Rached, M., Nobrega, K.Z., Dartora, C.A., and Hernández-Figueroa, H.E. (2003) On the localized superluminal solutions to the Maxwell equations. *IEEE J. Sel. Top. Quantum Electron.*, **9**, 59–73.

14. Recami, E. (1998) On localized X-shaped superluminal solutions to Maxwell equations. *Physica A*, **252**, 586–610.

15. Lu, J.-y., Greenleaf, J.F., and Recami, E. (1996) Limited diffraction solutions to Maxwell (and Schroedinger) equations, (Lanl Archives e-print physics/9610012), Report INFN/FM–96/01 (I.N.F.N.; Frascati).

16. Ziolkowski, R.W., Besieris, I.M., and Shaarawi, A.M. (2000) On the superluminal propagation of X-shaped localized waves. *J. Phys. A: Math.Gen.*, **33**, 7227–7254.

17. Bateman, H. (1915) *Electrical and Optical Wave Motion*, Cambridge University Press, Cambridge.

18. Courant, R. and Hilbert, D. (1966) *Methods of Mathematical Physics*, Vol. 2, John Wiley & Sons Inc., New York, p. 760.

19. Zamboni-Rached, M. and Recami, E. (2008) Subluminal wave bullets: exact localized subluminal solutions to the wave equations [e-print arXiv:0709.2372]. *Phys. Rev.*, **A77**, 033824.

20. Sônajalg, H. and Saari, P. (1996) Suppression of temporal spread of ultrashort pulses in dispersive media by Bessel beam generators. *Opt. Lett.*, **21**, 1162–1164.

21. Sônajalg, H., Ratsep, M., and Saari, P. (1997) Demonstration of Bessel-X pulse propagating with strong lateral and longitudinal localization in a dispersive medium. *Opt. Lett.*, **22**, 310–312.

22. Zamboni-Rached, M., Nóbrega, K.Z., Hernández-Figueroa, H.E., and Recami, E. (2003) Localized Superluminal solutions to the wave equation in (vacuum or) dispersive media, for

arbitrary frequencies and with adjustable bandwidth. *Opt. Commun.*, **226**, 15–23.

23. Conti, C., Trillo, S., Valiulis, G., Piskarkas, A., van Jedrkiewicz, O., Trull, J., and Di Trapani, P. (2003) Non-linear electromagnetic X-waves. *Phys. Rev. Lett.*, **90**, 170406.

24. Salo, J., Fagerholm, J., Friberg, A.T., and Salomaa, M.M. (1999) Nondiffracting bulk-acoustic X-waves in crystals. *Phys. Rev. Lett.*, **83**, 1171–1174.

25. Salo, J. and Saloma, M.M. (2003) Nondiffracting waves in anisotropic media. *Phys. Rev.*, **E67**, 056609.

26. Salo, J. and Friberg, A.T. (2008) Propagation-invariant fields: rotationally periodic and anisotropic nondiffracting waves, in *Localized Waves*, Chapter 5, (eds H.E. Hernandez, M. Zamboni-Rached and Recami E), John Wiley & Sons, Inc., New York.

27. Sheppard, C.J.R. (2002) Generalized Bessel pulse beams. *J. Opt. Soc. Am.*, **A19**, 2218–2222.

28. Longhi, S. (2004) Localized subluminal envelope pulses in dispersive media. *Opt. Lett.*, **29**, 147–149.

29. Salo, J. and Salomaa, M.M. (2001) Subsonic nondiffracting waves. *Acoust. Res. Lett. Online*, **21** (1), 31–36.

30. Lu, J.-y. and Greenleaf, J.F. (1995) Comparison of sidelobes of limited diffraction beams and localized waves. *Acoust. Imaging*, **21**, 145–152.

31. Mackinnon, L. (1978) A nondispersive de Broglie wave packet. *Found. Phys.*, **8**, 157.

32. Rodrigues, W.A., Vaz, J., and Recami, E. (1994) Free Maxwell equations, Dirac equation, and non-dispersive de Broglie wave packets, in *Courants, Amers, Écueils en Microphysique* (ed. G.P. Lochak), Paris, pp. 379–392.

33. Lu, J.-Y. and Greenleaf, J.F. (1995) Comparison of sidelobes of limited diffraction beams and localized waves, in *Acoustic Imaging*, Vol. 21 (ed. J.P. Jones), Plenum, New York, pp. 145–152.

34. Zamboni-Rached, M., Recami, E., and Besieris, I.M. (2010) Cherenkov radiation vs X-shaped Localized Waves. *J. Opt. Soc. Am.*, **A27**, 928–934.

35. Zamboni-Rached, M., Recami, E., and Besieris, I.M. (2012) Further comments on Cherenkov versus X-waves. *J. Opt. Soc. Am.*, **A29**, 2536–2541.

36. Utkin, A.B. (2012) Droplet-shaped waves: causal finite-support analogs of X-shaped waves. *J. Opt. Soc. Am.*, **A29**, 457–462.

37. Bouchal, Z., Wagner, J., and Chlup, M. (1998) Self-reconstruction of a distorted nondiffracting beam. *Opt. Commun.*, **151**, 207–211.

38. Grunwald, R., Griebner, U., Neumann, U., and Kebbel, V. (2004) Self-recontruction of ultrashort-pulse Bessel-like X-waves. CLEO/QELS Conference, San Francisco, CA; Paper No. CMQ7.

39. Brittingham, J.N. (1983) Focus wave modes in homogeneous Maxwell's equations: transverse electric mode. *J. Appl. Phys.*, **54**, 1179–1189.

40. Sezginer, A. (1985) A general formulation of focus wave modes. *J. Appl. Phys.*, **57**, 678–683.

41. McLeod, J.H. (1954) The Axicon: a new type of optical element. *J. Opt. Soc. Am.*, **44**, 592–597.

42. McLeod, J.H. (1960) Axicons and their use. *J. Opt. Soc. Am.*, **50**, 166–169.

43. Sheppard, C.J.R. and Wilson, T. (1978) Gaussian-beam theory of lenses with annular aperture. *IEEE J. Microw. Opt. Acoust.*, **2**, 105–112, 163–166.

44. Sheppard, C.J.R. (1977) The use of lenses with annular aperture. *Optik*, **48**, 329–334.

45. Durnin, J., Miceli, J.J., and Eberly, J.H. (1987) Diffraction-free beams. *Phys. Rev. Lett.*, **58**, 1499–1501.

46. Durnin, J. (1987) Exact solutions for nondiffracting beams: I. The scalar theory. *J. Opt. Soc. Am.*, **A4**, 651–654.

47. Zamboni-Rached, M. (1999) Localized solutions: structure and applications. MSc thesis. Phys. Dept., Campinas State University.

48. Zamboni-Rached, M. (2004) Localized waves in diffractive/dispersive media. PhD thesis. Universidade Estadual de Campinas, DMO/FEEC, *http://libdigi.unicamp.br/document/ ?code=vtls000337794* (accessed 27 April 2013).

49. Dartora, C.A., Zamboni-Rached, M., and Recami, E. (2003) General formulation for the analysis of scalar diffraction-free beams using angular modulation: Mathieu and Bessel beams. *Opt. Commun.*, **222**, 75–85.

50. Recami, E., Zamboni-Rached, M., and Hernández-Figueroa, H.E. (2008) Localized waves: a historical and scientific introduction, in *Localized Waves* (eds H.E. Hernandez Figueroa, M. Zamboni-Rached and E Recami), John Wiley & Sons, Inc., New York.

51. Zamboni-Rached, M., Recami, E., and Hernández-Figueroa, H.E. (2008) Structure of the nondiffracting waves, and some interesting applications, in *Localized Waves* (eds H.E. Hernandez Figueroa, M. Zamboni-Rached and E Recami), John Wiley & Sons, Inc., New York.

52. Besieris, I.M., Abdel-Rahman, M., Shaarawi, A., and Chatzipetros, A. (1998) Two fundamental representations of localized pulse solutions of the scalar wave equation. *Prog. Electromagn. Res. (PIER)*, **19**, 1–48.

53. Ziolkowski, R.W. (1989) Localized transmission of electromagnetic energy. *Phys. Rev.*, **A39**, 2005–2033.

54. Besieris, I.M., Shaarawi, A.M., and Ziolkowski, R.W. (1989) A bidirectional traveling plane wave representation of exact solutions of the scalar wave equation. *J. Math. Phys.*, **30**, 1254–1269.

55. Ziolkowski, R.W. (1991) Localized wave physics and engineering. *Phys. Rev.*, **A44**, 3960–3984.

56. Donnelly, R. and Ziolkowski, R.W. (1993) Designing localized waves. *Proc. R. Soc. Lond.*, **A440**, 541–565.

57. Ziolkowski, R.W., Besieris, I.M., and Shaarawi, A.M. (1993) Aperture realizations of exact solutions to homogeneous wave-equations. *J. Opt. Soc. Am.*, **A10**, 75–87.

58. Esposito, S. (1997) Classical solutions of Maxwell's equations with group-velocity different from *c*, and the photon tunneling effect. *Phys. Lett.*, **A225**, 203–209.

59. Friberg, A.T., Fagerholm, J., and Salomaa, M.M. (1997) Space-frequency analysis of nondiffracting pulses. *Opt. Commun.*, **136**, 207–212.

60. Shaarawi, A.M. and Besieris, I.M. (2000) On the Superluminal propagation of X-shaped localized waves. *J. Phys.*, **A33**, 7227–7254.

61. Recami, E. (2001) Superluminal motions? A bird's-eye view of the experimental status-of-the-art. *Found. Phys.*, **31**, 1119–1135.

62. Besieris, I. and Shaarawi, A. (2002) Three classes of Courant-Hilbert's progressing solutions to the scalar wave equation. *J. Electr. Waves Appl.*, **16** (8), 1047–1060.

63. Zamboni-Rached, M. (2009) Unidirectional decomposition method for obtaining exact localized wave solutions totally free of backward components. *Phys. Rev.*, **A79**, 013816.

64. Borisov, V.V. and Kiselev, A.P. (2000) A new class of relatively undistorted progressing waves. *Appl. Math. Lett.*, **13**, 83–86.

65. Kiselev, A.P. and Perel, M.V. (2000) Highly localized solutions of the wave equation. *J. Math. Phys.*, **41**, 1934–1955.

66. Zamboni-Rached, M., Nobrega, K.Z., Recami, E., and Hernández-Figueroa, H.E. (2002) Superluminal X-shaped beams propagating without distortion along a coaxial guide. *Phys. Rev.*, **E66** (036620).

67. Zamboni-Rached, M., Recami, E., and Fontana, F. (2001) Localized Superluminal solutions to Maxwell equations propagating along a normal-sized waveguide. *Phys. Rev.*, **E64** (066603), 6.

68. Zamboni-Rached, M., Fontana, F., and Recami, E. (2003) Superluminal localized solutions to Maxwell equations propagating along a waveguide: the finite-energy case. *Phys. Rev.*, **E67** (036620), 7.

69. Zamboni-Rached, M., Shaarawi, A., and Recami, E. (2004) Focused X-shaped pulses. *J. Opt. Soc. Am.*, **A21**, 1564–1574.

70. Shaarawi, A.M., Besieris, I.M., and Said, T.M. (2003) Temporal focusing by use of composite X-waves. *J. Opt. Soc. Am.*, **A20**, 1658–1665.

71. Zamboni-Rached, M., Hernández-Figueroa, H.E., and Recami, E. (2004) Chirped optical X-shaped pulses in material media. *J. Opt. Soc. Am.*, **A21**, 2455–2463.

72. (a) Sõnajalg, H. and Saari, P. (1996) Suppression of temporal spread of ultrashort pulses in dispersive media by Bessel beam generators. *Opt. Lett.*, **21**, 1162–1164; Cf. also (b) Sõnajalg, H., Rätsep, M., and Saari, P. (1997) Demonstration of the Bessel-X pulse propagating in a dispersive medium. *Opt. Lett.*, **22**, 310.

73. Porras, M.A., Valiulis, G., and Di Trapani, P. (2003) Unified description of Bessel X waves with cone dispersion and tilted pulses. *Phys. Rev.*, **E68**, 016613.

74. Longhi, S. (2003) Spatial-temporal Gauss-Laguerre waves in dispersive media. *Phys. Rev.*, **E68** (066612), 6.

75. Zamboni-Rached, M., Recami, E., and Balma, M. (2012) Simple and effective method for the analytic description of important optical beams when truncated by finite apertures. *Appl. Opt.*, **51**, 3370–3379, doi: 1559-128X/12/163370-10.

76. Zamboni-Rached, M. (2006) Analytical expressions for the longitudinal evolution of nondiffracting pulses truncated by finite apertures. *J. Opt. Soc. Am.*, **A23**, 2166–2176.

77. Lu, J.-Y., Zou, H.-H., and Greenleaf, J.F. (1993) Producing deep depth of field and depth independent resolution in NDE with limited diffraction beams. *Ultrason. Imaging*, **15**, 134–149.

78. Zamboni-Rached, M., Recami, E., and Balma, M. (2011) Proposal of apertures for generating non-diffracting beams of microwaves, arXiv:1108.2027 [physics].

79. Zamboni-Rached, M., Recami, E., and Balma, M. (2012) Analytical descriptions of optical beams truncated by finite apertures. Progress in Electromagnetics Research Symposium (PIERS) Proceedings, Moscow, Russia, Aug; pp. 464–468 [ISSN 1559-9450].

80. Saari, P. and Reivelt, K. (1997) Evidence of X-shaped propagation-invariant localized light waves. *Phys. Rev. Lett.*, **79**, 4135–4138.

81. Mugnai, D., Ranfagni, A., and Ruggeri, R. (2000) Observation of Superluminal behaviors in wave propagation. *Phys. Rev. Lett.*, **84**, 4830–4833.

82. Valtna, H., Reivelt, K., and Saari, P. (2007) Methods for generating wide-band localized waves of superluminal group-velocity. *Opt. Comm.*, **278**, 1–7.

83. Bowlan, P., Valtna-Luckner, H., Lõhmus, M., Piksarv, P., Saari, P., and Trebino, R. (2009) Measuring the spatiotemporal field of ultrashort Bessel X pulses. *Opt. Lett.*, **34**, 2276–2278.

84. Lu, J.-Y., Zou, H.-H., and Greenleaf, J.F. (1994) Biomedical ultrasound beam forming. *Ultrasound Med. Biol.*, **20**, 403–428.

85. Curtis, J.E., Koss, B.A., and Grier, D.G. (2002) Dynamic holographic optical tweezers. *Opt. Commun.*, **207**, 169–175.

86. Ambrosio, L.A. and Hernández-Figueroa, H.E. (2010) Gradient forces on double-negative particles in optical tweezers using Bessel beams in the ray optics regime. *Opt. Express*, **18**, 24287–24292.

87. Zamboni-Rached, M., Ambrosio, L.A., and Hernández-Figueroa, H.E. (2011) ''Diffraction-attenuation resistant beams: their higher-order versions and finite-aperture generation''. *Appl. Opt.*, **49**, 5861–5869.

88. Esposito, S., Majorana, E. Jr., vander Merwe, A., and Recami, E. (eds) (2003) *Ettore Majorana – Notes on Theoretical Physics*, Kluwer, Dordrecht and New York, pp. 512.

89. Barut, A.O., Maccarrone, G.D., and Recami, E. (1982) On the shape of tachyons. *Nuovo Cimento A*, **71**, 509–533.

90. Stratton, J.A. (1941) *Electromagnetic Theory*, McGraw-Hill, New York, p. 356.

91. Recami, E., Zamboni-Rached, M., and Dartora, C.A. (2004) The X-shaped, localized field generated by a Superluminal electric charge' [e-print physics/0210047]. *Phys. Rev.*, **E69**, 027602.

92. Hillion, P. (2001) Arrow Wave modes. *J. Opt. A: Pure Appl. Opt.*, **3**, 311–316.

93. Newell, A.C. and Molone, J.V. (1992) *Non-linear Optics*, Addison & Wesley, Redwood City, CA.

94. Durnin, J., Miceli, J.J., and Eberly, J.H. (1988) Comparison of Bessel and Gaussian beams. *Opt. Lett.*, **13**, 79–80.

95. Overfelt, P.L. and Kenney, C.S. (1991) Comparison of the propagation characteristics of Bessel, Bessel–Gauss, and Gaussian beams diffracted by a circular aperture. *J. Opt. Soc. Am. A*, **8**, 732–745.

96. Folman, R. and Recami, E. (1995) On the phenomenology of tachyon radiation. *Found. Phys. Lett.*, **8**, 127–134.

97. Besieris, I. and Shaarawi, A. (2004) Paraxial localized waves in free space. *Opt. Express*, **12**, 3848–3864.

98. Porras, M.A., Trillo, S., Conti, C., and Di Trapani, P. (2003) Paraxial envelope X waves. *Opt. Lett.*, **28**, 1090–1092.

99. Gradshteyn, I.S. and Ryzhik, I.M. (1965) *Integrals, Series and Products*, 5th edn, Academic Press, New York.

100. Goodman, J.W. (1996) *Introduction to Fourier Optics*, 2nd edn, McGraw-Hill, New York.

101. Gori, F. and Guattari, G. (1987) Bessel–Gauss beams. *Opt. Commun.*, **64**, 491–495.

102. Zamboni-Rached, M. and Hernández-Figueroa, H.E. (2000) A rigorous analysis of Localized Wave propagation in optical fibers. *Opt. Commun.*, **191**, 49–54.

103. Recami, E. (1986) Classical Tachyons and possible applications. *Rivista Nuovo Cim.*, **9** (6), 1–178; and refs therein.

104. (a) Dartora, C.A., Nóbrega, K.Z., Dartora, A., Viana, G.A., and Filho, H.T.S. (2006) A general theory for the frozen waves and their realizations through finite apertures. *Opt. Commun.*, **265**, 481; (b) (2007) Study of Frozen Waves' theory through continuous superpositions of Bessel beams. *Opt. Laser Technol.*, **39**, 1370.

105. Vieira, T.A., Gesualdi, M.R.R., and Rached, M. (2012) Frozen waves: experimental generation. *Opt. Lett.*, **37**, 2034–2036.

106. Recami, E. and Rodrigues, W.A. (1985) A model theory for tachyons in two dimensions, in *Gravitational Radiation and Relativity, Proceedings of the Sir Arthur Eddington Centenary Symposium*, Vol.3 (eds J. Weber and T.M. Karade), World Scientific, Singapore, pp. 151–203.

107. See, e.g., Recami, E. (ed.) (1978) *Tachyons, Monopoles, and Related Topics*, North-Holland, Amsterdam. pp. X + 285.

108. Recami, E. and Mignani, R. (1976) Magnetic monopoles and tachyons in special relativity. *Phys. Lett.*, **B62**, 41–43.

109. Recami, E. and Mignani, R. (1974) *Rivista Nuovo Cim.*, **4**, 209–290; E398.

110. Mignani, R. and Recami, E. (1973) Generalized Lorentz transformations and superluminal objects in four dimensions. *Nuovo Cimento*, **A14**, 169–189; A16, 206.

111. Saari, P. and Reivelt, K. (2004) Generation and classification of localized waves by Lorentz transformations in Fourier space. *Phys. Rev.*, **E69**, 036612; refs. therein.

112. Arlt, J., Garcés-Chavez, V., Sibbett, W., and Dholakia, K. (2001) Optical micromanipulation using a Bessel light beam. *Opt. Commun.*, **197**, 239–245.

113. Herman, R.M. and Wiggins, T.A. (1991) Production and uses of diffractionless beams. *J. Opt. Soc. Am.*, **A8**, 932–942.

114. Garcés-Chavez, V., McGloin, D., Melville, H., Sibbett, W., and Dholakia, K. (2002) Simultaneous micromanipulation in multiple planes using a self-reconstructing light beam. *Nature*, **419**, 145–147.

115. Garcés-Chávez, V., Roskey, D., Summers, M.D., Melville, H., McGloin, D., Wright, E.M., and Dholakia, K. (2004) Optical levitation in a Bessel light beam. *Appl. Phys. Lett.*, **85**, 4001–4003.

116. Milne, G., Dholakia, K., McGloin, D., Volke-Sepulveda, K., and Zemánek, P. (2007) Transverse particle dynamics in a Bessel beam. *Opt. Express*, **15**, 13972–13987.

117. Neuman, K.C. and Block, S.M. (2004) Optical trapping. *Rev. Sci. Instrum.*, **75**, 2787–2809.

118. Ashkin, A. (1992) Forces of a single-beam gradient laser trap on a dielectric sphere in the ray optics regime. *Biophys. J.*, **61**, 569–582.

119. Volke-Sepulveda, K., Chávez-Cerda, S., Garcés-Chávez, V., and Dholakia, K. (2004) Three-dimensional optical forces and transfer of orbital angular momentum from multi-ringed light beams to spherical particles. *J. Opt. Soc. Am.*, **B21**, 1749.

120. Garcés-Chávez, V., Volte-Sepulveda, K., Chávez-Cerda, S., Sibbett, W., and Dholakia, K. (2002) Transfer of orbital angular momentum to an optically trapped low-index particle. *Phys. Rev.*, **A66**, 063402.

121. Rubinov, A.N., Afanas'ev, A.A., Ermolaev, I.E., Kurochkin, Y.A., and Mikhnevich, S.Y. (2003) Localization of spherical particles under the action of gradient forces in the field of a zero-order Bessel beam. Rayleigh-Gans approximation. *J. Appl. Spectrosc.*, **70**, 565–572.

122. Gouesbet, G. and Gréhan, G. (1982) Sur la généralisation de la théorie de Lorenz–Mie. *J. Opt. (Paris)*, **13**, 97–103.

123. Maheu, B., Gouesbet, G., and Gréhan, G. (1988) A concise presentation of the generalized Lorenz–Mie theory for arbitrary incident profile. *J. Opt. (Paris)*, **19**, 59–67.

124. Lock, J.A. and Gouesbet, G. (2009) Generalized Lorenz–Mie theory and applications. *J. Quant. Spectrosc. Radiat. Transf.*, **110**, 800–807.

125. Gouesbet, G. (2009) Generalized Lorenz–Mie theories, the third decade: a perspective. *J. Quant. Spectrosc. Radiat. Transf.*, **110**, 1223–1238.

126. Gouesbet, G. and Gréhan, G. (2010) *Generalized Lorenz–Mie theories*, Springer-Verlag.

127. Gouesbet, G., Grhan, G., and Maheu, B. (1988) Expressions to compute the coefficients g_n^m in the generalized Lorenz–Mie theory using finite series. *J. Opt. (Paris)*, **19**, 35–48.

128. Gouesbet, G., Gréhan, G., and Maheu, B. (1989) On the generalized Lorenz–Mie theory: first attempt to design a localized approximation to the computation of the coefficients g_n^m. *J. Opt. (Paris)*, **20**, 31–43.

129. Gouesbet, G., Grhan, G., and Maheu, B. (1990) Localized interpretation to compute all the coefficients g_n^m in the generalized Lorenz–Mie theory. *J. Opt. Soc. Am.*, **A7**, 998–1007.

130. Gouesbet, G. and Lock, J.A. (1994) Rigorous justification of the localized approximation to the beam-shape coefficients in generalized Lorenz–Mie theory. I. On-axis beams. *J. Opt. Soc. Am.*, **A11**, 2503–2515.

131. Gouesbet, G. and Lock, J.A. (1994) Rigorous justification of the localized approximation to the beam-shape coefficients in generalized Lorenz–Mie theory. II. Off-axis beams. *J. Opt. Soc. Am.*, **A11**, 2516–2525.

132. Ambrosio, L.A. and Hernández-Figueroa, H.E. (2011) Integral localized approximation description of ordinary Bessel beams and application to optical trapping forces. *Biomed. Opt. Express*, **2**, 1893–1906.

133. Ren, K.F., Gouesbet, G., and Gréhan, G. (1998) Integral localized approximation in generalized Lorenz–Mie theory. *Appl. Opt.*, **37**, 4218–4225.

134. Ambrosio, L.A. and Hernández-Figueroa, H.E. (2011) Radiation pressure cross section and optical forces over negative refractive index spherical particles by ordinary Bessel beams. *Appl. Opt.*, **50**, 4489–4498.

135. Li, R., Ren, K.F., Han, X., Wu, Z., Guo, L., and Gong, S. (2012) Analysis of radiation pressure force exerted on a biological cell induced by high-order Bessel beams using Debye series. *J. Quant. Spectrosc. Radiat. Transf.*. http://dx.doi.org/10.1016/j.jqsrt.2012.07.030.

136. Neves, A.A.R., Fontes, A., Padilha, L.A., Rodriguez, E., Cruz, C.H.D., Barbosa, L.C., and Cesar, C.L. (2006) Exact partial wave expansion of optical beams with respect to an arbitrary origin. *Opt. Lett.*, **31**, 2477–2479.

137. Neves, A.A.R., Fontes, A., Pozzo, L.D.Y., de Thomaz, A.A., Chillce, E., Rodriguez, E., Barbosa, L.C., and Cesar, C.L. (2006) Electromagnetic forces for an arbitrary optical trapping

of a spherical dielectric. *Opt. Express*, **14**, 13101–13106.

138. Bouchal, Z. and Olivík, M. (1995) Non-diffracting vector Bessel beams. *J. Modern Opt.*, **42**, 1555–1566.

139. Veselago, V.G. (1968) The electrodynamics of substances with simultaneously negative values of ϵ and μ. *Sov. Phys. Usp.*, **10**, 509–514.

140. Smith, D.R., Padilla, W.J., Vier, D.C., Nemat-Nasser, S.C., and Schultz, S. (2000) Composite medium with simultaneously negative permeability and permittivity. *Phys. Rev. Lett.*, **84**, 4184–4187.

141. Shelby, R.A., Smith, D.R., and Schultz, S. (2001) Experimental verification of a negative index of refraction. *Science*, **292**, 77–79.

142. Siviloglu, G.A. and Christodoulides, D.N. (2007) Accelerating finite energy airy beams. *Opt. Lett.*, **32**, 979–981.

143. Siviloglu, G.A., Broky, J., Dogariu, A., and Christodoulides, D.N. (2007) Observation of accelerating airy beams. *Phys. Rev. Lett.*, **99**, 213901.

144. Besieris, I.M. and Shaarawi, A.M. (2008) Accelerating Airy wave packets

in the presence of quadratic and cubic dispersion. *Phys. Rev.*, **E78**, 046605.

145. Siviloglu, G.A., Broky, J., Dogariu, A., and Christodoulides, D.N. (2008) Ballistic dynamics of airy beams. *Opt. Lett.*, **33**, 207.

146. Lotti, A., Faccio, D., Couairon, A., *et al.* (2011) Stationary non-linear Airy beams. *Phys. Rev.*, **A84**, 021807.

147. Olkhovsky, V.S. and Recami, E. (1992) Recent developments in the time analysis of tunnelling processes. *Phys. Rep.*, **214**, 339–357, and refs therein.

148. Olkhovsky, V.S., Recami, E., and Jakiel, J. (2004) Unified time analysis of photon and nonrelativistic particle tunneling. *Phys. Rep.*, **398**, 133–178.

149. Privitera, G., Recami, E., Salesi, G., and Olkhovsky, V.S. (2003) Tunnelling times: an elementary introduction. *Rivista Nuovo Cim.*, **26**, monographic issue (4), 54.

150. Barbero, A.P.L., Hernández-Figueroa, H.E., and Recami, E. (2000) On the propagation speed of evanescent modes. *Phys. Rev.*, **E62**, 8628–8635.